

Self-Interference Cancellation in Full-Duplex Communication Systems

Ruozhu Li



Department of Electrical & Computer Engineering
McGill University
Montreal, Canada

April 2017

A thesis submitted to McGill University in partial fulfillment of the requirements for the degree
of Master of Engineering.

© 2017 Ruozhu Li

Abstract

Full-duplex (FD) wireless communications can potentially double the spectral efficiency by transmitting and receiving simultaneously over the same frequency at a cost of a large power difference between the high-power self-interference (SI), and the low-power intended signal received from the remote transmitter. SI can be reduced gradually by a combination of radio-frequency (RF) and baseband SI-cancellation stages. Each stage requires the estimation of various distortions that the SI endures, such as SI-channel and transceiver nonlinearities. This thesis deals with the development of SI-cancellation techniques that are well adapted to FD operations.

We address SI-cancellation for FD operations in the presence of imperfect RF components. In particular, we develop a new scheme to jointly estimate the IQ mixer imbalance, power amplifier (PA) nonlinearities, up-/down-conversion phase-noise and SI-channel. First, we study and develop a baseband model that captures the most significant transceiver RF imperfections, for both separate- and common-oscillator structures used in the up- and down-conversions. A basis expansion model (BEM) is then derived to approximate the time-varying phase-noise, and to transform the problem of estimating the time-varying phase-noise into the estimation of a set of static coefficients. Using the method of maximum likelihood (ML) criterion, the likelihood function is derived in the presence of the unknown intended signal, which leads to the joint estimation of the intended channel, the SI-channel, the nonlinear impairments and the phase-noise. When the intended signal is unknown, an iterative procedure is developed to find the ML estimate of the different parameters based on its own known transmitted data, the known pilot symbols, and the statistic of the unknown intended signal received from the intended transmitter. We consider the two pilot-insertion structures used in LTE for the frequency-multiplexed pilots and the time-multiplexed pilots. Compared to training-based techniques, the full use of the received signal significantly reduces the required number of pilot symbols. Simulation results indicate that the proposed algorithms can offer a superior SI-cancellation performance, with the resulting signal-to-SI-and-noise ratio (SINR) being very close to the signal-to-noise ratio (SNR).

Moreover, we study the power of SI after each cancellation stage, taking into account the transceiver impairments. One SI-cancellation scheme, which combines antenna cancellation, RF cancellation and digital cancellation, provides results from real world experiments that show the feasibility of an FD design. In general, it is difficult to assess the exact level of the SI reduction that is obtainable due to the interactions among factors such as transceiver impairments, wireless propagation channel and estimation error. We hereby identify the main factors that affect the

cancellation performance. This allows for a better understanding of the obtained performance, and leads to the development of new methods that improves the cancellation capability of FD systems. We address the impact of each transceiver impairment in FD systems, and specify the limiting factors of the RF and baseband SI-cancellation stages for a given architecture. In addition, we demonstrate that reducing the SI before the LNA/ADC, via the RF SI-cancellation stage is necessary to avoid high quantization noise from the ADC. The analysis further reveals that the transmitter nonlinearities need to be modeled and canceled in the baseband SI-cancellation stage. Finally, in light of our simulation results, we discuss the trade-off between the amount of SI-cancellation and the number of cancellation stages, and propose the potential case scenarios for operations with one digital cancellation.

Sommaire

La transmission en duplex intégral (full-duplex ou DF) peut potentiellement doubler l'efficacité spectrale des systèmes semi-duplex. Elle est achevée en utilisant la même ressource temporelle et fréquentielle pour la transmission et la réception au prix d'une large interférence (self-interference ou SI) comparée à la puissance du signal utile reçu de l'autre émetteur. La SI peut être graduellement réduite par une combinaison d'étages de réduction au niveau radiofréquence (RF) et en bande de base. Chaque étage requiert l'estimation des différentes distorsions que la SI subit, tels que le canal de propagation et les non-linéarités de l'émetteur. Cette thèse propose des techniques pour réduire la SI qui sont bien adaptées à l'opération en FD.

Nous adressons la réduction de la SI pour opérer en FD en présence de composants RF imparfaits. En particulier, nous développons un nouveau schéma pour estimer conjointement le dérèglement du mélangeur, la non-linéarité de l'amplificateur de puissance (PA), le bruit de phase du convertisseur de fréquence et le canal de propagation. Premièrement, nous détaillons un modèle en bande de base qui capture les imperfections de l'émetteur les plus importantes, utilisant soit deux oscillateurs séparés pour les conversions de fréquence ou un même oscillateur. Un modèle d'expansion de base (BEM) est ensuite dérivé pour approximer la variation temporelle du bruit de phase et pour transformer le problème d'estimer des coefficients variables au cours du temps à l'estimation d'un ensemble de coefficients statiques. En utilisant le critère du maximum de vraisemblance (ML), la fonction de vraisemblance est dérivée en présence du signal inconnu, qui résulte à l'estimation jointe des canaux de propagation de la SI et du signal utile, des imperfections de l'émetteur et du bruit de phase. Quand le signal utile est non connu, une procédure itérative est développée pour trouver l'estimé au maximum de vraisemblance des différents paramètres en se basant sur le signal transmis, les symboles pilotes et la statistique du signal utile inconnu. Nous considérons les deux structures utilisées en LTE pour l'insertion des symboles pilotes en les multiplexant en temps ou en fréquence. Comparée aux techniques supervisées, l'utilisation complète du signal reçu réduit considérablement le nombre de pilotes requis. Les résultats de simulation indiquent que l'algorithme proposé offre des performances supérieures en terme d'annulation de SI, résultant en un rapport signal sur SI plus bruit très proche du rapport signal sur bruit (SNR).

De plus, nous étudions la puissance de la SI après chaque étage d'annulation, en prenant en compte les imperfections de l'émetteur. En général, il est difficile de trouver le niveau exact de la SI après chaque étage d'annulation à cause de l'interaction de plusieurs facteurs tels que

les imperfections de l'émetteur, le canal de propagation et l'erreur d'estimation. En identifiant les facteurs principaux qui dictent la performance d'annulation, nous pouvons développer les méthodes appropriées qui traitent ces facteurs. Nous évaluons l'impact de chaque composant dans les systèmes FD et nous spécifions les facteurs limites des étages d'annulation en RF et en bande de base. En plus, nous démontrons que réduire la SI avant les LAN/ADC, à travers l'étage d'annulation RF, est nécessaire pour éviter un large bruit de quantification de l'ADC. L'analyse révèle aussi que les non-linéarités de l'émetteur doivent être modélées et réduites en bande de base. Finalement, à travers nos résultats de simulations, nous discutons le compromis entre le taux d'annulation et le nombre d'étages d'annulation et nous proposons le scénario d'opération utilisant un étage d'annulation en bande de base.

Acknowledgments

First, I would like to express my deepest and sincere gratitude to my supervisor, Professor Tho Le-Ngoc, for his inspiring guidance, warm encouragement and continuous support during my studies at McGill University. His broad knowledge, sharp judgment, enthusiasm and dedication to top-quality research have been of great value for me, and will continue to benefit me through my research journey. I would like to acknowledge the financial supports received from the Natural Sciences and Engineering Research Council of Canada (NSERC) and Huawei Canada.

My deep appreciation goes to Dr. Ahmed Masmoudi for his patient, productive research coaching and collaboration. He has helped me countless times in various aspects of my research and I have learned a great deal in working closely with him.

I am really grateful to all my fellow lab-mates in the Broadband Communications Research Lab (BCRL), especially Robert, Fei, Xiaowei, Rajesh, Alfred, Yue, Chao, Gowdemy, Atoosa, Pragyan, Vikas and Yahya for the beneficial discussions, and for making my journey at McGill amusing and memorable.

I am also thankful to my friends at McGill University: Wenrui Duan, Rui Li, Siting Ni, Junqian Zhang, Bofan Wang, Ryan Razani and Laure DC. It has been your company that made life away from home interesting and meaningful.

Finally, my deepest love and gratitude are devoted to my parents who give meaning to my life. To them, I dedicate this thesis.

Contents

1	Introduction	1
1.1	Motivation	1
1.2	Contributions	5
2	SI-Cancellation in Full-Duplex Systems	7
2.1	SI-Channel Modeling	7
2.2	Antenna SI-Cancellation	9
2.2.1	Antenna Separation	9
2.2.2	Antenna Direction	10
2.2.3	Antenna Placement	10
2.3	RF SI-Cancellation	11
2.4	Baseband/Digital SI-Cancellation	13
2.5	Chapter Summary	15
3	BEM Based Maximum Likelihood-Based SI-Cancellation	16
3.1	System Model for Frequency-Multiplexed Pilot Transmission	17
3.1.1	Signal model	17
3.1.2	Basis expansion model	20
3.2	Parameter Estimation and SI-Cancellation for Frequency-Multiplexed Pilot Transmission	26
3.3	Signal Model and SI-Cancellation Parameter Estimation for Time-Multiplexed Pilots Transmission	29
3.3.1	LS and ML Estimators for Time-Multiplexed Pilots Transmission	30
3.4	Simulation Results	32
3.4.1	Performance Evaluation with Separate- and Common-Oscillator Structures	33

3.4.2	Performance of Frequency-Multiplexed and Time-Multiplexed Pilot Transmission	35
3.5	Chapter Summary	40
4	SI-Cancellation Performance and Limiting Factors	41
4.1	Overview of Simulink FD Communications System Platform	41
4.2	Simulation of FD Communication System	43
4.2.1	Limiting Factors in SI-Cancellation	45
4.2.2	Performance of The First Architecture	49
4.2.3	Performance of The Second Architecture	59
4.3	Limitation of Cancellation	69
4.3.1	Limitation of RF SI-Cancellation Stage	70
4.3.2	Limitation of baseband SI-cancellation stage	70
4.4	Potential Scenarios with fewer cancellation stages	70
4.4.1	Potential Scenarios for operation without RF SI-cancellation stage	71
4.4.2	Potential Scenarios for operation without baseband SI-cancellation stage	72
4.5	Chapter Summary	73
5	Conclusions and Future Work	74
5.1	Summary	74
5.2	Potential Future Research	75
	References	77

List of Figures

1.1	An FD wireline communication system with echo cancellation.	2
1.2	Illustration of the SI in an FD point-to-point wireless communication system. . .	3
2.1	Illustration of the SI-channel for separate and shared antenna architectures. . . .	8
2.2	A FD base station can receive in the uplink from one mobile station while transmitting in the downlink to another mobile station.	10
2.3	Block diagram of antenna placement.	11
2.4	RF/analog SI-cancellation stage using TDL circuit.	12
2.5	Transversal FIR structure.	13
2.6	Simplified block diagram of the FD transceiver with RF and baseband SI-cancellation stages.	14
3.1	Time-multiplexed pilots transmission.	29
3.2	SINR before and after baseband SI-cancellation versus SNR in separate-oscillator and common-oscillator cases.	33
3.3	Phase-noise in the <i>separate</i> oscillator case (solid line) and its approximations (dashed lines) using different basis expansion order Q	34
3.4	Phase-noise in the <i>common</i> oscillator case (solid line) and its approximations (dashed lines) using different basis expansion order Q	35
3.5	SI-channel MSE versus SNR in different numbers of iterations.	36
3.6	SI-channel estimation MSE versus input SNR.	37
3.7	Output SINR versus input SNR after cancellation.	38
3.8	SI-cancellation gain versus input SNR after cancellation.	39
4.1	Top Level Block Diagram of Simulink FD Communications System Platform. . .	42

4.2	Simplified block diagram of the FD transceivers with RF and baseband SI-cancellation stages.	44
4.3	Cancellation performance in the absence of quantization noise and nonlinearities in architecture 1.	49
4.4	Receive ADC resolution effect in architecture 1.	50
4.5	RF cancellation output DAC resolution effect in architecture 1.	51
4.6	Transmitter DAC resolution effect in architecture 1.	52
4.7	Combined ADC and DAC resolution effect in architecture 1.	53
4.8	PA nonlinearity effect in architecture 1.	53
4.9	Combined PA nonlinearity and Quantization effect in architecture 1.	54
4.10	LNA nonlinearity effect in architecture 1.	57
4.11	Combined LNA nonlinearity and quantization effect in architecture 1.	57
4.12	TD-SICv4 case and TD-SICv5 case in architecture 1.	58
4.13	Cancellation performance in the absence of quantization noise and nonlinearities in architecture 2.	59
4.14	Receive ADC resolution effect in architecture 2.	60
4.15	Transmitter reference ADC resolution effect in architecture 2.	61
4.16	RF cancellation output DAC resolution effect in architecture 2.	62
4.17	Transmitter DAC resolution effect in architecture 2.	63
4.18	Combined ADC and DAC resolution effect in architecture 2.	63
4.19	PA nonlinearity effect in architecture 2.	64
4.20	Combined PA nonlinearity and Quantization effect in architecture 2.	65
4.21	LNA nonlinearity effect in architecture 2.	67
4.22	Combined LNA nonlinearity and quantization effect in architecture 2.	68
4.23	TD-SICv4 case and TD-SICv5 case in architecture 2.	69

List of Tables

4.1	Analog SI-Cancellation nonlinearity effect in architecture 1.	55
4.2	Combined analog SI-cancellation nonlinearity and quantization effect in architecture 1.	56
4.3	Analog SI-Cancellation nonlinearity effect in architecture 2.	65
4.4	Combined analog SI-cancellation nonlinearity and quantization effect in architecture 2.	66
4.5	The parameters of ADC	71
4.6	The parameters of LNA	72

List of Acronyms

ADC	Analog-to-digital converter
AGC	automatic gain control
BEM	Basis expansion model
CCP	Co-channel nonlinear distortion power
CPE	Common phase error
DAC	Digital-to-analog converter
FD	Full-duplex
FDD	Frequency-division duplex
FFT	Fast Fourier transform
FIR	Finite impulse response
FSPL	Free-space path loss
HD	Half-duplex
ICC	Intercarrier interference
IMD3	Third-order Inter-Modulation Distortion
IQ mixer	In-phase/quadrature mixer
LNA	Low noise amplifier
LoS	Line-of-sight
LS	Least square
LTE	Long-Term Evolution
MIMO	Multiple-input multiple-output
ML	Maximum likelihood
MMSE	Minimum mean square error
MSE	Mean square error
OFDM	Orthogonal frequency-division multiplexing

OIP3	Third-order intercept point
PA	Power amplifier
PAPR	Peak-to-Average Power Ratio
PDP	Power delay profile
PLL	Phase-locked loop
QAM	Quadrature amplitude modulation
RF	Radio-frequency
SC-FDMA	Single Carrier FDMA
SI	Self-interference
SISO	Single-input single-output
SINR	Signal-to-interference noise ratio
SIR	Signal-to-interference ratio
SNR	Signal-to-noise ratio
SNIR	Signal-to-noise-and-interference noise ratio
TDD	time-division duplex
TDL	Tapped delay lines
VGA	Variable gain amplifier
dB	Decibel
dBm	Decibel-milliwatts

Chapter 1

Introduction

Currently, wireless communications systems operate in half-duplex (HD) [1]. To avoid the potentially strong self-interference (SI) from its own transmission to its reception, a transceiver in a HD system has to transmit and receive in non-overlapping time-slots (time-division duplex (TDD)), or frequency-slots (frequency-division duplex (FDD)), or in different orthogonal spectrum-spreading codes. Since the demand on data rates offered by communications systems is rapidly increasing, it is necessary to improve the spectral efficiency of these networks. Although many advanced techniques, for example orthogonal frequency division multiplexing (OFDM) [2] and multiple-input–multiple-output (MIMO) [3], have been proposed to increase the spectral efficiency, current operational wireless communications systems [4], which employ only HD operations, still cannot meet the demand for the fast growth of wireless communications. Therefore, relying solely on HD transmission leads to under-utilization of resources. Full-duplex (FD) operations by simultaneous transmission and reception over the same frequency slot, can increase the spectral efficiency to overcome the limitations of HD systems [5].

1.1 Motivation

Despite the aforementioned benefits promised by FD operations, the main challenge remains in dealing with the SI signal that arises from the node's own transmission. This SI is much stronger than the signal of interest from the remote node [6], and results in very low signal-to-interference-and-noise ratio (SINR). In fact, the strong SI reduces the capacity of an FD system to a level below that of an HD system. Moreover, SI signals cause transceiver oscillations [4, 7]. Therefore, when

implementing FD communications systems, it is critical to keep SI sufficiently low in order to effectively detect the intended but lower-powered signal. The notion of FD operations is not new, and has been successfully used in wired communications systems. In this case, the interference, or the line echo, arises from the coupling between transmitting and receiving wires, as well as from the impedance mismatch of the hybrid circuit at the two/four-wires conversion interface [8], as shown in Fig. 1.1. This line echo is about 3 – 6 dB lower than the intended signal [9], which requires a relatively low cancellation level in the range of 20 – 30 dB.

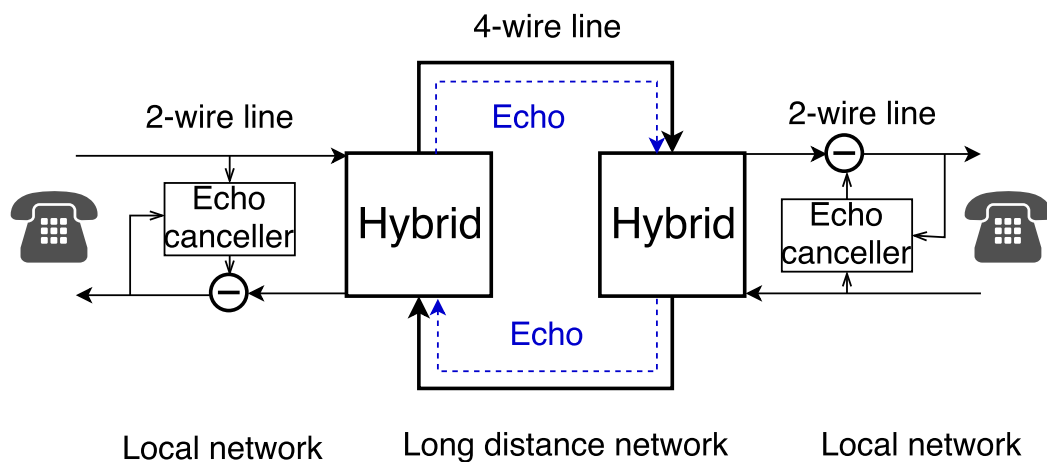


Fig. 1.1 An FD wireline communication system with echo cancellation.

However, it is more challenging for current wireless communications systems to operate in FD mode. As shown in Fig. 1.2, when transceivers communicate in FD, the receiver, due to its own transmission, would experience a co-channel SI. Due to the large distance that the intended signal crosses, the SI is often several orders of magnitude stronger than the intended signal [10]. For example, given two transceivers that are separated by 1 km, then for each, the intended signal coming from the other would be attenuated by approximately 100 dB, assuming free-space path loss (FSPL). Supposing that the transmit and receive antennas within one transceiver are isolated by 15 dB, the resulting SI would be 85 dB stronger than the intended signal. The difference in power level between the SI and the intended signal becomes even larger as the distance between them increases. Consequently, FD wireless systems require a much higher SI-cancellation, compared with echo cancellation in wired communications systems. This in turn suggests the need for developing more advanced cancellation techniques and strategies.

Various works have proposed to suppress the SI by combining successive cancellation stages

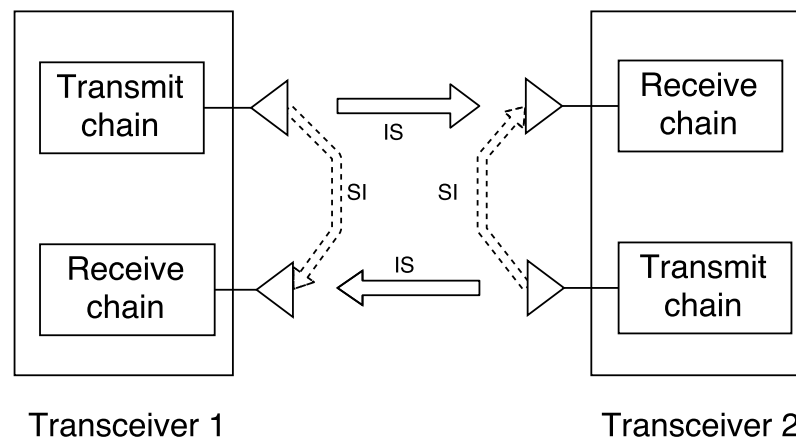


Fig. 1.2 Illustration of the SI in an FD point-to-point wireless communication system.

[11, 12]. First, the antenna SI-cancellation stage exploits the designed antennas and supporting structures on the same transceiver to reduce the transmitter-receiver coupling. Subsequently, a radio-frequency (RF) SI-cancellation stage is introduced prior to the low-noise amplifier (LNA) and the analog-to-digital converter (ADC) to further suppress the SI. This brings down the SI to a sufficiently low level, to avoid overloading or saturating these components. Further cancellation of the residual SI can be done after the ADC at the baseband.

Due to the non-ideality of transceiver components, reducing only the linear part of the SI leaves a large amount of residual SI, which needs to be further suppressed by digital SI cancelers at baseband. Actually, the IQ mixer creates an inband image signal, about 25 dB lower than the main signal [13]. The IQ imbalance on the FD transceiver results in considerable residual SI [14] that cannot be ignored. In [15], a widely-linear least-square (LS) estimation technique was proposed to compensate the IQ imbalance caused by IQ mixers in the transceiver. Moreover, the transmit power amplifier (PA) generates nonlinear components [10, 16–18]. Cancellation of the nonlinearities induced by the PA in FD transceivers is discussed in [15], where the PA output is approximated by a Hammerstein model and an LS-based estimator is used to find the model coefficients. In [19], an iterative algorithm is proposed to jointly estimate the SI-channel and the nonlinear-PA coefficients using LS criterion. The estimated coefficients are then used to construct an estimate of the received SI to be subtracted from the received signal.

The analytical and experimental results from [10, 20, 21] show that the power of phase-noise induced distortion is high relative to the intended signal. Thus it has to be canceled in order to accurately detect the intended signal. In generally, phase-noise in OFDM systems has a two-fold

effect: It generates a common phase error (CPE), which is a constant phase shift affecting all subcarriers, and intercarrier interference (ICI) [20]. The CPE can be compensated by most of the current SI-cancellation methods. However, ICI causes the power of a subcarrier to spread into adjacent ones, which limits the performance of SI cancellation.

The experimental results in [22] show how phase-noise affects narrow band signals in an FD transceiver, in which the transmitter and receiver have separate oscillators. However, since FD operations use the same frequency for transmission and the reception, it is more convenient to share the same oscillator between the transmit and receive chains. Both common and separate oscillator scenarios were studied in [20] in terms of the resulting SI. Using one common oscillator, the phase-noise affecting the signal in the up-conversion and down-conversion is the same, with some delay due to signal propagation. On the other hand, when using separate oscillators, the signal is affected by two independent phase-noises, making the effect of the phase-noise more severe. For generality, both independent/separate oscillators and common/shared oscillator will be discussed in this work. To suppress the oscillator phase-noise in FD systems, we need first to estimate the phase-noise that affects the received SI, shift the reference signal in order to produce a replica of the SI, which is subtracted from the received signal at baseband. However, the time-varying nature of the phase-noise makes the estimation process challenging. A frequency-domain and a time-domain estimation procedures were proposed in [23], using the minimum-mean-square-error (MMSE) and LS criteria by alternatively estimating the phase-noise and the SI-channel, while considering the intended signal as additive noise. Compared to the frequency-domain technique, the time-domain technique achieves better performance due to the linear interpolation performed, which uses the estimated samples to obtain an estimate for the residual samples in each OFDM symbol [23].

Using an estimation of the SI-channel, the transmitter nonlinearities and the phase-noise, a replica of the received SI can be generated from the known transmitted signal, then subtracted from the received signal in the baseband. All the previous methods we mentioned, which can be considered as training based techniques, ignore the intended signal by considering it as additive noise or using a training period. The assumption made in [15] and [19] that the intended signal is not present during the SI estimation stage, is not practical in a real FD communications system. Moreover, since the phase-noise is a time varying process, it cannot be estimated during training periods since. Other methods consider the intended signal as noise, which increases the estimation error in these methods [24]. This estimation error will directly affect the cancellation performance for the reconstructed SI is different from the actual received SI. Since

the presence of the intended signal significantly influences the estimation performance, it is more appropriate to jointly estimate the SI-channel, intended channel, transmitter nonlinearities and the phase-noise [25]. To that end, we need an accurate model to capture all these parameters.

1.2 Contributions

The first objective of this work is to develop a novel and effective baseband SI-cancellation stage for FD wireless communications systems. To achieve this goal, we study and develop appropriate estimation algorithm to reduce the residual SI accurately after the RF cancellation. The second objective is to build a platform of FD communications systems to evaluate the SI-cancellation performance. The research contributions of this work are highlighted along with the thesis organization as follows.

In Chapter 2, we start with a brief survey of the most relevant state-of-the-art cancellation techniques. We summarize the existing architectures to design the SI canceler. Then, a brief overview of the existing estimation algorithms used to reconstruct the SI for SI-cancellation is presented. We also summarize the spatial cancellation techniques applicable to SI suppression. These background materials will be the starting point for the developments of new algorithms and methods for SI-cancellation.

In Chapter 3, we incorporate the intended signal in the estimation process instead of considering it as additive noise and we cancel all transmitter impairments. To that end, we develop a new method to jointly estimate the transmitter nonlinearities, phase-noise and both the SI- and intended-channel at the baseband. To deal with the time-varying aspect of the phase-noise, a Basis Expansion Model (BEM) [26–28] is adopted to model the combined phase-noise, nonlinearities and SI-channel coefficients. To estimate the BEM coefficients, we rely on the Maximum-Likelihood (ML) criteria. The proposed ML estimator uses the known transmitted SI signal, and both the known pilot symbols and unknown data symbols received from the other transmitter. The required number of pilot symbols is able to be reduced by making the full use of each block of the received signal [29]. To formulate the likelihood function, the unknown signal is modeled as a Gaussian process. An iterative procedure is proposed to find the global maximum of the likelihood function. While an ML-based estimator was previously developed to estimate the SI and intended channels [29], it was not explored to mitigate the effect of transmitter impairments. Our preliminary results in [28] focus on the phase-noise mitigation

without considering the intended transmitter impairments. The development of the joint estimation scheme to simultaneously mitigate the PA, the IQ mixer and the phase-noise effects will be presented in this thesis. We consider both LTE pilot insertion schemes used for the frequency-multiplexed pilots (i.e., base-station transmission) and time-multiplexed pilots (i.e., user transmission) [13]. For the frequency-multiplexed pilots, the base-station transmitted signal contains the known pilot symbols in the specified/reserved sub-carriers and unknown data symbols in the other sub-carriers. Different from the frequency-multiplexed pilots, the time-multiplexed pilots transmission reserves certain time slots for pilot transmission. According to the pilot distribution in time-multiplexed pilots transmission time-slots, the proposed method to estimate the BEM coefficients is based on the combination of LS and ML criteria. For unknown data blocks, the intended signal is considered as Gaussian noise. An iterative procedure is proposed to find the global maximum of the likelihood function.

First, we briefly introduce the SIMULINK platform and explain the practical settings in Chapter 4. Then, for the two commonly used architectures of SI-cancellation, we discuss the main limitation factor of each cancellation stage [10] with a complete set of simulation results. In our platform, we focus on the quantization and nonlinearity, and study scenarios of individual impairment. The limitation factor that we take into consideration is distortion introduced by ADC and DAC, nonlinearity of analog SI-cancellation stage, nonlinearity of PA and nonlinearity of LAN. By presenting the performance with each limitation factor, the effect of each limitation on cancellation is shown directly. Based on these results, we analyze the dominant factors that limit the SI-cancellation. Last, we discuss the potential scenarios for operation with only two SI-cancellation stages: RF/Analog and Baseband/Digital.

Finally, Chapter 5 concludes this thesis.

Chapter 2

SI-Cancellation in Full-Duplex Systems

This chapter provides a brief overview of FD communications systems and SI-cancellation techniques. We first discuss the nature of the SI-channel then model it by power delay profile. Based on this model, we propose several successive cancellation stages, including an antenna cancellation stage, an analog RF SI-cancellation stage and a digital cancellation stage. We present a survey on each stage, describing the techniques applied to each stage and discussing their advantages and limitations.

2.1 SI-Channel Modeling

Several works have been done to analyze and measure the SI-channel. Considering the typical and popular architecture of antenna, the same antenna is used to transmit and receive signals simultaneously via a three-port circulator. As shown in Fig.2.1(a), the SI-channel is divided into three components: leakage, antenna internal reflection, and external reflection [30]. Leakage occurs due to the practically limited isolation in the circulator and the impedance mismatch in the circulator ports [30]. Antenna internal reflection (i.e., part of the transmitted signal is reflected from the antenna) results from the impedance mismatch between the isolator and antenna [30]. External reflections from the surrounding environment [30], mainly closely located objects, typically have larger delays and weaker levels than leakage and antenna internal reflection.

It was reported in [30] that power levels of the leakage and antenna internal reflection are more stable, and they exceed the external reflections by about 30 dB. When using two different antennas to transmit and receive, the line-of-sight (LoS) components and the path coming from the electromagnetic waves reflected from the transceiver structure represent the most significant paths [31]. The different reflection paths that constitute the SI-channel between the two antenna configurations are represented in Fig.2.1(b). The antenna internal reflection is almost static because there is no relative movement between the two antennas, while the external reflections change according to the surrounding environment.

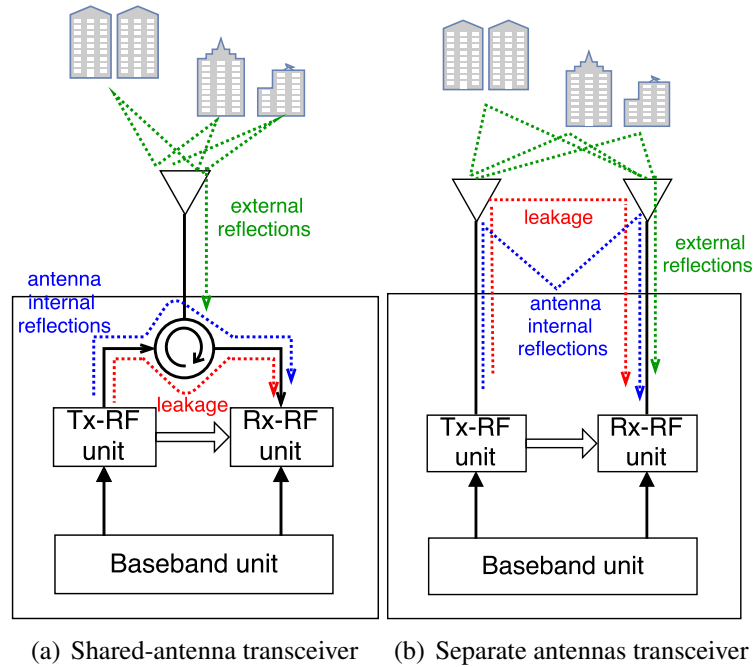


Fig. 2.1 Illustration of the SI-channel for separate and shared antenna architectures.

For both architectures, in general, the power delay profile (PDP) of the SI-channel is written as [30]:

$$P_{PDP}(t, \tau) = P_{pl}\delta(t - \tau_{pl}) + P_{ar}\delta(t - \tau_{ar}) + \sum_{l=1}^L P_l\delta(t - \tau_l), \quad \tau_{pl} > \tau_{ir} \geq \tau_l \quad (2.1)$$

where $\{P_{pl}, \tau_{pl}\}$, $\{P_{ar}, \tau_{ar}\}$ and $\{P_l, \tau_l\}$ are the power delays of the leakage path, the antenna reflection path, and the external reflection multipath, respectively, and L is the number of the

external reflection multipath components [30].

2.2 Antenna SI-Cancellation

Antenna SI-cancellation techniques are intended to reduce SI by means of an appropriate design of transmitting and receiving antenna structures. A FD transceiver can (i) use one common antenna shared by its transmitter and receiver via a circulator, or (ii) use 2 separate antennas, one for its transmitter and the other for its receiver, shown in Fig. 2.1. In a separate-antenna FD transceiver, strong SI can occur via direct leakage from transmit to receive antennas, and reflections due to the transceiver structure. On the other hand, in a shared-antenna FD transceiver, leakage is via the circulator and the reflections comes from the antenna impedance mismatch. In both architectures, these two components are quasi-static and are referred to as internal reflections. Furthermore, for both architectures, SI is also contributed by external reflections due to surrounding environmental conditions, which vary over time and cannot be reduced by the antenna design.

Antenna SI-cancellation, or passive SI-cancellation, can be achieved by using antenna separation [32, 33], directional antennas [34, 35] or antennas placement to create null space at the receive antennas [36, 37].

2.2.1 Antenna Separation

Antenna separation is the basic method of implementing passive suppression [4], because in practice increasing the path-loss between the transmit antenna and receive antenna is an effective approach to attenuate the SI signal for systems. Consider a system in which each node has one transmit and one receive antenna, higher SI suppression capability is achieved by the larger separation between the transmit and the receive antennas [32, 33]. For FD communications systems in practice, however, the isolation cancellation by antenna separation is insufficient, therefore the employment of RF and digital SI-cancellation stages is necessary to further reduce the power of residual SI [4].

2.2.2 Antenna Direction

Antenna-directional SI suppression is a technique that minimizes the intersection of main radiation side lobes of the transmit and receive antennas of an FD node [38]. The topology of Fig. 2.2 is an example of an FD base station that can exploit directional diversity [34]. These techniques imply that the transceiver's transmit direction is different from its receive direction [34, 35]. In this case, SI suppression can be achieved by applying directional antennas at FD base station, which directs its transmit signal to the downlink mobile and thus away from its receive antenna, which directs the uplink mobile [35].

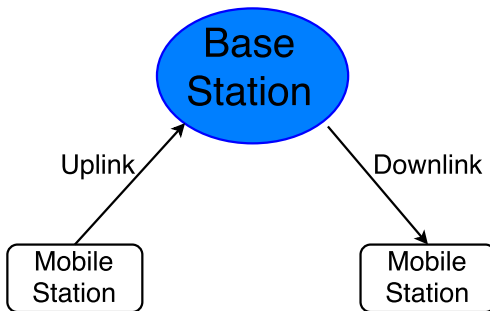


Fig. 2.2 A FD base station can receive in the uplink from one mobile station while transmitting in the downlink to another mobile station.

2.2.3 Antenna Placement

Antenna placement can be achieved by employing two transmit antennas and a single receive antenna, where the pair of transmit antennas is placed at distances of d and $d + \lambda/2$ away from the receive antenna respectively, with λ representing the wavelength of the transmitted signal [37]. Positioned appropriately, the distances between the receive antenna and the transmit antennas differ by an odd multiple of $\lambda/2$, which results in the transmit signals to be superimposed with each other [36, 37]. Fig. 2.3 illustrates this technique. The destructive interference becomes excellent when the signal impulses impinging on the receive antenna from the pair of transmit antennas are identical, thereby generating a zero at the position of the receive antenna [4].

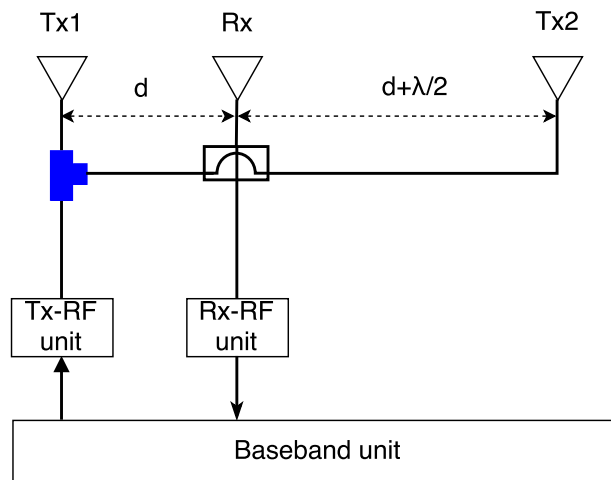


Fig. 2.3 Block diagram of antenna placement.

2.3 RF SI-Cancellation

RF SI-cancellation aims to use the knowledge of the transmitted SI to cancel it before the receiving LNA. In general, RF SI-cancellation can be implemented in two stages. The first RF/analog stage takes part of the RF/analog transmitted signal from the PA output, passes it through an analog tapped-delay line (TDL) circuit to reconstruct the estimated SI replica for cancellation at the receiver input as shown in Fig. 2.4 [10, 17]. The second RF/digital stage (not shown in Fig. 2.4) passes the transmitted baseband digital signal through a digital SI-channel estimator and then to an auxiliary transmit chain with DAC, and up-converter to produce an estimated RF SI-replica to be subtracted from the received signal prior to the LNA [39–41].

The SI-channel can be divided into internal reflections (near-field) having fewer paths, shorter delays as well as larger amplitudes, and external reflections (far-field) with more paths, longer delays and smaller amplitudes, as discussed in Section 2.2. Internal reflections are quasi-static, and depend on the components and structure of transceivers, while external reflections vary in accordance with environmental conditions.

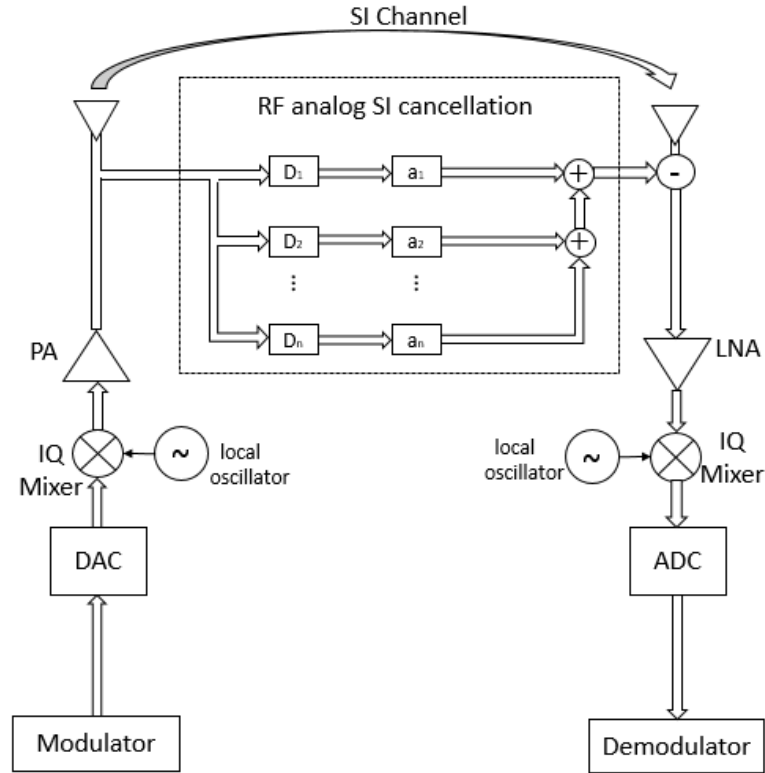


Fig. 2.4 RF/analog SI-cancellation stage using TDL circuit.

Based on this multi-tap structure, as shown in Fig. 2.4, the first RF/analog SI-cancellation stage uses a TDL circuit with adjustable delays and coefficients. The TDL method achieves an SI reduction of 30 to 45 dB [42, 43]. Although the TDL can match the short delay of the internal reflections, the interaction between the delays and attenuators makes the tuning very complex. A 4-tap analog RF cancellation is proposed in [43, 44]. Each tap consists of variable attenuator and phase. The antenna domain suppression was implemented by ring array antenna with optimized beamformer [45]. In [42], a 12-tap analog RF cancellation is proposed with variable attenuator and fixed delay lines. The method proposed in [36, 46] consists of using a cancelling circuit based on balance transformer such as QHx220 chip. To match the received SI, this chip takes the transmitted SI as input, then subtracts the resulting signal from the received signal by changing its amplitude and phase. This method is able to achieve about 20 dB reduction in the received SI [36].

A large amount of residual SI is left to be reduced in the subsequent cancellation stages.

Moreover, being sensitive to environmental conditions, more adaptive cancellation methods are needed to cancel external reflections, which can be done by using digital domain processing. RF/digital SI-cancellation can be applied to adapt to random external reflections, and to suppress SI components due to external reflections by using a digital symbol-synchronous finite-impulse-response filter [36, 41, 47]. The idea of using an initial HD period to initiate the RF/digital SI-cancellation stage has been used in [48], where the baseband transmit signal is rotated at each subcarrier and the rotated signal is used to represent the received SI. This second RF/digital SI-cancellation stage requires additional hardware resources for each antenna, such as an up-converter and a DAC, potentially making it too costly for MIMO system [25]. In addition, since the reference signal was tapped at baseband, the PA nonlinear distortion, as well as output noise will not be reduced, leaving a large amount of SI.

RF SI-cancellation is combined with antenna cancellation to reduce the SI signal power to prevent receiver saturation [16], and reduce ADC quantization noise, since quantization noise is a key factor in limiting the performance of SI-cancellation [49, 50].

2.4 Baseband/Digital SI-Cancellation

Digital SI-cancellation is an effective mitigation mechanism in the baseband [4]. In practice, digital cancellation includes two steps: i) Estimate the SI-channel; ii) Construct an estimate of the received SI from the channel estimate and the known transmit signal, then subtract it from the received signal [46]. By exploiting the knowledge of the SI signal, received SI is canceled after quantization of the received signal by the ADC [36, 40].

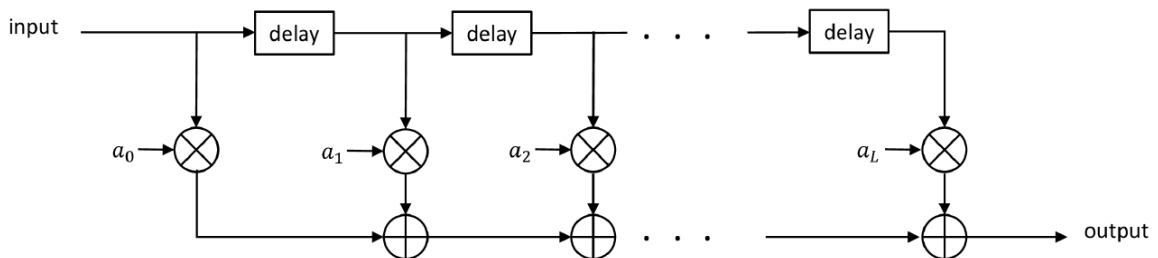


Fig. 2.5 Transversal FIR structure.

which requires accurate estimates of SI-channel and transceiver impairments. To that end, we need to get every impairment that may happen to the transmitted SI along the way, including propagation channel and nonlinearities of RF components like in-phase/quadrature (IQ) mixer and power amplifier (PA) [10].

To achieve the goal of SI-cancellation in baseband, many works have provided different methods [15, 19, 23, 29, 51]. A joint detection procedure is developed in [29] based on subspace that can accurately estimate the SI channel coefficients and the nonlinear parameters without any pilot symbols from the intended signal. The author in [15] proposed a separate channel and phase-noise estimation for compensating the image component of the SI signal, which occurs due to IQ imbalances in the transmitter and receiver IQ mixers. An iterative technique is proposed in [19], which is used to jointly estimate the SI-channel and the nonlinearity coefficients to suppress the distortion signal. A closed-form expression of baseband SI-cancellation is derived in [51] by alternatively estimating the SI-channel with IQ imbalance and PA nonlinearity. An MMSE procedure proposed in [23] considers the intended signal as additive noise. However, it suffers from two kinds of errors: the phase-noise increases the estimation error of the SI-channel, and that in turn degrades the phase-noise estimation performance.

In the next chapters, we discuss the existing techniques in more details, improve some of them and propose new cancellation techniques.

2.5 Chapter Summary

This chapter provides an overview of the existing works on SI-cancellation in FD wireless systems. Estimating the SI-channel is seen as a central issue in developing efficient cancellation methods. Due to the large power of SI, successive cancellation stages are needed to properly detect the intended signal.

Chapter 3

BEM Based Maximum Likelihood-Based SI-Cancellation ¹

This chapter addresses the self-interference cancellation for FD operation in the presence of imperfect radio-frequency components. In particular, we develop a new scheme to jointly estimate and cancel the IQ mixer imbalance, power amplifier nonlinearities, up-/down-conversion phase-noise and the SI-channel. First, we develop a detailed baseband model that captures the most significant transceiver RF imperfections for both separate- and common-oscillator structures used in the up- and down-conversions. A basis expansion model is derived to approximate the time-varying phase-noise and to transform the problem of estimating the time-varying phase-noise into the estimation of a set of time-invariant coefficients. Subsequently, the likelihood function is derived in the presence of the unknown intended signal to formulate the joint estimation of the intended channel, the SI-channel, nonlinear impairments and phase-noise, under the maximum likelihood criterion. An iterative procedure is developed to find the ML estimate of the different parameters based on the known transmitted data, the known pilot symbols, and the statistics of the unknown intended signal received from the intended transmitter. The full use of the received signal significantly reduces the required number of pilot symbols as compared to training-based

¹Parts of this chapter have been presented in [28].

techniques. We consider the two pilot-insertion structures used in LTE: frequency- and time-multiplexed pilots. Simulation results indicate that the proposed ML algorithms can offer a superior SI-cancellation performance with the resulting signal-to-SI-and-noise ratio (SINR) very close to the signal-to-noise ratio (SNR).

3.1 System Model for Frequency-Multiplexed Pilot Transmission

In this section, we present the signal model for FD systems in the presence of transceiver impairments, and transmit and receive phase-noise. Consider an FD transceiver that transmits and receives simultaneously over the same frequency slot. This FD operation creates SI that needs to be canceled in order to reliably detect the intended signal from the other transmitter. The block diagram of the considered FD transceiver along with the other intended transmitter² is presented in Fig. 2.6. In addition to the transmit and receive chains, the transceiver contains SI-cancellation stages. RF SI-cancellation stages are assumed to suppress the SI to a sufficiently low level before the LNA to avoid receiver saturation/overloading. Then, baseband SI-cancellation stage, after the ADC, further reduces the residual SI.

3.1.1 Signal model

We consider an OFDM system with N subcarriers and focus on the received signal at one transceiver. After processing by the digital-to-analog converter (DAC), the m^{th} transmitted OFDM signal, denoted by $x_m(t)$, is passed through the IQ mixer. Due to the inherent mismatches between the amplitudes and phases of the I and Q branches, a mirror image of the original signal is added. The local oscillator used for up-conversion generates random phase-noise, denoted by $\phi^{\text{up,i}}(t)$. The signal at the output of the transmit IQ mixer is written as³ [52]:

$$x_m^{\text{IQ}}(t) = (g_1 x_m(t) + g_2 x_m^*(t)) e^{j\phi^{\text{up,i}}(t)}, \quad (3.1)$$

where g_1 is the response of the IQ mixer for the direct signal component, and g_2 is the response for the image component.

²For simplicity, the receiver of the other transceiver is not shown in Fig. 2.6.

³For brevity, we use the equivalent complex-valued baseband representation (i.e., with zero carrier frequency.)

Before transmission, the signal is passed through the transmit PA, whose response is modeled with a Hammerstein nonlinearity [53, 54] presented as:

$$x_m^{\text{PA}}(t) = \left(\sum_{k=0}^K \alpha_{2k+1} x_{m,2k+1}(t) \right) * f(t), \quad (3.2)$$

where α_1 is the linear gain of PA, and α_{2k+1} , for $k = 1, \dots, K$ is the gain of $(2k + 1)^{\text{th}}$ order component⁴, $2K + 1$ is the total order of PA nonlinear component, $f(t)$ denotes the memory model of the PA, $*$ denotes the convolution operator, and $x_{m,2k+1}(t) = x_m^{\text{IQ}}(t) |x_m^{\text{IQ}}(t)|^{2k}$ results from the cascaded IQ and PA [55].

At the receiver, in the presence of the intended signal, the m^{th} received OFDM block (including one OFDM symbol of N subcarriers and N_{cp} cyclic prefix) is written in time domain as:

$$y_m^{\text{RF}}(t) = (x_m^{\text{PA}}(t) e^{j\phi^{\text{up.i}}(t)}) * h^{\text{SI}}(t) + (s_m(t) e^{j\phi^{\text{up.s}}(t)}) * h^{\text{s}}(t) + w_m^{\text{G}}(t), \quad (3.3)$$

where $\phi^{\text{up.i}}(t)$ and $\phi^{\text{up.s}}(t)$ are the phase-noise processes affecting the SI and the intended signal, respectively. $h^{\text{SI}}(t)$ is the SI-channel and $h^{\text{s}}(t)$ is the intended channel, and $w_m^{\text{G}}(n)$ is the additive Gaussian noise.

After SI-cancellation at the RF stage, the received signal can be expressed as:

$$y_m^{\text{rsi}}(t) = y_m^{\text{RF}}(t) - x_m^{\text{PA}}(t) * a(t), \quad (3.4)$$

where $a(t)$ is an estimate of the SI-channel [36, 41]. Typically, RF SI-cancellation provides 30 dB suppression of the SI signal [41].

In this paper, we assume the receiver implements a direct down-converter with IQ correction [56], such that the IQ imbalance is removed. Phase-noise generated by the local transceiver oscillator used for down-conversion is denoted by $\phi^{\text{down}}(t)$. Thus, the m^{th} received OFDM signal

⁴We ignore the even-order nonlinearities, which are out of the band of the signal.

is written as:

$$\begin{aligned}
 y_m(n) = & \left((\alpha_1 g_1 x_m(n) + \alpha_1 g_2 x_m^*(n)) e^{j\phi^{\text{up},i}(n)} \right) * h^{\text{rsi}}(n) e^{-j\phi^{\text{down}}(n)} \\
 & + \left(\sum_{k=1}^K \alpha_{2k+1} x_{m,2k+1}(n) e^{j\phi^{\text{up},i}(n)} \right) * h^{\text{rsi}}(n) e^{-j\phi^{\text{down}}(n)} \\
 & + \left(s_m(n) e^{j\phi^{\text{up},s}(n)} \right) * h^s(n) e^{-j\phi^{\text{down}}(n)} + w_m(n).
 \end{aligned} \tag{3.5}$$

for $n = 1, 2, \dots, N$, where $x_m(n)$ and $s_m(n)$ are the SI and intended signal, respectively, the residual SI-channel after RF cancellation is $h^{\text{rsi}}(n) = h^{\text{SI}}(n) - a(n)$, and $w_m(n)$ is the overall noise.

We assume that the length of cyclic prefix N_{cp} satisfies $N_{cp} > L$. For L-tap propagation channels, the received signal can be written as:

$$\begin{aligned}
 y_m(n) = & \sum_{l=0}^{L-1} \alpha_1 g_1 x_m(n-l) h^i(l) e^{j\phi^i(n-l)} + \\
 & \alpha_1 g_2 x_m^*(n-l) h_{IQ}^i(l) e^{j\phi^i(n-l)} + \\
 & \sum_{k=1}^K \alpha_{2k+1} x_{m,2k+1}(n-l) h_{PA,k}^i(l) e^{j\phi^i(n-l)} + \\
 & s_m(n-l) h^s(l) e^{j\phi^s(n-l)} + w_m(n),
 \end{aligned} \tag{3.6}$$

where $h_{PA,k}^i(l)$, for $k = 0, \dots, K$, is the equivalent SI-channel for the k^{th} order of PA nonlinear component, $x_{m,2k+1}(n)$ is approximated by $g_1 x_m(n) |x_m(n)|^{2k} + g_2 x_m^*(n) |x_m(n)|^{2k}$ [15], and $\phi^i(n-l) = \phi^{\text{up},i}(n-l) - \phi^{\text{down}}(n)$, $\phi^s(n-l) = \phi^{\text{up},s}(n-l) - \phi^{\text{down}}(n)$ are the global phase-noise processes affecting the SI and intended signals, respectively. The equivalent SI and intended channels for the individual signal components combined with the phase-noise on both transmitter and receiver are:

$$\begin{aligned}
 h^i(n, l) &= \alpha_1 g_1 h^{\text{rsi}}(l) e^{j\phi^i(n-l)}, \\
 h_{IQ}^i(n, l) &= \alpha_1 g_2 h^{\text{rsi}}(l) e^{j\phi^i(n-l)},
 \end{aligned}$$

$$\begin{aligned}
h_{PA,k}^i(n, l) &= \alpha_{2k+1} g_1 h^{\text{rsi}}(l) e^{j\phi^i(n-l)}, \\
h_{PA,IQ,k}^i(n, l) &= \alpha_{2k+1} g_2 h^{\text{rsi}}(l) e^{j\phi^i(n-l)}, \\
h^s(n, l) &= h^s(l) e^{j\phi^s(n-l)}.
\end{aligned} \tag{3.7}$$

The up-converter and down-converter oscillators in a full-duplex communications system can be either separate, where the resulting phase-noise processes $\phi^{\text{up},i}(n)$ and $\phi^{\text{down}}(n)$ are statistically independent, or common where $\phi^{\text{up},i}(n) = \phi^{\text{down}}(n)$, which is possible for co-located transmit and receive chains. The global phase-noise process changes from one sample to another. Thus, the equivalent channel coefficients in (3.7) are time-varying. In this case, the number of parameters to estimate is much larger than the number of received samples. In fact, each additional sample results in $2K + 3$ unknowns. To avoid this problem, we adopt the approach detailed in the following section.

3.1.2 Basis expansion model

In general, a function can be approximated by a decomposition over a set of elementary functions. Considering the combined channel coefficient and phase-noise $h^i(n, l_0) = h^{\text{rsi}}(l_0) e^{j\phi^i(n-l_0)}$ as a function of time n for a given l_0 , it can be approximated by a set of elementary functions of n .

In this situation, $h^i(n, l_0)$ can be expanded over a basis of complex exponentials. Specifically, the variation of the impulse responses, caused by the time-varying phase-noise, is captured in a deterministic way by the means of a basis expansion as follows:

$$h^i(n, l) = \sum_{q=1}^Q a_q^{\text{rsi}}(l) b_q(n) + \epsilon_q^i(n), \tag{3.8}$$

where $\epsilon_q^i(n)$ is the remainder of the expansion, $b_q(n)$, for $q = 1, \dots, Q$, form the known basis used for the development, Q is the order of the development, and $a_q^{\text{rsi}}(l)$, for $q = 1, \dots, Q$, are the unknown coefficients, which are time-invariant. The coefficients $\{a_q^{\text{rsi}}(l)\}_{q=1}^Q$, together with the basis $\{b_q(n)\}_{q=1}^Q$, characterize the system.

Various BEM designs have been suggested to model time-varying channel [26] such as Polynomial BEM (P-BEM), Discrete Karhunen-Loève BEM (DKL-BEM), and Complex Exponential

BEM (CE-BEM). For the problem at hand, the combined phase-noise and channel coefficients are complex-valued, making the real-valued P-BEM not suitable. On the other hand, the DKL-BEM offers the lowest estimation error, but requires knowledge of the channel statistics, which may not be available in practice. Due to its tractability, the complex exponential basis, given by $b_q(n) = e^{jw_q n}$, is widely used to model the wireless channel. It can be seen as a special case of the Karhunen-Loève BEM based on white spectrum. Therefore, we apply CE-BEM in our model.

The method to estimate the frequencies of the exponential basis $\{w_q\}_{q=1}^Q$ proposed in [27] is time-consuming and thus impractical in real implementation. The variation of the channel and phase-noise can be represented by *i*) the time-invariant BEM coefficients \mathbf{a} , and *ii*) the Fourier basis $e^{jw_q n}$, that captures the time-variation. According to the characteristics of channel and phase-noise responses over the block duration [57], and the property of Fourier transform, the basis used to jointly model the channel and phase-noise is given by:

$$b_q(n) = e^{j2\pi(q-Q/2)n/N}. \quad (3.9)$$

The remainder of the expansion $\epsilon_q^{\text{rsi}}(n)$ tends to zero under the following conditions: *i*) For a sufficient approximation order Q ; or *ii*) For a small variation of the phase-noise. For a particular oscillator, the phase-noise is a slowly varying process with respect to the sampling rate; thus $\epsilon_q^{\text{rsi}}(n)$ can be neglected to obtain the equivalent SI and intended channels for the individual signal components combined with the phase-noise:

$$\begin{aligned} h^i(n, l) &= \sum_{q=1}^Q a_q^{\text{rsi}}(l) b_q(n), \\ h_{IQ}^i(n, l) &= \sum_{q=1}^Q a_{q,IQ}^{\text{rsi}}(l) b_q(n), \\ h_{PA}^i(n, l) &= \sum_{q=1}^Q a_{q,PA}^{\text{rsi}}(l) b_q(n), \\ h_{PA,IQ}^i(n, l) &= \sum_{q=1}^Q a_{q,PA,IQ}^{\text{rsi}}(l) b_q(n), \end{aligned}$$

$$h^s(n, l) = \sum_{q=1}^Q a_q^s(l) b_q(n), \quad (3.10)$$

where $a_{q,PA}^{\text{rsi}}(l)$, $a_{q,PA,IQ}^{\text{rsi}}(l)$ and $a_q^s(l)$, $q = 1, 2, \dots, Q$ are the unknown coefficients, related to their corresponding channels. The objective of the formulation in (3.10), referred to as BEM [27], is to reduce the number of parameters to be estimated and to transform the original under-determined problem to a more tractable one.

For an OFDM transmitted signal, the symbol sequence $\{S_m(k)\}_0^{N-1}$ is transformed into time domain signal $s_m(n)$ using an IFFT block (i.e., $s_m(n) = \sum_0^{N-1} S_m(k) e^{j2\pi kn/N}$). For frequency-multiplexed pilot transmission, the base-station transmitted signal contains the known pilot symbols in the specified/reserved sub-carriers and unknown data symbols in the other sub-carriers. By denoting $\mathcal{N}_p = \{p_1, \dots, p_P\}$ as the index set of subcarriers that are used for pilot symbols, where P is the number of pilots. We represent the transmitted signal $s_m(n)$ from the intended transceiver as the sum of two signals $s_m(n) = s_m^p(n) + s_m^d(n)$ where:

$$\begin{aligned} s_m^p(n) &= \sum_{i=1}^P S_m(n_i) e^{j2\pi p_i n/N}, \\ s_m^d(n) &= \sum_{k \notin \mathcal{N}_p} S_m(k) e^{j2\pi kn/N}. \end{aligned} \quad (3.11)$$

Then, we rewrite (3.6) as:

$$\begin{aligned} y_m(n) &= \sum_{l=0}^{L-1} \sum_{q=1}^Q x_m(n-l) a_{q,1}^{\text{rsi}}(l) b_q(n) + \\ & x_m^*(n-l) a_{q,IQ}^{\text{rsi}}(l) b_q(n) + \\ & x_m(n-l) |x_m(n-l)|^2 a_{q,PA}^{\text{rsi}}(l) b_q(n) + \\ & x_m^*(n-l) |x_m(n-l)|^2 a_{q,PA,IQ}^{\text{rsi}}(l) b_q(n) + \\ & s_m^p(n-l) a_q^s(l) b_q(n) + \\ & s_m^d(n-l) a_q^s(l) b_q(n) + w_m(n). \end{aligned} \quad (3.12)$$

The estimation of the time-varying channels turns into that of the sets of the time-invariant BEM coefficients given by:

$$\begin{aligned}
\mathbf{a}^{\text{rsi}}(l) &= [a_1^{\text{rsi}}(l), \dots, a_Q^{\text{rsi}}(l)]^T, \\
\mathbf{a}_{IQ}^{\text{rsi}}(l) &= [a_{1,IQ}^{\text{rsi}}(l), \dots, a_{Q,IQ}^{\text{rsi}}(l)]^T, \\
\mathbf{a}_{PA}^{\text{rsi}}(l) &= [a_{1,PA}^{\text{rsi}}(l), \dots, a_{Q,PA}^{\text{rsi}}(l)]^T, \\
\mathbf{a}_{PA,IQ}^{\text{rsi}}(l) &= [a_{1,PA,IQ}^{\text{rsi}}(l), \dots, a_{Q,PA,IQ}^{\text{rsi}}(l)]^T, \\
\mathbf{a}^s(l) &= [a_1^s(l), \dots, a_Q^s(l)]^T.
\end{aligned} \tag{3.13}$$

For a more compact representation of (3.10), we gather the basis and coefficients for the residual SI-channel in matrix form as:

$$h^{\text{rsi}}(n, l) = \mathbf{b}_n^T \mathbf{a}^{\text{rsi}}(l), \tag{3.14}$$

where $\mathbf{b}_n = [b_1(n), \dots, b_Q(n)]^T$ is the basis vector at time n . Applying the same manipulation for all individual channel coefficients yields the following relations:

$$\begin{aligned}
h_{IQ}^{\text{rsi}}(n, l) &= \mathbf{b}_n^T \mathbf{a}_{IQ}^{\text{rsi}}(l), \\
h_{PA}^{\text{rsi}}(n, l) &= \mathbf{b}_n^T \mathbf{a}_{PA}^{\text{rsi}}(l), \\
h_{PA,IQ}^{\text{rsi}}(n, l) &= \mathbf{b}_n^T \mathbf{a}_{PA,IQ}^{\text{rsi}}(l), \\
h^s(n, l) &= \mathbf{b}_n^T \mathbf{a}^s(l).
\end{aligned} \tag{3.15}$$

By gathering the different paths in vector forms as:

$$\begin{aligned}
\mathbf{h}_n^{\text{rsi}} &= [h^{\text{rsi}}(n, 0), \dots, h^{\text{rsi}}(n, L-1)]^T, \\
\mathbf{h}_{n,IQ}^{\text{rsi}} &= [h_{IQ}^{\text{rsi}}(n, 0), \dots, h_{IQ}^{\text{rsi}}(n, L-1)]^T, \\
\mathbf{h}_{n,PA}^{\text{rsi}} &= [h_{PA}^{\text{rsi}}(n, 0), \dots, h_{PA}^{\text{rsi}}(n, L-1)]^T, \\
\mathbf{h}_{n,PA,IQ}^{\text{rsi}} &= [h_{PA,IQ}^{\text{rsi}}(n, 0), \dots, h_{PA,IQ}^{\text{rsi}}(n, L-1)]^T, \\
\mathbf{h}_n^s &= [h^s(n, 0), \dots, h^s(n, L-1)]^T,
\end{aligned} \tag{3.16}$$

all the channel coefficients to be estimated are collected as:

$$\begin{aligned} \mathbf{h}_n &= \left[\mathbf{h}_n^{\text{rsi}T}, \mathbf{h}_{n,IQ}^{\text{rsi}T}, \mathbf{h}_{n,PA}^{\text{rsi}T}, \mathbf{h}_{n,PA,IQ}^{\text{rsi}T}, \mathbf{h}_n^{\text{s}T} \right]^T \\ &= \mathbf{B}_n \mathbf{a}, \end{aligned} \quad (3.17)$$

where $\mathbf{a} = [\mathbf{a}^{\text{rsi}T}, \mathbf{a}_{IQ}^{\text{rsi}T}, \mathbf{a}_{PA}^{\text{rsi}T}, \mathbf{a}_{PA,IQ}^{\text{rsi}T}, \mathbf{a}^{\text{s}T}]^T$ is the $5QL \times 1$ vector gathering all the BEM coefficients where the vectors of coefficients are related to the SI-channel $\mathbf{a}^{\text{rsi}} = [\mathbf{a}^{\text{rsi}}(0), \mathbf{a}^{\text{rsi}}(1), \dots, \mathbf{a}^{\text{rsi}}(L-1)]^T$ for direct component, $\mathbf{a}_{IQ}^{\text{rsi}} = [\mathbf{a}_{IQ}^{\text{rsi}}(0), \mathbf{a}_{IQ}^{\text{rsi}}(1), \dots, \mathbf{a}_{IQ}^{\text{rsi}}(L-1)]^T$ for image component, $\mathbf{a}_{PA}^{\text{rsi}} = [\mathbf{a}_{PA}^{\text{rsi}}(0), \mathbf{a}_{PA}^{\text{rsi}}(1), \dots, \mathbf{a}_{PA}^{\text{rsi}}(L-1)]^T$ for direct part of PA component, $\mathbf{a}_{PA,IQ}^{\text{rsi}} = [\mathbf{a}_{PA,IQ}^{\text{rsi}}(0), \mathbf{a}_{PA,IQ}^{\text{rsi}}(1), \dots, \mathbf{a}_{PA,IQ}^{\text{rsi}}(L-1)]^T$ for image part of PA component, and $\mathbf{a}^{\text{s}} = [\mathbf{a}^{\text{s}}(0), \mathbf{a}^{\text{s}}(1), \dots, \mathbf{a}^{\text{s}}(L-1)]^T$ for intended channel. The $5L \times 5QL$ basis matrix \mathbf{B}_n is given by:

$$\begin{aligned} \mathbf{B}_n &= \begin{bmatrix} \mathbf{b}_n^T & 0 & \cdots & 0 & 0 \\ 0 & \mathbf{b}_n^T & \cdots & 0 & 0 \\ \vdots & \vdots & \ddots & \vdots & \\ 0 & 0 & \cdots & \mathbf{b}_n^T & 0 \\ 0 & 0 & \cdots & 0 & \mathbf{b}_n^T \end{bmatrix} \\ &= \mathbf{I}_{N \times N} \otimes \mathbf{b}_n^T, \end{aligned} \quad (3.18)$$

where \otimes denotes the Kronecker product.

Using the sequence $\{x_m(n)\}$, we define the $N \times L$ Toeplitz matrix $\mathbf{X}_{\text{toep},m}$, with the first row $[x_m(1), x_m(N), \dots, x_m(N-L+2)]$, and the first column⁵ $[x_m(1), x_m(2), \dots, x_m(N)]$. The Toeplitz matrices $\mathbf{X}_{IQ,\text{toep},m}$, $\mathbf{X}_{PA,\text{toep},m}$, $\mathbf{X}_{PA,IQ,\text{toep},m}$ and $\mathbf{S}_{\text{toep},m}^{\text{p}}$ are defined in the same way as $\mathbf{X}_{\text{toep},m}$ using the sequence $\{x_m^*(n)\}$, $\{x_m(n)|x_m(n)|^2\}$, $\{x_m^*(n)|x_m(n)|^2\}$ and $\{s_m^{\text{p}}(n)\}$, in-

⁵Note that the remaining i, j elements of a Toeplitz matrix \mathbf{A} satisfy the relation: $a_{i,j} = a_{i-1,j-1}$.

instead of $\{x_m(n)\}$, respectively. Using $\mathbf{X}_{toep,m}$, the $N \times LQ$ matrix $\mathbf{X}_{basis,m}$, combining the direct component of the SI data sequence and the basis, is defined as⁶ $\mathbf{X}_{basis,m}(n, :) = \mathbf{X}_{toep,m}(n, :) \otimes \mathbf{b}_n^T$. Similarly, $\mathbf{X}_{IQ,basis,m}$, $\mathbf{X}_{PA,basis,m}$ and $\mathbf{X}_{PA,IQ,basis,m}$ combine $X_{IQ,toep,m}$, $X_{PA,toep,m}$ and $X_{PA,IQ,toep,m}$, respectively, with the basis b_n , instead of $X_{toep,m}$, and the matrix $\mathbf{S}_{basis,m}^p$, containing the intended pilot symbols, is defined in the same way using $\mathbf{S}_{toep,m}^p$. Then, we express the received vector $\mathbf{y}_m = [y_m(1), \dots, y_m(N)]^T$ as:

$$\begin{aligned}
 \mathbf{y}_m &= \mathbf{X}_{basis,m} \mathbf{a}^{\text{rsi}} + \mathbf{X}_{IQ,basis,m} \mathbf{a}_{IQ}^{\text{rsi}} + \mathbf{X}_{PA,basis,m} \mathbf{a}_{PA}^{\text{rsi}} + \mathbf{X}_{PA,IQ,basis,m} \mathbf{a}_{PA,IQ}^{\text{rsi}} + \\
 &\quad \mathbf{S}_{basis,m}^p \mathbf{a}^s + \mathbf{H}_m^s \mathbf{s}_m^d + \mathbf{w}_m \\
 &= \mathbf{D}_{basis,m} \mathbf{a} + \mathbf{H}_m^s \mathbf{s}_m^d + \mathbf{w}_m,
 \end{aligned} \tag{3.19}$$

where $\mathbf{D}_{basis,m} = [\mathbf{X}_{basis,m}, \mathbf{X}_{IQ,basis,m}, \mathbf{X}_{PA,basis,m}, \mathbf{X}_{PA,IQ,basis,m}, \mathbf{S}_{basis,m}^p]$ is the matrix collecting all the known SI symbols of direct component, image component and nonlinear PA component, as well as the known pilot symbols from the intended signal. In (3.19), \mathbf{H}_m^s is the intended channel matrix of m^{th} block defined as:

$$\mathbf{H}_m^s = \begin{bmatrix} h^s(1,0) & 0 \cdots & h^s(1,L-1) & \cdots & h^s(1,1) \\ h^s(2,1) & h^s(2,0) & \cdots & h^s(2,L-1) \cdots & h^s(2,2) \\ \vdots & \ddots & \ddots & \ddots & \vdots \\ h^s(L,L-1) & \cdots & h^s(L,0) & 0 \cdots & 0 \\ \vdots & \ddots & \ddots & \ddots & \vdots \\ 0 \cdots & 0 \cdots & h^s(N,L-1) & \cdots & h^s(N,0) \end{bmatrix}. \tag{3.20}$$

The formulation of the received signal in (3.19) allows us to express the parameters to estimate

⁶ $\mathbf{X}_{toep,m}(n, :)$ is the n^{th} row of Toeplitz matrix $\mathbf{X}_{toep,m}$, $\mathbf{X}_{basis,m}(n, :)$ is the n^{th} row of matrix $\mathbf{X}_{basis,m}$

in a linear form.

3.2 Parameter Estimation and SI-Cancellation for Frequency-Multiplexed

Pilot Transmission

This section studies the estimation of the SI-channel, nonlinearities, and phase-noise based on the previous developments. We consider the problem of estimating the time-invariant BEM coefficients \mathbf{a} from the sample \mathbf{y}_m .

To reduce the SI in (3.19), we need to estimate the vector $\tilde{\mathbf{a}}^{\text{rsi}} = [\mathbf{a}^{\text{rsi}T}, \mathbf{a}_{IQ}^{\text{rsi}T}, \mathbf{a}_{PA}^{\text{rsi}T}, \mathbf{a}_{PA,IQ}^{\text{rsi}T}]^T$ from \mathbf{y}_m . Since the $\mathbf{X}_{basis,m}$, $\mathbf{X}_{IQ,basis,m}$, $\mathbf{X}_{PA,basis,m}$ and $\mathbf{X}_{PA,IQ,basis,m}$ are known, the straightforward procedure to estimate $\tilde{\mathbf{a}}^{\text{rsi}}$ is to resort to a linear estimator using the matrix $\tilde{\mathbf{X}}_{basis,m} = [\mathbf{X}_{basis,m}, \mathbf{X}_{IQ,basis,m}, \mathbf{X}_{PA,basis,m}, \mathbf{X}_{PA,IQ,basis,m}]$. However, this strategy gives poor performance since the intended signal is considered as noise. As an alternative, we exploit the statistics of the unknown part of the intended signal to jointly estimate $\tilde{\mathbf{a}}^{\text{rsi}}$ and \mathbf{a}^s . The received signal is modeled as a Gaussian random process⁷ with mean $\mathbf{D}_{basis,m}\mathbf{a}$ and covariance matrix \mathbf{R} given by:

$$\begin{aligned} \mathbf{R} &= \mathbb{E} \left\{ (\mathbf{H}_m^s \mathbf{s}_m^d + \mathbf{w}_m)(\mathbf{H}_m^s \mathbf{s}_m^d + \mathbf{w}_m)^H \right\} \\ &= \mathbb{E}_H \left\{ \mathbf{H}_m^s \mathbb{E}_s \{ \mathbf{s}_m^d \mathbf{s}_m^{dH} \} \mathbf{H}_m^{sH} \right\} + \mathbb{E} \{ \mathbf{w}_m \mathbf{w}_m^H \} \\ &= \alpha^2 \mathbb{E} \left\{ \mathbf{H}_m^s \mathbf{H}_m^{sH} \right\} + \sigma^2 \mathbf{I}_N, \end{aligned} \quad (3.21)$$

where $(\cdot)^H$ denotes the Hermitian transpose, α^2 and σ^2 are the variances of the intended signal and additive Gaussian thermal noise, respectively, and $\mathbb{E} \{ \mathbf{H}_m^s \mathbf{H}_m^{sH} \}$ depends on the statistical properties of the phase-noise process and the intended channel coefficients. The statistical properties of the phase-noise are determined by the oscillator type (i.e., PLL-based oscillator or a free-running oscillator [59]). According to the Gaussian model, the log-likelihood function is

⁷The Gaussian approximation is well justified for OFDM signals [58].

given by:

$$\mathcal{L}(\mathbf{a}) = -M \log |\mathbf{R}| - \sum_{m=1}^M (\mathbf{y}_m - \mathbf{D}_{basis,m} \mathbf{a})^H \mathbf{R}^{-1} (\mathbf{y}_m - \mathbf{D}_{basis,m} \mathbf{a}), \quad (3.22)$$

where M is the total number of received blocks, $|\cdot|$ returns the determinant of a matrix.

The ML estimator of \mathbf{a} is obtained by maximizing the log-likelihood function $\mathcal{L}(\cdot)$ shown in (3.22). According to its definition, \mathbf{H}_m^s depends on the intended channel and phase-noise equivalent on \mathbf{a}^s . Therefore, the dependency between \mathbf{R} and \mathbf{a} makes the direct maximization of the log-likelihood function with respect to \mathbf{a} difficult. To overcome this complexity, we ignore the relation between \mathbf{a} and \mathbf{R} and we maximize the log-likelihood function with respect to \mathbf{a} and \mathbf{R} , treated as two separate terms. In other words, the new optimization problem is split into two independent optimization problems, each with respect to only one variable, \mathbf{a} or \mathbf{R} while fixing the other. This separability is exploited to solve the problem in a low-complexity manner.

By separately considering variables \mathbf{a} and \mathbf{R} , it is possible to maximize (3.22) with respect to one variable. If the matrix \mathbf{R} is available, the vector \mathbf{a} that maximizes the log-likelihood function is given by:

$$\mathbf{a}_{ML}(\mathbf{R}) = \left(\sum_{m=1}^M \mathbf{D}_{basis,m}^H \mathbf{R}^{-1} \mathbf{D}_{basis,m} \right)^{-1} \times \sum_{m=1}^M \mathbf{D}_{basis,m}^H \mathbf{R}^{-1} \mathbf{y}_m. \quad (3.23)$$

Conversely, given \mathbf{a} , we can solve the maximization of log-likelihood function with respect to \mathbf{R} as:

$$\mathbf{R}_{ML}(\mathbf{a}) = \frac{1}{M} \sum_{m=1}^M (\mathbf{y}_m - \mathbf{D}_{basis,m} \mathbf{a})(\mathbf{y}_m - \mathbf{D}_{basis,m} \mathbf{a})^H. \quad (3.24)$$

Thus, using (3.23) and (3.24), we develop the following iterative algorithm: Given covariance matrix \mathbf{R}_{k-1} , estimate of \mathbf{a} at the k^{th} iteration is obtained by $\mathbf{a}_k = \mathbf{a}_{ML}(\mathbf{R}_{k-1})$; Then, we update the k^{th} estimate of \mathbf{R} as $\mathbf{R}_k = \mathbf{R}_{ML}(\mathbf{a}_k)$. In the proposed algorithm, \mathbf{R}_k acts as a weighting matrix that improves the performance of parameter estimation as more iterations are performed. This algorithm continues until the difference between the estimated values from two successive

iterations is considered to be negligibly small. In the absence of a prior knowledge of \mathbf{R} , we initialize the algorithm by $\mathbf{R}_0 = \mathbf{I}_N$ which gives an LS estimator of the vector coefficients at first iteration as:

$$\mathbf{a}_{LS} = \left(\sum_{m=1}^M \mathbf{D}_{basis,m}^H \mathbf{D}_{basis,m} \right)^{-1} \sum_{m=1}^M \mathbf{D}_{basis,m}^H \mathbf{y}_m. \quad (3.25)$$

In order to demonstrate the validity of this iterative algorithm, we need to show the convergence of the ML solution. Noting that the objective function is maximized with respect to one variable \mathbf{a} or \mathbf{R} while fixing the other, the value of the objective function is increased after every iteration. The proof of convergence to the global maximum of the log-likelihood function is not straightforward because the function at hand is not verified to be convex. In fact, when initializing the algorithm with $\mathbf{R}_0 = \mathbf{I}$, the algorithm returns, in the second iteration, the same channel estimate given in the closed-form solution [29] as:

$$\mathbf{h}_{ML} = \left(\sum_{m=1}^M \mathbf{D}_{basis,m}^H \tilde{\mathbf{R}}^{-1} \mathbf{D}_{basis,m} \right)^{-1} \times \sum_{m=1}^M \mathbf{D}_{basis,m}^H \tilde{\mathbf{R}}^{-1} \mathbf{y}_m, \quad (3.26)$$

where $\tilde{\mathbf{R}} = 1/M \sum_{m=1}^M \mathbf{d}_m \mathbf{d}_m^H$, and $\mathbf{d}_m = \mathbf{y}_m - \mathbf{D}_{basis,m} \mathbf{a}_{LS}$. That is, after two iterations, the algorithm operates close to the ML solution. We have:

$$\begin{aligned} \mathcal{L}(\mathbf{h}_i, \mathbf{R}_i) &= \max_{\mathbf{R}} \mathcal{L}(\mathbf{h}_i, \mathbf{R}) \\ &\geq \mathcal{L}(\mathbf{h}_i, \mathbf{R}_{i-1}) \\ &= \max_{\mathbf{h}} \mathcal{L}(\mathbf{h}, \mathbf{R}_{i-1}) \\ &\geq \mathcal{L}(\mathbf{h}_{i-1}, \mathbf{R}_{i-1}). \end{aligned} \quad (3.27)$$

Therefore, the log-likelihood function increases after each iteration, and the convergence to global maximum is fast, given a suitable initialization. The simulation results presented in Section 3.4 also confirm that, when the algorithm is initialized by $\mathbf{R}_0 = \mathbf{I}$, the iterative algorithm converges

to the ML solution after a reasonable number of iterations [29].

The computational complexity of the LS estimator comes mainly from the inversion of $\left(\sum_{m=1}^M \mathbf{D}_{basis,m}^H \mathbf{D}_{basis,m}\right)$, while compared to the LS estimator, the proposed ML algorithm needs to calculate an additional inversion of $N \times N$ matrix \mathbf{R} in each iteration [29].

3.3 Signal Model and SI-Cancellation Parameter Estimation for Time-Multiplexed Pilots Transmission

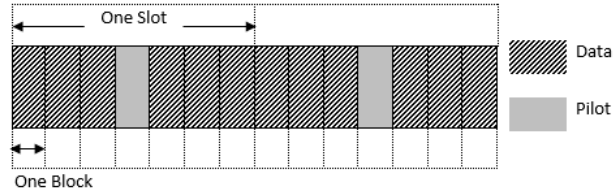


Fig. 3.1 Time-multiplexed pilots transmission.

The algorithm developed in the previous section follows the frequency-multiplexed pilots insertion, as used for the downlink from the base station to the mobile users in the LTE standard [13].

When Single Carrier FDMA (SC-FDMA) is used in LTE, the pilots are multiplexed in time domain by introducing one pilot symbol every 7 time-blocks, as shown in Fig. 3.1. Thus, the intended received signal $s(n)$ from users can contain either pilot or data time-slots. We denote by \mathcal{M}_P and \mathcal{M}_D the index sets for pilot and data time-blocks, respectively. When the received symbol in time m corresponds to a pilot symbol (i.e., $m \in \mathcal{M}_P$), the received signal can be written as:

$$\begin{aligned} \mathbf{y}_{m|m \in \mathcal{M}_P} &= \mathbf{X}_{basis,m} \mathbf{a}^{rsi} + \mathbf{X}_{IQ,basis,m} \mathbf{a}_{IQ}^{rsi} + \mathbf{X}_{PA,basis,m} \mathbf{a}_{PA}^{rsi} + \mathbf{X}_{PA,IQ,basis,m} \mathbf{a}_{PA,IQ}^{rsi} \\ &\quad + \mathbf{S}_{basis,m}^p \mathbf{a}^s + \mathbf{w}_m \\ &= \mathbf{D}_{basis,m} \mathbf{a} + \mathbf{w}_m, \end{aligned} \quad (3.28)$$

where \mathbf{a}^{rsi} , \mathbf{a}_{IQ}^{rsi} , \mathbf{a}_{PA}^{rsi} and $\mathbf{a}_{PA,IQ}^{rsi}$ are $QL \times 1$ vectors gathering all the coefficients necessary to

reduce the SI, and \mathbf{a}^s is the $QL \times 1$ vector collecting the channel coefficients of intended signal. For data-carrying symbols (i.e., $m \in \mathcal{M}_D$), the received signal is expressed in a slightly different way as:

$$\begin{aligned} \mathbf{y}_{m|m \in \mathcal{M}_D} &= \mathbf{X}_{basis,m} \mathbf{a}^{\text{rsi}} + \mathbf{X}_{IQ,basis,m} \mathbf{a}_{IQ}^{\text{rsi}} + \mathbf{X}_{PA,basis,m} \mathbf{a}_{PA}^{\text{rsi}} + \mathbf{X}_{PA,IQ,basis,m} \mathbf{a}_{PA,IQ}^{\text{rsi}} \\ &\quad + \mathbf{H}_m^s \mathbf{s}_m^d + \mathbf{w}_m \\ &= \widetilde{\mathbf{X}}_{basis,m} \widetilde{\mathbf{a}}^{\text{rsi}} + \mathbf{H}_m^s \mathbf{s}_m^d + \mathbf{w}_m. \end{aligned} \quad (3.29)$$

In what follows we describe the estimation process to find $\widetilde{\mathbf{a}}^{\text{rsi}}$.

3.3.1 LS and ML Estimators for Time-Multiplexed Pilots Transmission

The objective is to estimate the SI-channel and the transmitter impairments, and then to regenerate the SI to be subtracted from the received signal. Since the transmitted SI signal $\mathbf{D}_{basis,m}$ is known, the straightforward way is to use the LS estimator as:

$$\mathbf{a}_{LS|m \in \mathcal{M}_P} = \left(\sum_{m \in \mathcal{M}_P} \mathbf{D}_{basis,m}^H \mathbf{D}_{basis,m} \right)^{-1} \times \left(\sum_{m \in \mathcal{M}_P} \mathbf{D}_{basis,m}^H \mathbf{y}_m \right). \quad (3.30)$$

The estimate in (3.30) is based on the received symbols corresponding to pilots (i.e., $m \in \mathcal{M}_P$). Therefore, a better estimate of \mathbf{a} can be obtained if we exploit all the received signals both pilot $m \in \mathcal{M}_P$ and data symbols $m \in \mathcal{M}_D$. In the following, we propose an estimation algorithm that incorporates the intended signal both in pilot time slots and data time slots. By modeling the unknown data as Gaussian random variable, the received signal \mathbf{y}_m during the non-pilot period is a Gaussian random vector with mean $\widetilde{\mathbf{X}}_{basis,m} \widetilde{\mathbf{a}}^{\text{rsi}}$ and covariance matrix $\mathbf{R}_{\mathcal{M}_D} = \alpha^2 \mathbb{E}\{\mathbf{H}_m^s \mathbf{H}_m^s\} + \sigma^2 \mathbf{I}_N$. Furthermore, during the pilot period, the received signal \mathbf{y}_m is a Gaussian variable with mean $\mathbf{D}_{basis,m} \mathbf{a}$ and covariance matrix $\mathbf{R}_{\mathcal{M}_P} = \sigma^2 \mathbf{I}_N$. Considering the statistical properties of the received signal, the log likelihood function is given by:

$$\mathcal{L}(\widetilde{\mathbf{a}}^{\text{rsi}}, \mathbf{a}^s) = -M_d \log |\mathbf{R}_{\mathcal{M}_P}| - \sum_{m \in \mathcal{M}_P} (\mathbf{y}_m - \widetilde{\mathbf{X}}_{basis,m} \widetilde{\mathbf{a}}^{\text{rsi}} - \mathbf{S}_{basis,m}^p \mathbf{a}^s)^T \times$$

$$\begin{aligned}
 & (\mathbf{y}_m - \widetilde{\mathbf{X}}_{basis,m} \widetilde{\mathbf{a}}^{rsi} - \mathbf{S}_{basis,m}^p \mathbf{a}^s) - \\
 & \sum_{m \in \mathcal{M}_D} (\mathbf{y}_m - \widetilde{\mathbf{X}}_{basis,m} \widetilde{\mathbf{a}}^{rsi})^T \mathbf{R}_{\mathcal{M}_P}^{-1} (\mathbf{y}_m - \widetilde{\mathbf{X}}_{basis,m} \widetilde{\mathbf{a}}^{rsi}). \quad (3.31)
 \end{aligned}$$

Therefore, the ML estimates of $\widetilde{\mathbf{a}}^{rsi}$ and \mathbf{a}^s are obtained by maximizing $\mathcal{L}(\cdot, \cdot)$ in (3.31). Note that, in the above objective function, the matrix $\mathbf{R}_{\mathcal{M}_P}$ depends on \mathbf{a}^s making the direct maximization of $\mathcal{L}(\cdot, \cdot)$ intractable since it involves a multidimensional grid search. To solve the problem, we first maximize (3.31) with respect to $\widetilde{\mathbf{a}}^{rsi}$ for fixed \mathbf{a}^s and $\mathbf{R}_{\mathcal{M}_P}$. Therefore, taking the gradient of $\mathcal{L}(\cdot, \cdot)$ with respect to $\widetilde{\mathbf{a}}^{rsi}$ and setting it to zero yields:

$$\begin{aligned}
 \widehat{\mathbf{a}}_{ML}^{rsi} = & \left(\sum_{m \in \mathcal{M}_P} \widetilde{\mathbf{X}}_{basis,m}^H \widetilde{\mathbf{X}}_{basis,m} + \sum_{m \in \mathcal{M}_D} \widetilde{\mathbf{X}}_{basis,m}^H \mathbf{R}_{\mathcal{M}_P}^{-1} \widetilde{\mathbf{X}}_{basis,m} \right)^{-1} \times \\
 & \left(\sum_{m \in \mathcal{M}_P} \widetilde{\mathbf{X}}_{basis,m}^H (\mathbf{y}_m - \mathbf{S}_{basis,m}^p \mathbf{a}^s) + \sum_{m \in \mathcal{M}_D} \widetilde{\mathbf{X}}_{basis,m}^H \mathbf{R}_{\mathcal{M}_P}^{-1} \mathbf{y}_m \right). \quad (3.32)
 \end{aligned}$$

On the other hand, for fixed $\widetilde{\mathbf{a}}^{rsi}$, the covariance matrix $\mathbf{R}_{\mathcal{M}_P}$ can be estimated as:

$$\widehat{\mathbf{R}}_{\mathcal{M}_P, ML} = \frac{1}{M} \sum_{m=1}^T (\mathbf{y}_m - \widetilde{\mathbf{X}}_{basis,m} \widetilde{\mathbf{a}}^{rsi}) (\mathbf{y}_m - \widetilde{\mathbf{X}}_{basis,m} \widetilde{\mathbf{a}}^{rsi})^H. \quad (3.33)$$

and the coefficients related to the intended channel are obtained from:

$$\widehat{\mathbf{a}}_{ML}^s = \left(\sum_{m \in \mathcal{M}_P} \mathbf{S}_{basis,m}^{pH} \mathbf{S}_{basis,m}^p \right)^{-1} \times \left(\sum_{m \in \mathcal{M}_P} \mathbf{S}_{basis,m}^{pH} (\mathbf{y}_m - \widetilde{\mathbf{X}}_{basis,m} \widetilde{\mathbf{a}}^{rsi}) \right). \quad (3.34)$$

Clearly, the estimate of $\widetilde{\mathbf{a}}^{rsi}$ in (3.32) depends on \mathbf{a}^s and $\mathbf{R}_{\mathcal{M}_P}$. At the same time, the estimate of $\mathbf{R}_{\mathcal{M}_P}$ in (3.33) and \mathbf{a}^s in (3.34), depends on the value of $\widetilde{\mathbf{a}}^{rsi}$. Therefore, here we resort to an iterative procedure to find the different parameters. At the k^{th} iteration, the estimate $\widehat{\mathbf{a}}^{\widehat{rsi}, k-1}$ obtained at iteration $k-1$ is used to find $\widehat{\mathbf{R}}_{\mathcal{M}_P}^k$ and $\widehat{\mathbf{a}}^{s,k}$. Then, the estimate of $\widetilde{\mathbf{a}}^{rsi}$ is updated at iteration k using the obtained values of $\mathbf{R}_{\mathcal{M}_P}$ and \mathbf{a}^s . To initiate this procedure, we use the pilot symbols to estimate $\widetilde{\mathbf{a}}^{rsi}$ and \mathbf{a}^s as equation (3.30).

There are two differences between the ML solution in (3.32) and the LS solution in (3.30). The ML estimate is obtained by using the received signal corresponding to both pilot and data symbols, while the LS estimate only uses the received signal corresponding to pilot symbols.

The proof of convergence to the global maximum of the log-likelihood function is similar to that in the previous section.

3.4 Simulation Results

We evaluate the performance of the proposed algorithm in terms of the estimation mean square error (MSE), intended-signal-to-SI-plus-thermal-noise power ratio (SINR) and the SI-cancellation gain versus the intended-signal-to-thermal-noise power ratio (SNR). The SI-cancellation gain is defined as the power ratio of the initial SI before cancellation to the residual SI after cancellation. Also, the intended-signal-to-interference power ratio (SIR) at the output of the RF cancellation stage is assumed to be -20 dB. The wireless channels are represented by a multipath Rayleigh fading model with $L = 7$ paths and an average path gain vector $[0, -1, -5, -10, -8, -15, -25]$ dB for the intended channel and $[20, 19, 15, 10, 12, 5, -5]$ dB for the SI channel corresponding to SIR of -20 dB.

There are two widely used oscillator types: free-running and phase-locked loop (PLL) based oscillators. Phase-noise in a free-running oscillator can be modeled as a Wiener process [59]. In a PLL-based oscillator, phase-noise is controlled by the feed-back loop and can be modeled as an Ornstein Uhlenbeck process [60]. In the following, we consider free-running oscillators in use, and the corresponding Wiener phase-noise at the n^{th} sample is related to the previous sample as: $\phi(n) = \phi(n-1) + \beta$, where β is a Gaussian random process with zero mean and variance $\sigma^2 = 4\pi f_{3dB} T_s$. T_s denotes the sample interval and f_{3dB} is the 3 dB bandwidth of the phase-noise Lorentzian spectrum [59], indicating the quality of the oscillator (i.e., large f_{3dB} corresponding to large phase-noise). In the following numerical results, we set $\sigma^2 = 0.001$, $f_{3dB} = 100$ Hz.

In the simulation, we use MATLAB to implement the various blocks shown in Fig.2.6. The generated OFDM signals cover both frequency-multiplexed pilots and time-multiplexed pilots. The non-linear PA polynomial model coefficients are derived from our SimRF amplifier operating at 2.08896 GHz in SIMULINK, as $\alpha_1 = 10$, $\alpha_3 = -0.2$, $\alpha_5 = 2.95 \times 10^{-4}$, $\alpha_7 = -1.14 \times 10^{-7}$. Based on these coefficients, we calculate the power gain $G = 20\log_{10}(\alpha_1) = 20$ dB, output third-order intercept point $OIP3 = 10\log_{10}\frac{\alpha_1^3}{|\alpha_3|} + 14.26 = 51.24$ dBm, and the output 1dB-

compression point as $P_{1dB} = OIP3 - 10.6 = 40.64$ dBm. The effects of the IQ-imbalance are modeled by introducing an image signal to the actual transmit signal with a signal-to-image power ratio of 40 dB, where $g_1=1$ and $g_2=0.0029 - 0.013i$. The thermal noise is modeled as a white Gaussian component added to the received signal and SI at the receiver input, after which its power is increased according to the receiver component gains and noise figures.

3.4.1 Performance Evaluation with Separate- and Common-Oscillator Structures

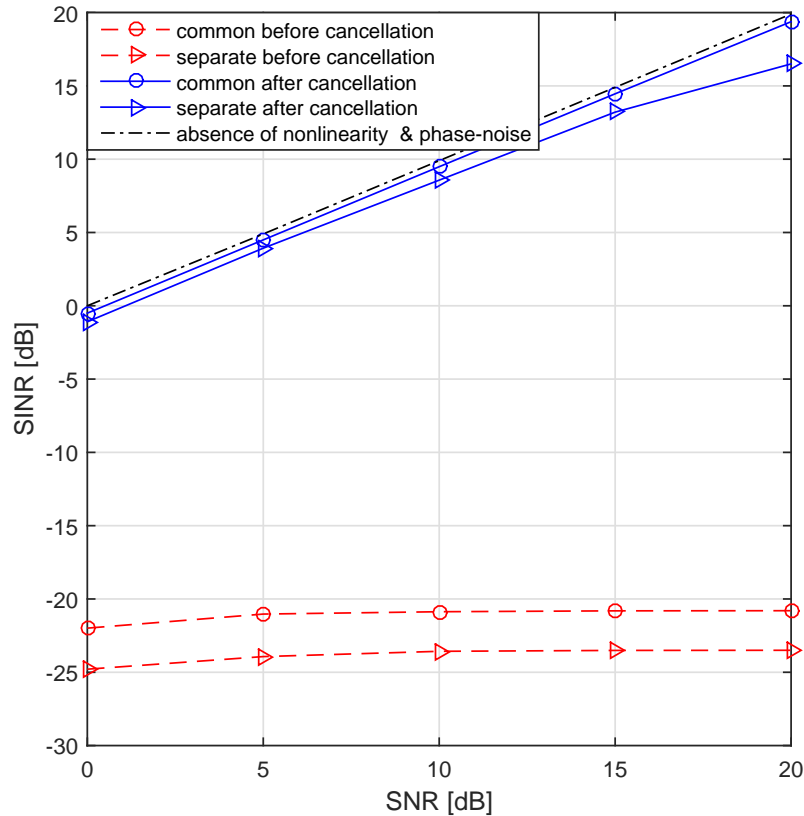


Fig. 3.2 SINR before and after baseband SI-cancellation versus SNR in separate-oscillator and common-oscillator cases.

In this section, we compare the effect of phase-noise introduced by two oscillator structures, where nonlinearity is not included. When using a common oscillator, the phase-noise is partially compensated by the oscillator on the receiver's side, making the effects of the phase-noise lower than using two separate oscillators, where the transmit and receive SI signals are affected by

two independent phase-noise realizations [20]. Fig. 3.2 compares the SINR's before and after baseband SI-cancellation for the: separate- and common-oscillator scenarios. The plots indicate a large SINR gap of about 2.7 dB between the separate- and common-oscillator cases, before baseband SI-cancellation. In the common-oscillator case, part of the up-conversion phase-noise $\phi^{\text{up}}(n)$ can be compensated for in down-conversion phase-noise $\phi^{\text{down}}(n)$, resulting in less phase-noise, and hence less SI. The baseband SI-cancellation stage effectively reduces the SI as shown in Fig. 3.2.

After baseband SI-cancellation, the SINR in the common-oscillator case is almost equal to the SNR, and the SINR gap between the common- and separate-oscillator cases is reduced to less than 1 dB for $\text{SNR} < 5$ dB. However, with increasing SNR, this SINR gap is increased. At $\text{SNR} = 20$ dB, the SINR gap is about 2.7 dB, similar to the SINR gap before baseband SI-cancellation.

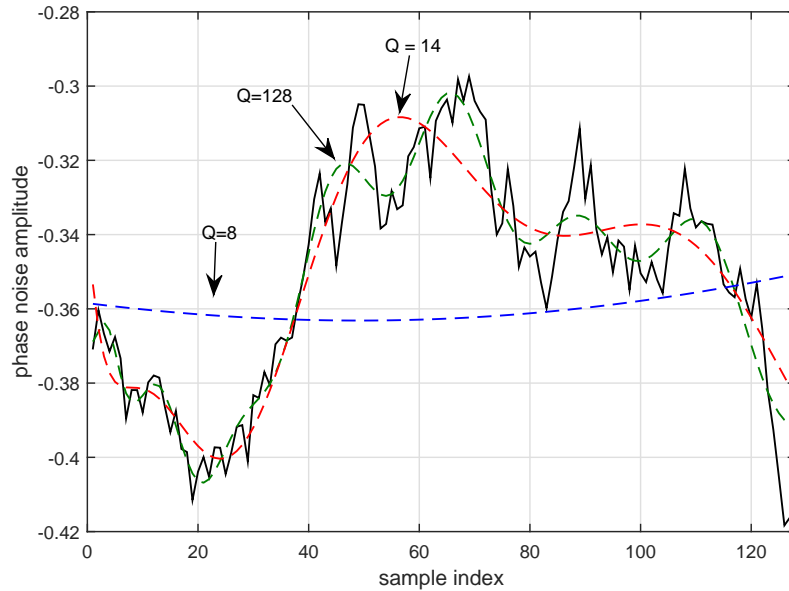


Fig. 3.3 Phase-noise in the *separate* oscillator case (solid line) and its approximations (dashed lines) using different basis expansion order Q .

In a multipath channel, each resolvable path has a different delay, resulting in different global phase-noise $\phi = \phi^{\text{up}}(n - l) - \phi^{\text{down}}(n)$. Figs. 3.3 and 3.4 plot the phase-noise samples, along with BEM approximations, of one channel path for separate and common oscillators, respectively. Higher expansion orders result in a better approximation of the phase-noise, as shown in Fig. 3.3 and Fig. 3.4, but at the cost of increasing the number of parameters to estimate (i.e., the size of \mathbf{a} is related to Q as $5QL$). The problem is identifiable when the number of samples considered

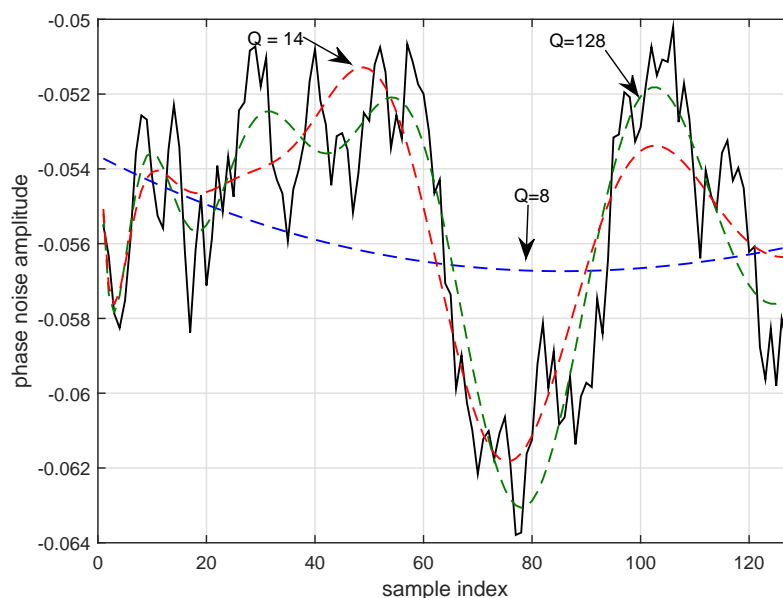


Fig. 3.4 Phase-noise in the *common* oscillator case (solid line) and its approximations (dashed lines) using different basis expansion order Q .

for the estimation is larger than the number of parameters (i.e., the order of basis should satisfy $5QL \leq N$). In the simulation, we choose $Q = \lfloor N/(5L) \rfloor = 14$.

3.4.2 Performance of Frequency-Multiplexed and Time-Multiplexed Pilot Transmission

For the frequency-multiplexed pilots, we consider an OFDM system with $N = 512$ subcarriers, using 4QAM and a cyclic prefix of $N_{cp} = 16$. The number of observed OFDM blocks is set to be $T = 140$ in all simulations. The pilot symbols are inserted periodically in some subcarriers before the IFFT operation. Fig. 3.5 plots the channel MSE versus the SNR for different numbers of iterations in the case of frequency-multiplexed pilots. From the plot, it can be seen that 5 iterations are sufficient to obtain a good performance.

We also evaluate the performance of the proposed algorithm in the case of time-multiplexed pilots, in a SC-FDMA system with $N = 512$ data subcarriers, using 4QAM and a cyclic prefix of $N_{cp} = 16$. The number of observed SC-FDMA blocks is $T = 140$. The pilot symbols are inserted periodically in the fourth block of every slot. For reference, we also evaluate the performance of the algorithm proposed in [23], under the same conditions. The approach proposed in [23] consists of the following two steps: First, it assumes no phase-noise and estimates the SI-channel

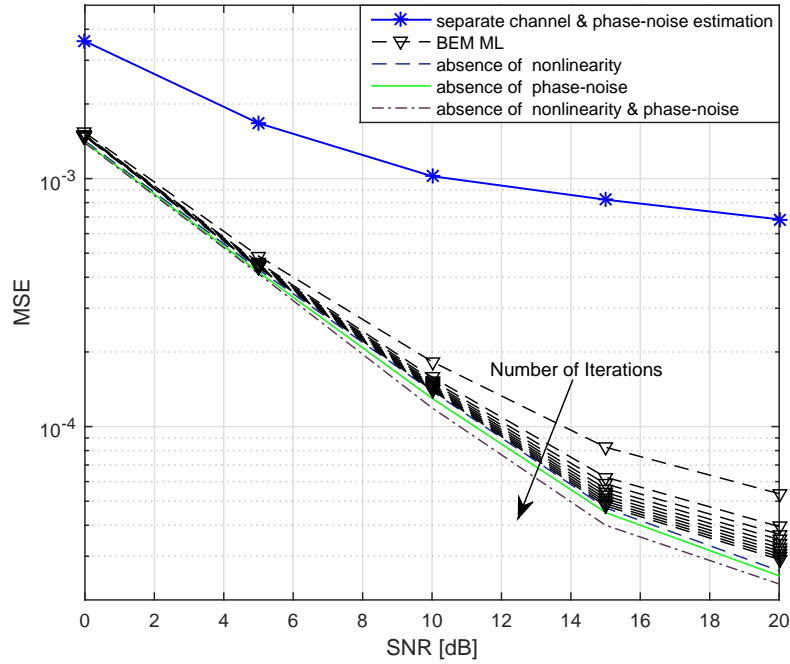


Fig. 3.5 SI-channel MSE versus SNR in different numbers of iterations.

using the LS criterion; Then, with the estimated SI-channel, it estimates the phase-noise using the MMSE criterion. This method suffers from two kinds of estimation errors: Channel estimation error when estimating the phase-noise, and errors from the unknown intended signal, which is treated as additive noise.

Regarding the computational complexity, the complexity of the proposed algorithm is mainly related to the calculation of matrix inversion of the $N \times N$ matrix \mathbf{R} at each iteration. This inversion sets the complexity of such technique to $O(N^2)$. In addition to matrix inversion, the SI signal is reconstructed using an $O(N)$ multiplication process. The main complexity of the algorithm proposed in [23] comes from the calculation of an $N \times N$ weighting matrix that involves matrix inversion with complexity order of $O(N^2)$. Reconstructing the SI signal involves a multiplication process of order $O(N)$. In addition, the MMSE estimation requires an inverse discrete Fourier transform (IDFT) process to with complexity order of $O(N \log_2 N)$.

Fig. 3.6 plots the MSE of the SI-channel estimation as a function of SNR, with the performance of the algorithm proposed in [23] (labeled as “separate channel and phase-noise estimation” in Fig. 3.6). For simplicity, we just compute and compare the SI-channel corresponding to the direct component of the SI signal h^i . For both frequency- and time-multiplexed pilots,

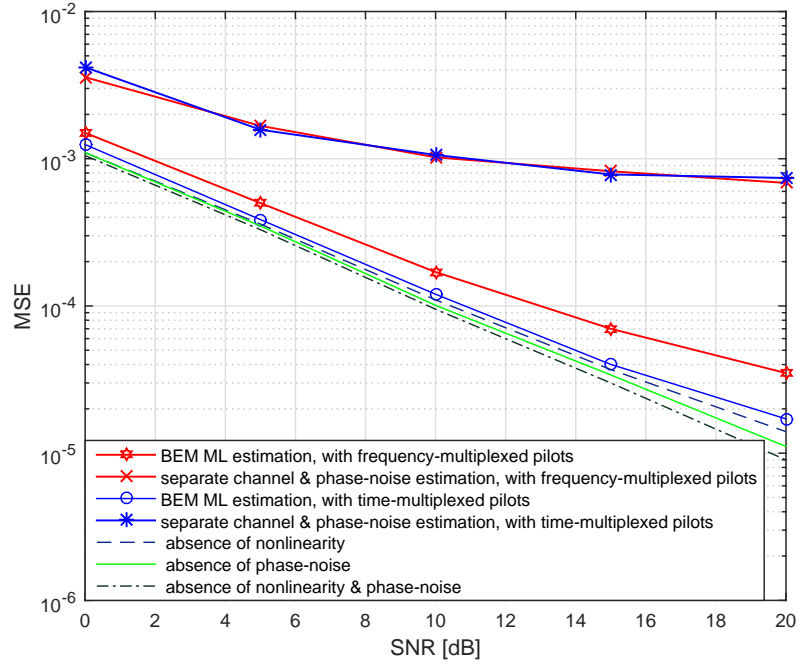


Fig. 3.6 SI-channel estimation MSE versus input SNR.

the simulation results indicate that the performance of [23] saturates at high SNR because it is affected by both phase-noise and additive Gaussian noise. Moreover, at high SNR, even if the phase-noise is suppressed, the transmitter nonlinearity considerably increases the noise floor, limiting the estimation performance and resulting in a large residual SI. Thus, the suppression of the transmitter nonlinearity in our algorithm improves the performance significantly.

Fig. 3.7 shows the relationship between the SINR after cancellation and the SNR in presence of the phase-noise in the separate-oscillator case, for both the frequency-multiplexed and time-multiplexed pilots. In general, the SINR is always smaller than the SNR due to the non-zero residual SI after cancellation. Without phase-noise, the resulting SINR is almost the same as the operating SNR. It can be seen that larger phase-noise induces higher residual SI and hence larger degradation in cancellation performance (i.e., lower SINR). With phase-noise, the proposed algorithm closely approaches the SINR performance in the case of no phase-noise (< 0.5 dB for $\text{SNR} \leq 10$ dB, < 1 dB for $\text{SNR} \leq 20$ dB), and outperforms the algorithm in [23], more noticeable at high SNR > 10 dB when the resulting SINR of the algorithm in [23], becomes saturated at around 12 dB. In all cases, the frequency-multiplexed pilots provide better SINR performance than the time-multiplexed pilots.

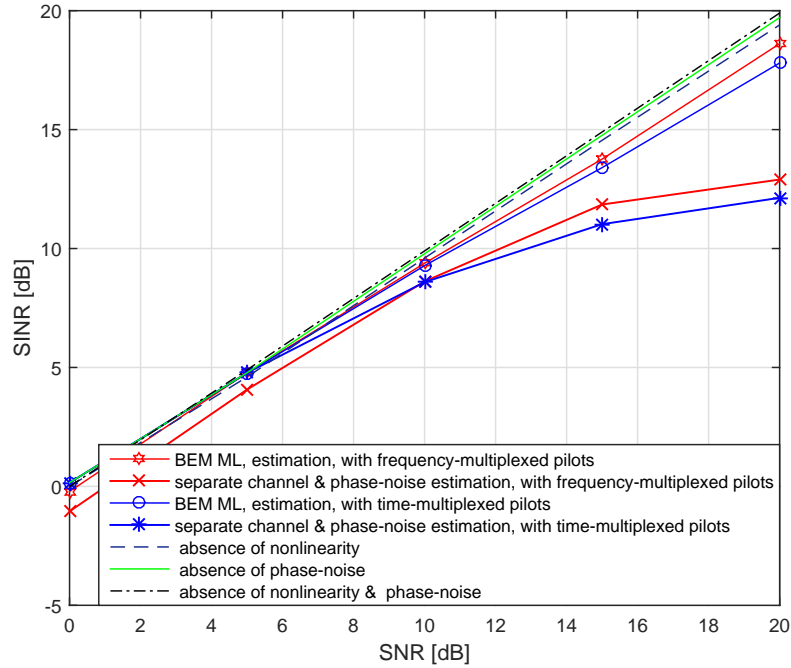


Fig. 3.7 Output SINR versus input SNR after cancellation.

We consider a typical case when the average power of the SI (before cancellation) is about 70 dB to 90 dB higher than that of the intended signal. Results in [36, 41] indicate an antenna SI isolation of more than 30 dB plus a RF SI-cancellation of about 20 dB, so that the SI-to-intended-signal power ratio (ISR) after the RF SI-cancellation stage (at the LNA input in Fig. 2.6) is about 20 dB ($= 70 \text{ dB} - 30 \text{ dB} - 20 \text{ dB}$) to 40 dB ($= 90 \text{ dB} - 30 \text{ dB} - 20 \text{ dB}$). The baseband SI-cancellation stage offers further reduction/suppression of the residual SI, which can be expressed as SI-cancellation gain (in dB). Fig. 3.8 plots the SI-cancellation gain versus the SNR achieved by the proposed algorithm and the algorithm of [23] for $\text{ISR} = 20 \text{ dB}$ and 40 dB . For the frequency-multiplexed pilots, the results shows that the proposed BEM-ML algorithm outperforms that of [23] by 3 dB when $\text{ISR} = 20 \text{ dB}$ and 6 dB when $\text{ISR} = 40 \text{ dB}$. The results for the time-multiplexed pilots show that the performance difference of two algorithms is not obvious at low SNR, but becomes clearer at high SNR. At $\text{SNR} = 20 \text{ dB}$ the proposed BEM-ML algorithm outperforms that of [23] by 8 dB in both cases.

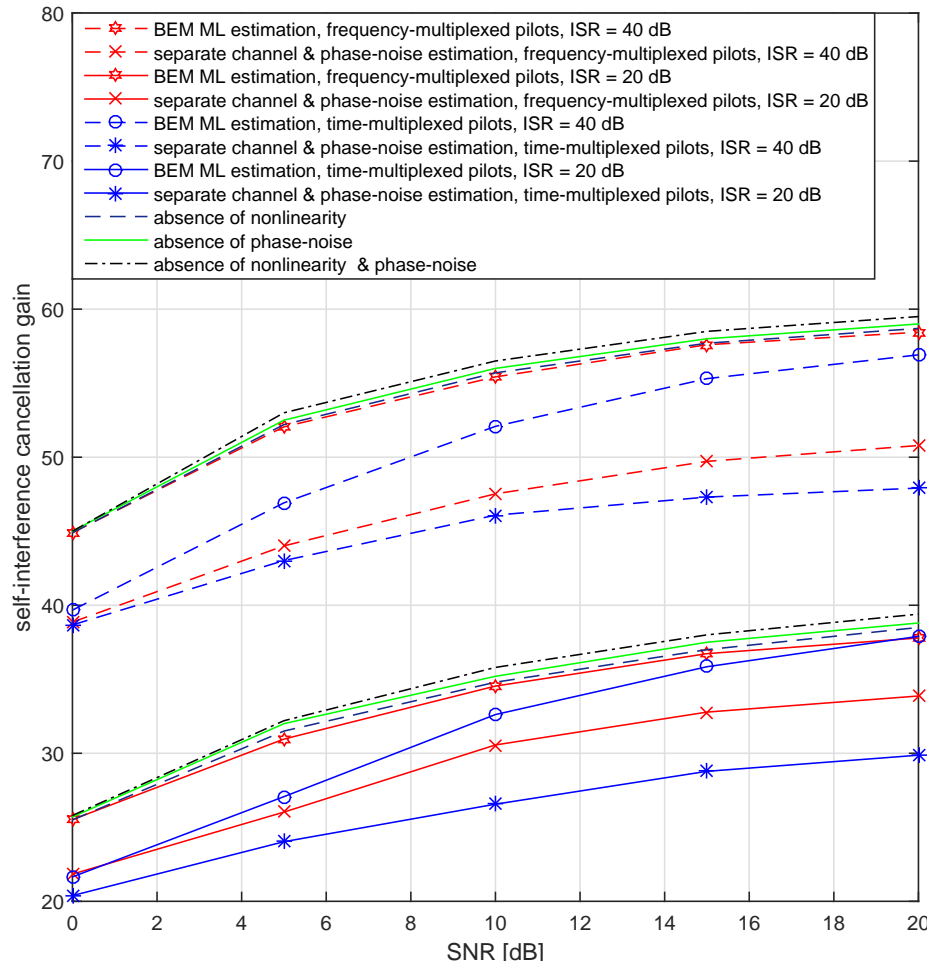


Fig. 3.8 SI-cancellation gain versus input SNR after cancellation.

3.5 Chapter Summary

In this chapter, a phase-noise and nonlinearity mitigation scheme has been proposed to reduce the SI in FD systems. The BEM is adopted to transform the problem of estimating the time-varying phase-noise to the estimation of a set of time-invariant coefficients. Then, an ML scheme is developed to find the BEM coefficients. Incorporating the intended signal into the estimation process represents the main advantage of the proposed method. By exploiting the pilot symbols and second-order statistics of the unknown intended signal, the proposed method incorporates the unknown intended signal in an iterative process by jointly both estimating the SI and intended-signal channels. For time-multiplexed pilot transmission, we combined the LS and the ML schemes. First, the LS algorithm is used to exploit the pilot symbols and to jointly estimate the SI and intended-signal channels. Then, the ML algorithm is applied to exploit second-order statistics of the unknown intended data signal and incorporates the unknown intended signal in an iterative process. Simulation results are presented and confirm the superior performance of the proposed algorithm in achieving SI-cancellation.

Chapter 4

SI-Cancellation Performance and Limiting Factors

4.1 Overview of Simulink FD Communications System Platform

In this chapter, we study the SI-cancellation performance and its characteristics in different scenarios through simulation using experimental results.

We first implement an FD communication system using 20 MHz OFDM centered at 2.27 GHz with 30 dBm. This OFDM signal has 12 dB peak-to-average power ratio (PAPR), similar to LTE signals. Fig. 4.1 depicts the top level block diagram of the implemented FD communication system platform. The signal was generated by waveform simulator implemented in Simulink with 3/4 channel coding and 16-QAM modulation. The signal goes through a DAC, where quantization noise is introduced, before being sent through a PA, which amplifies its power to 30 dBm. The PA introduces nonlinear distortion as well as adding some output noise. For the SI channel with an analog SI-cancellation stage (S1), both measured and theoretical SI channels are used in the Matlab Simulink Platform. An LNA is used at the receiver. One active RF SI-cancellation stage (S2) is applied before LNA. Moreover, to incorporate the effect of quantization noise into the simulations, the ADC is modeled explicitly as a uniform quantization process. The imple-

mentation of the baseband SI-cancellation stage (S3) follows directly after the ADC. The effect of thermal noise is realized by fixed noise power. For example, in our platform the thermal noise power spectral density is -174 dBm/Hz while the SNR is 20 dB.

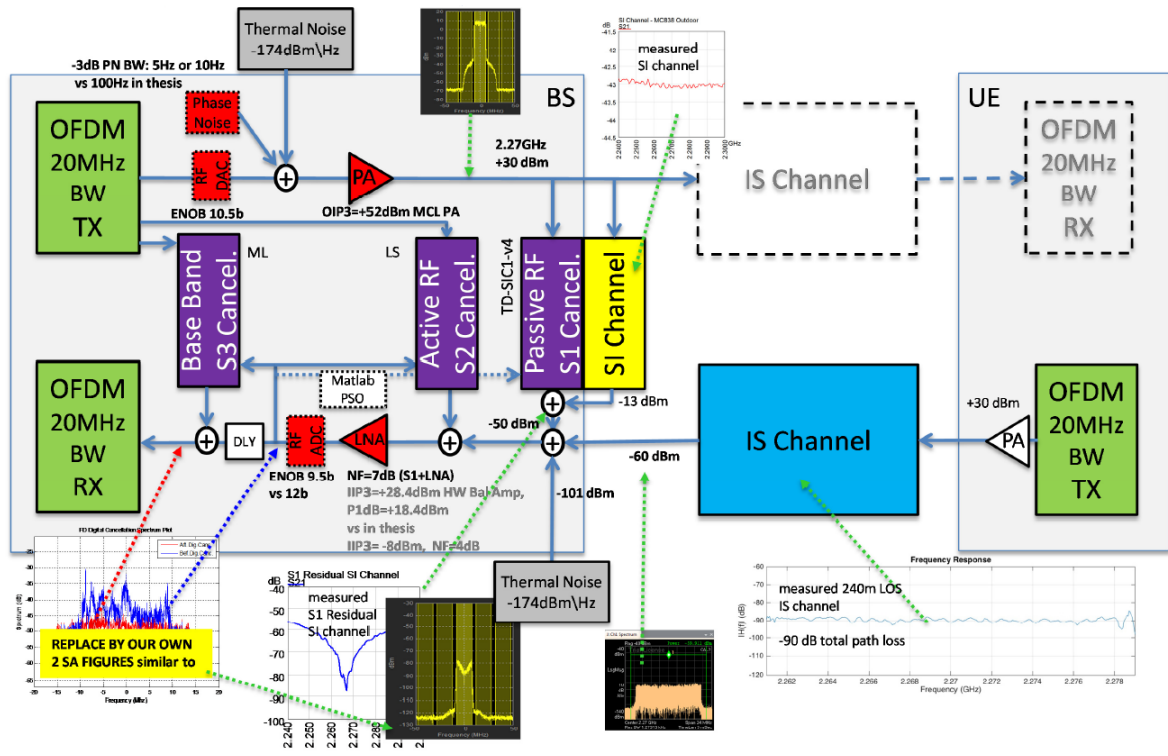


Fig. 4.1 Top Level Block Diagram of Simulink FD Communications System Platform.

For the analog SI-cancellation stage, we apply the method in [49]. The SI channel could be split into two sections, namely internal SI channel and external SI channel. The internal SI channel is due to the intrinsic characteristics of antenna structures, which are independent of environment. However, the external SI channels are related to the dynamic reflections of the environment. The purpose of analog cancellation is three-fold: suppressing the internal reflection, preventing receiver saturation, and minimizing the quantization noise. For a 20 MHz OFDM signal with transmitted power of 30 dBm, in order to keep the degradation of the effective SNR of the intended signal within 0.4 dB, the co-channel nonlinear distortion power generated by analog cancellation must be at least 10 dB lower than the thermal noise floor. This requires the IIP3 of analog cancellation to be higher than 78 dBm. The prototype analog cancellation with 2 taps was measured and characterized using a 20MHz OFDM signal centered at 2.27 GHz with

30 dBm signal. In an outdoor environment, analog cancellation combined with custom dual-polarized antenna separation of approximately 50 dB suppression would provide 80 – 90 dB cancellation for an FD system. In an indoor environment, due to the rich multipath effects, the analog cancellation improves to be about 17 dB cancellation over 48 dB antenna suppression, yielding 65 dB of cancellation in total. The signal after analog cancellation was captured and fed into a digital cancellation simulation platform. In our simulation, we implemented the analog SI-cancellation stage, while taking into account measurements from actual indoor and outdoor SI channels.

To avoid overloading or saturation of these components, a radio frequency SI-cancellation stage is introduced prior to the LNA and ADC to suppress the SI to a level sufficiently low. As previously discussed, the major task in the RF SI-cancellation stage is to estimate the SI channel vector. The initial SI channel estimate is obtained during the short HD period at the start of the RF SI-cancellation stage, also called the estimation period of S2. Since the transmitted SI signal is known, it is straightforward to use the least-square method for estimation. After the SI channel is estimated, the simulation moves to the cancellation period of S2, which lies in the FD period of the RF cancellation, where the SI is suppressed.

RF cancellation attenuates only the direct coupling component of the SI channel. Therefore, to suppress the residual SI and RF impairments, a baseband SI-cancellation stage is introduced after the ADC. During FD operations, detection of the intended signal requires the knowledge of the channel between the two transceivers. An ML algorithm is implemented in baseband cancellation to jointly estimate the residual SI channel with transmitter nonlinearity and the intended channel, based on the known transmitted symbols from its own transmitter as well as the known pilot symbols from the other intended transmitter. Here, the RF impairments include PA and LNA nonlinearities. An iterative algorithm is implemented to improve the estimation performance.

4.2 Simulation of FD Communication System

Following a typical direct conversion architecture [61–63], the structures of the transceivers being analyzed are given in Fig. 4.2. The calculations are mostly dedicated to identifying the limiting factors of the SI-cancellation performance. One significant component of SI-cancellation is the reference signal for the RF and the baseband SI-cancellation stages [10]. In the simulation, we apply these two commonly used architectures and analyze the SI-cancellation performance of

each architecture. In the first one, the reference signals are directly taken from the transmitter baseband for both RF and baseband stages, where an auxiliary transmitter chain is required to convert the baseband signal to RF [10]. The second architecture takes the reference signals from the output of the PA. As a result, an additional receive chain is needed to obtain the reference signal for baseband stage [10].

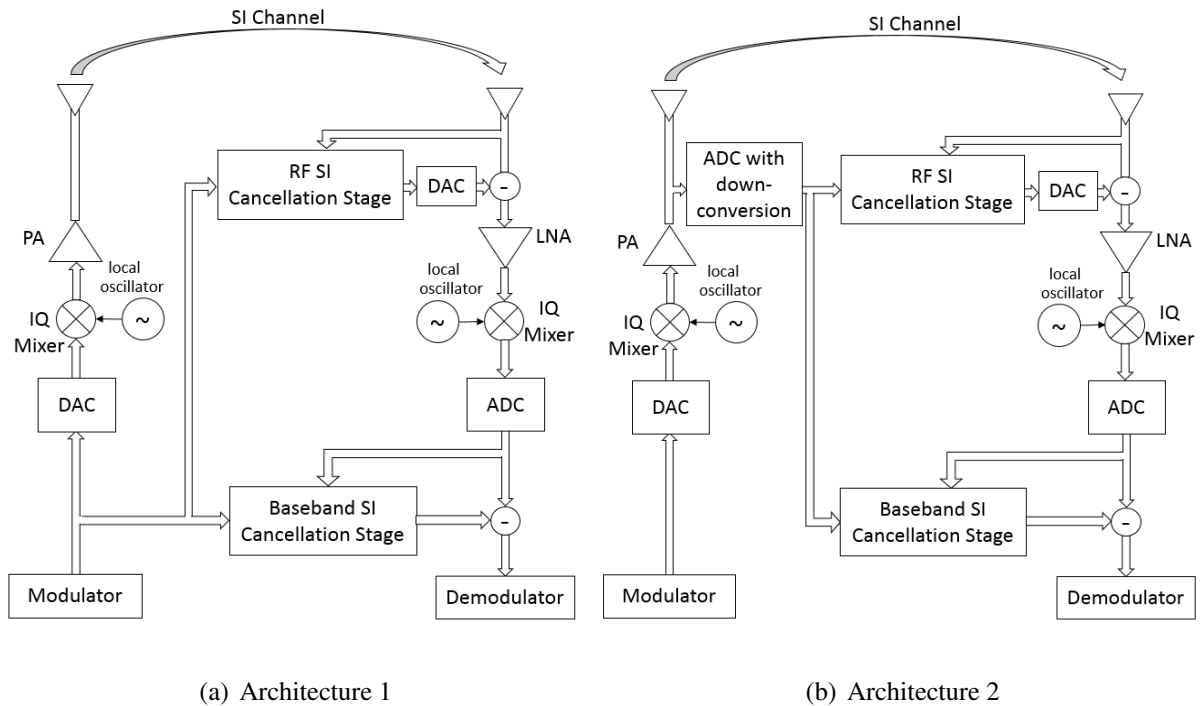


Fig. 4.2 Simplified block diagram of the FD transceivers with RF and baseband SI-cancellation stages.

In the first architecture, distortion caused by the transmitter cannot be suppressed by the RF cancellation, and it increases the quantization noise. However, baseband cancellation can reduce the PA-induced nonlinearity. In the second architecture, the distortion is reduced by the RF cancellation since it has already been included in the reference signal. But the additional transmitter reference ADC increases the quantization noise.

4.2.1 Limiting Factors in SI-Cancellation

To reduce the SI in an FD system, successive cancellation stages are needed to properly detect the intended signal due to its large power. In general, it is difficult to give an accurate estimate of the obtainable SI reduction because of the interactions among many factors such as transceiver impairments, wireless propagation channel, estimation error and so on. In the following, we briefly discuss the impact of the transceiver impairments in FD systems that limit the cancellation of SI.

Quantization Noise

There are two quantization noise sources, one from the finite-resolution DAC, and the other from the ADC [64]. Since the amount of the SI-cancellation performed in the digital domain is very large, in order to avoid the low resolution of the weak intended signal, an additional dynamic range is required in the interfaces of ADC and DAC, otherwise, the low resolution limits the overall performance of the transceiver [16].

The uniform ADCs with equidistant quantization levels at 2^b are mostly used in communications systems, where b is the number of bits of the ADC. Assuming that the level of the output signal from the ADC is limited between $+1$ and -1 , the quantization function under these conditions is [64, 65]:

$$Q(x) = \begin{cases} -1, & \text{if } x \leq \frac{2-2^b}{2^b-1}, \\ 2\frac{q-1}{2^b-1} - 1, & \text{if } \frac{2q-2-2^b}{2^b-1} < x \leq \frac{2q-2^b}{2^b-1}, q = 2, \dots, 2^b - 1, \\ 1, & \text{if } x \geq \frac{2^b-2}{2^b-1}. \end{cases} \quad (4.1)$$

In practice, as the receiver automatic gain control (AGC) with adjustable gain g_{AGC} keeps the total ADC input level within the fixed scale of the quantization block $Q(\cdot)$. In our development, we make sure that the AGC operates optimally to minimize the the quantization noise.

Let us assume the transmission of OFDM signals, which are very close to Gaussian by the central limit theorem when the number of subcarriers is large [66]. Therefore, the classical formula of signal-to-quantization noise ratio is $\rho = 6.02b + 1.76dB$, assuming a sinusoidal input signal is no longer valid. f_s is the sampling rate of signal before quantization. The resulting sam-

ples are denoted by $y(n)$. Using the Bussgang's theorem [67] for nonlinear memoryless systems, the output of the ADC is the sum of the input attenuation version and the statistical independent Gaussian term. Thus the input-output relation of the ADC is given by [64]:

$$y_{ADC}(n) = \alpha\sqrt{g_{AGC}}y(n) + \omega_{AGC}(n), \quad (4.2)$$

where $\omega_{ADC}(n)$ is the clipping-plus-quantization noise uncorrelated with the input $y(n)$ and α is the attenuation given as follows [64]:

$$\alpha = \sqrt{g_{AGC}} \frac{\mathbb{E}\{y(n) * y_{ADC}(n)\}}{\mathbb{E}\{|y(n)|^2\}}. \quad (4.3)$$

The power of $\omega_{ADC}(n)$ is obtained by rearranging the terms in (4.2) as:

$$P_{ADC} = \mathbb{E}\{|y_{ADC}(n)|^2\} - \alpha^2 g_{AGC} \mathbb{E}\{|y(n)|^2\}. \quad (4.4)$$

The various expectations in (4.3) and (4.5) can be easily calculated given that the input signal follows a Gaussian distribution:

$$\begin{aligned} \mathbb{E}\{|y_{ADC}(n)|^2\} &= \int_{-\infty}^{\infty} Q^2(x) f(x, gP_{in}) dx, \\ \mathbb{E}\{y(n) \times y_{ADC}(n)\} &= \int_{-\infty}^{\infty} \frac{xQ(x)}{\sqrt{g_{AGC}}} f(x, gP_{in}) dx. \end{aligned} \quad (4.5)$$

where P_{in} is the power of the input signal of the ADC and $f(x, \sigma_x^2)$ is the probability distribution function of a Gaussian random variable x with zero mean and σ_x^2 variance [64].

Nonlinearity

While it is relatively easy to reduce the linear part of the SI, reducing the different nonlinearity impairments from the transmitter and receiver chains is more challenging. Analog SI-cancellation nonlinearity, PA nonlinearity and LNA nonlinearity are recognized as the dominant nonlineari-

ties.

Nonlinearity of analog SI-cancellation is introduced by the process of S1. The power of co-channel nonlinear distortion (P_{CC}), which occurs due to the analog SI-cancellation, limits the cancellation performance of entire FD system. In order to avoid a significant fall in SNR, P_{CC} should be kept below the noise floor at the receiver by a certain amount. The limiting factors of overall cancellation are co-channel nonlinearity, signal bandwidth and noise figure of the receiver [68]. Hence, the total achievable cancellation P_{TC} at the receiver is presented as follows [68]:

$$P_{TC} = P_{Tx} - (-174 + 10\log_{10}B_w + P_{TNF} + P_{CC}), \quad (4.6)$$

where P_{Tx} is the transmitted power, P_{TNF} is the noise figure of the receiver with analog SI-Cancellation, B_w is the signal bandwidth [69].

To prevent a degradation exceeding 0.4 dB to the intended signal's effective SNR, the in-band P_{CC} should be 10 dB lower than the noise floor at receiver ($-174 + 10\log_{10}B_w - 10 + P_{tnf}$) [68]. The relation between P_{CC} and two tone third-order Inter-Modulation Distortion components (IMD3) is provided by [69]:

$$\begin{aligned} P_{CC} &= 10\log_{10}\left(\frac{64}{3}P_{IMD_3}\right) \\ &= P_{IMD_3} + 13.3, \end{aligned} \quad (4.7)$$

where P_{IMD_3} is the power of IMD3. By equation 4.7, we can transform the requirement of co-channel nonlinear distortion into that of IMD3, which is frequently used in measuring system nonlinearity [68].

In addition, the third-order intercept point (OIP3) of analog SI-Cancellation with 10 dB P_{CC} margin is given by [68]:

$$P_{OIP_3} = \frac{2}{3}(P_{Tx} - P_{AS}) - \frac{1}{2}(-174 + 10\log_{10}B_w - 10 - 13.4 + P_{TNF}) \quad (4.8)$$

where P_{AS} is the cancellation power of antenna suppression.

As mentioned in the previous section, PA nonlinearity can be modeled with a Hammerstein nonlinearity.

The low noise amplifier (LNA) is an important component of RF receiver. The distortion performance of LAN is its significant properties [70], typically specified in terms of IIP2 and IIP3.

The k_{th} order nonlinearity produced by transmit PA and receive LNA is presented as [61]:

$$p_{k,nl} = \frac{p_{in}^k g}{p_{iipk}^{k-1}}, \quad (4.9)$$

where g is the linear gain of the component, p_{in} is the power of the input signal and p_{iipk} is the k^{th} order input reference intercept point.

Transceiver Noise

The thermal noise represented by the additive Gaussian noise is inherent in the transceiver circuits, and it is usually characterized by the noise factor. Considering the multiple stages in Fig. 4.2, the receiver's output noise power is

$$p_{noise,Rx} = kT_0 F_{Rx} B_w (g_{LNA}), \quad (4.10)$$

where g_{LNA} is the power gain of the LNA, B_w is the bandwidth of the signal, $kT_0 = 10^{-174/10}$ mW/Hz is the thermal noise power spectral density, and F_{Rx} is the overall noise factor of the receiver. By Friis' formula, F_{Rx} can be derived from F_{LNA} and F_{AGC} , which refer to the individual noise factors of LNA and AGC respectively, as

$$F_{Rx} = F_{LNA} + \frac{F_{AGC} - 1}{g_{LNA}}. \quad (4.11)$$

Noise emission from the transmitter to its own receiver also affects the performance of FD systems. While being partially suppressed in the second architecture, the noise remains unchecked in the first one, it still has to be derived. Let $F_{Tx} = F_{PA} - 1$ be the noise factor of the transmitter

chain, its noise emission, $p_{noise,Tx}$, is then given by [10]:

$$p_{noise,Tx} = kT_0 F_{Tx} B_w g_{PA}, \quad (4.12)$$

where g_{PA} is the gain of the PA. In the previous expression, it is assumed that compared to the noise generated by the PA, the noise generated by other devices (such as low-pass and band-pass filters) is negligible.

4.2.2 Performance of The First Architecture

In the first architecture, the estimate by RF and baseband SI-cancellation stages take the reference signals from the transmitter baseband, therefore an auxiliary transmitter chain is required to convert the baseband signal to RF [10].

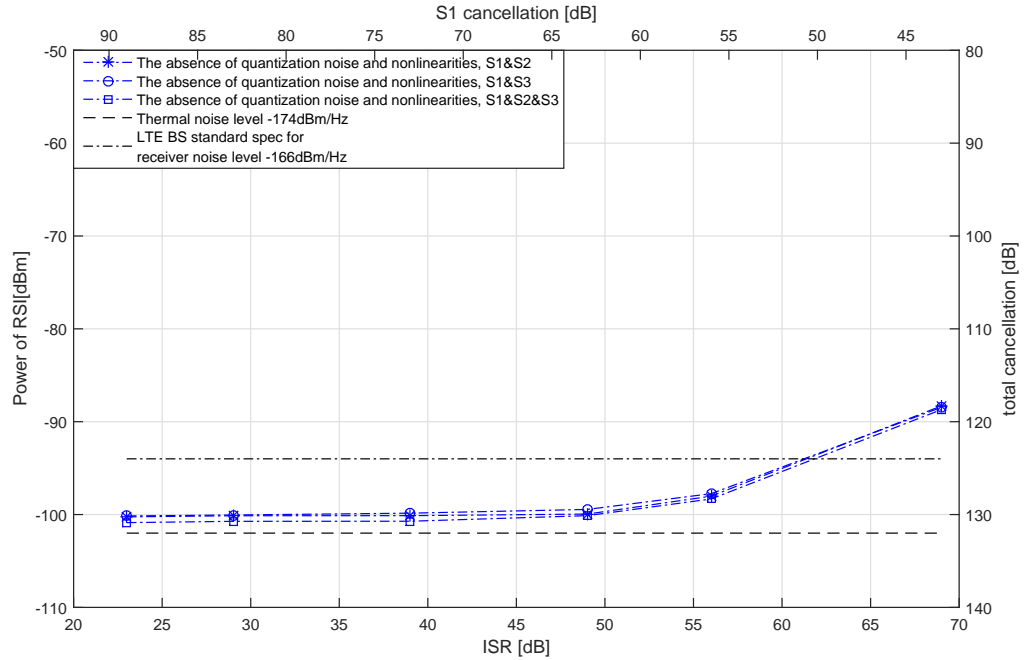


Fig. 4.3 Cancellation performance in the absence of quantization noise and nonlinearities in architecture 1.

Quantization Effect

As shown in Fig. 4.2 (a), quantization noise is introduced by one ADC and two DACs. In the transmitter chain, a DAC is added before up-converting signal from baseband to RF band, in which signals having a few defined (digital) levels are converted into ones having a theoretically infinite number of (analog) levels that result in some distortion. In the output of S2 cancellation, an additional DAC and an up-converting radio chain for generating the RF signal are needed. The additional components slightly change the generated SI leading to residual SI, thereby introducing a part of quantization bits noise. Moreover, an ADC is required in the receiver chain. Actually, the ADC is preceded by AGC with adjustable gain. As a result, the strong SI in the received signal significantly reduces the amount of bits that can be used for intended signal. In the following figures, we show the quantization effects of each of these components.

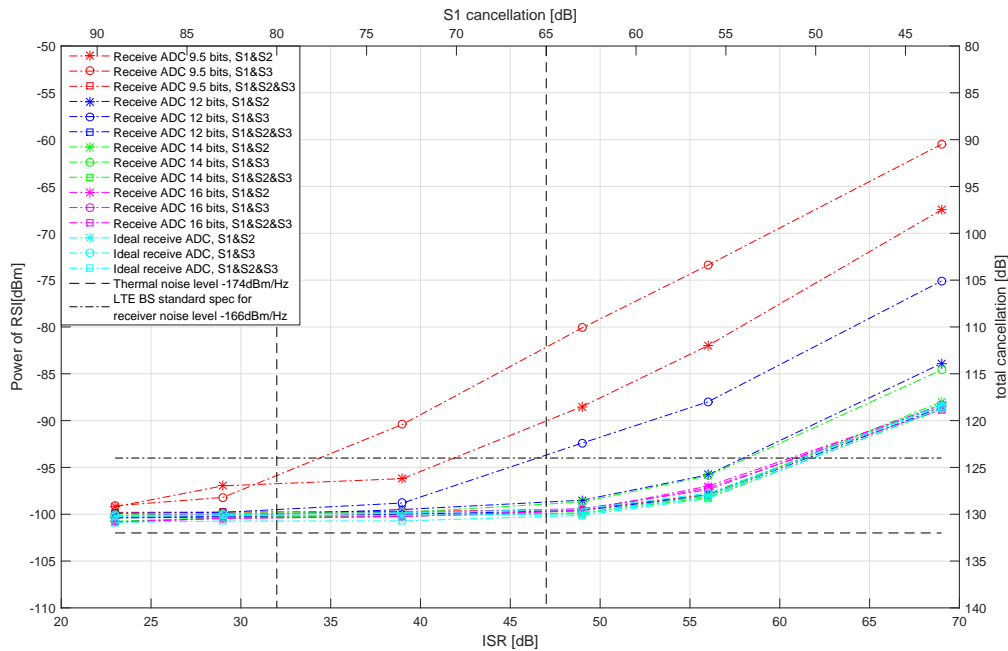


Fig. 4.4 Receive ADC resolution effect in architecture 1.

To better illustrate the quantization effects of ADC in the receiver, Fig. 4.4 plots the cancellation performance with various resolutions of ADC. It is clear that the quantization noise introduced by ADC in the receiver greatly limits the cancellation ability of our system, especially when the ADC resolution is low (i.e., 9.5 bits). When we increase the resolution, the power of

residual SI decreases quickly. Baseband SI-cancellation stage is more sensitive to receiver ADC compared with RF SI-cancellation stage, particularly with high ISR. This is due to the fact that without RF SI-cancellation stage the high residual SI passes the ADC and leads to large amount of quantization, which becomes the dominant noise and makes baseband SI-cancellation stage unable to estimate the SI channel accurately. Thus the ability of cancellation in the system is weakened. According to Fig. 4.4 we can see that even when the quantization noise is sufficiently low, the power of residual SI still increases with ISR of the receiver. In this situation, noise figure of PA and LNA become the main limiting factor of cancellation.

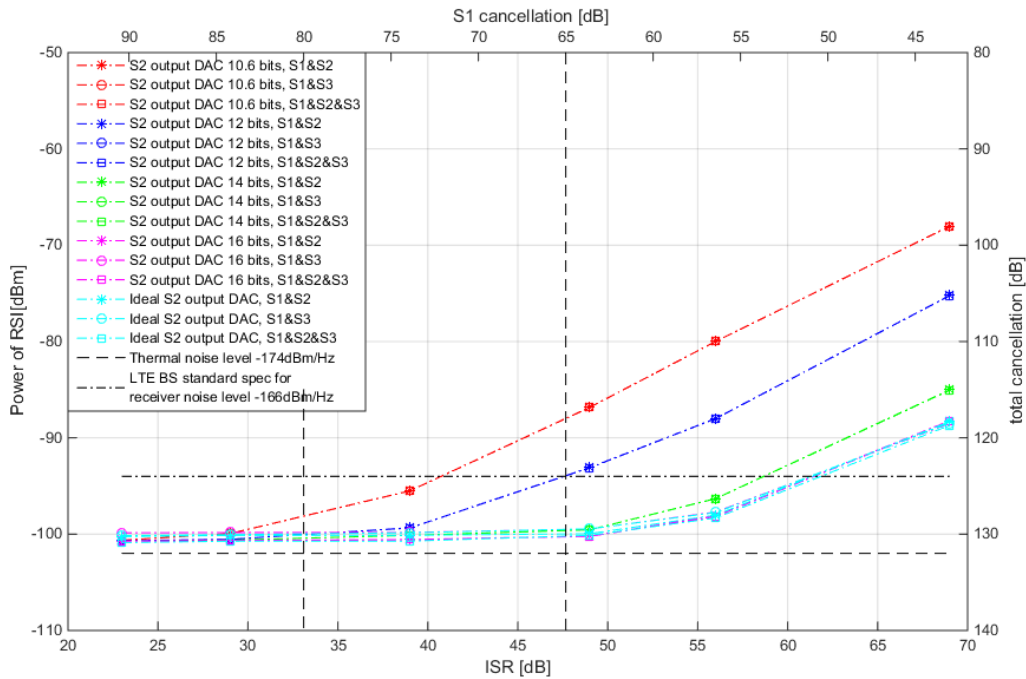


Fig. 4.5 RF cancellation output DAC resolution effect in architecture 1.

Fig. 4.5 presents the cancellation performance with various resolutions of DAC, showing that the distortion introduced by S2 DAC, especially with low resolution, greatly limits the cancellation performance. However, when we only apply analog and baseband SI-cancellation stages (with the absence of RF-cancellation stage), the quantization noise from the DAC at RF cancellation output is of no concern.

Fig. 4.6 shows the cancellation performance with various resolutions of transmitter DAC. It indicates that transmitter DAC does not have much influence on RF SI-cancellation stage or

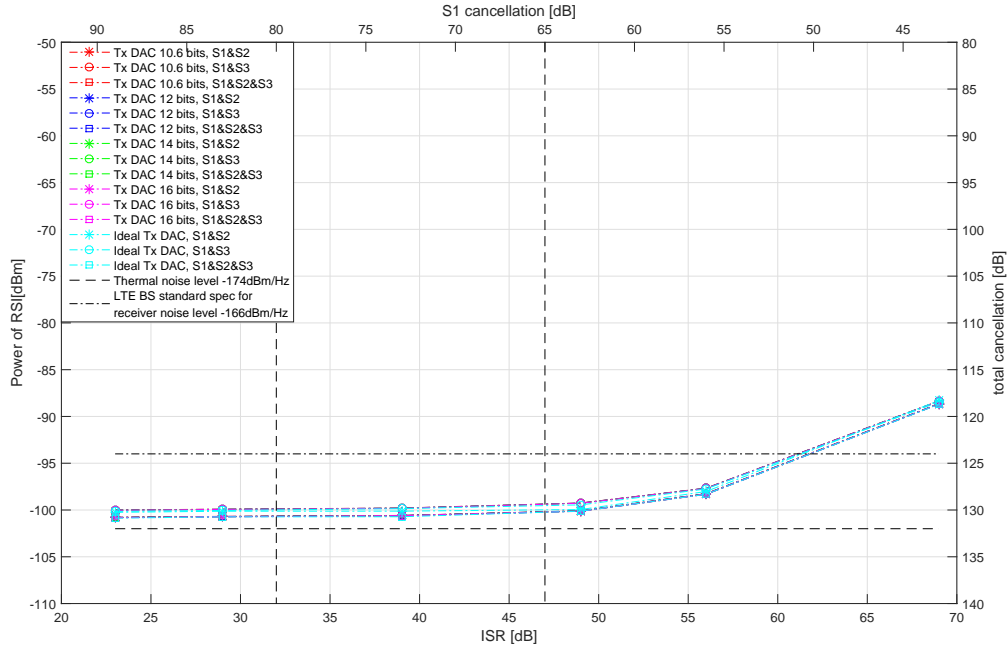


Fig. 4.6 Transmitter DAC resolution effect in architecture 1.

baseband SI-cancellation stage. The noise figure of PA and LNA are the main limitations of cancellation.

The quantization noise introduced by receiver ADC and S2 DAC is the main quantization factor that limits the RF SI-cancellation stage and baseband SI-cancellation stage. Fig. 4.7 plots the combined cases with ADC and DACs. Having a high quality receiver ADC and S2 DAC is very important. For negligible contribution to total cancellation limit (128 dB), the receiver ADC and S2 DAC should have at least 12 and 14 effective bits, respectively. Otherwise, with 9.5-bit ADC and 10.6-bit DAC, the total cancellation will be mostly limited by 10.6-bit S2 DAC to about 118 dB (for the case of S1 cancellation of 65 dB).

PA Nonlinearity Effect

The nonlinear distortion from the transmitter PA can contribute significantly to the SI signal and limit the efficiency of digital cancellation. Through the following figures, the effect of PA nonlinearity becomes clear.

Fig. 4.8 plots the cancellation performance with PA nonlinearity. We compare the perfor-

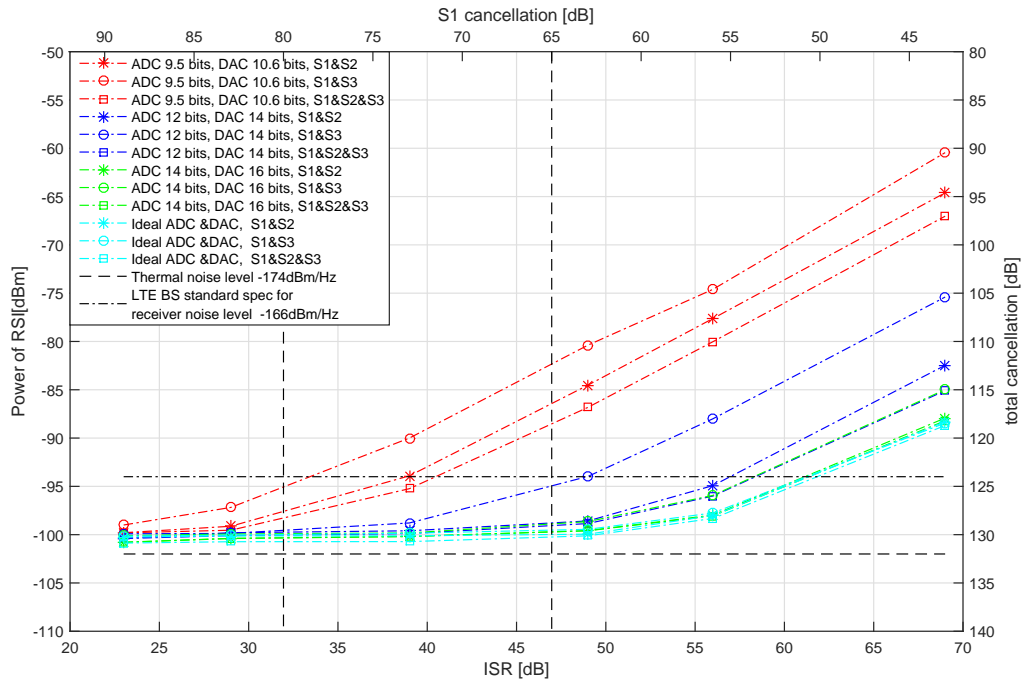


Fig. 4.7 Combined ADC and DAC resolution effect in architecture 1.

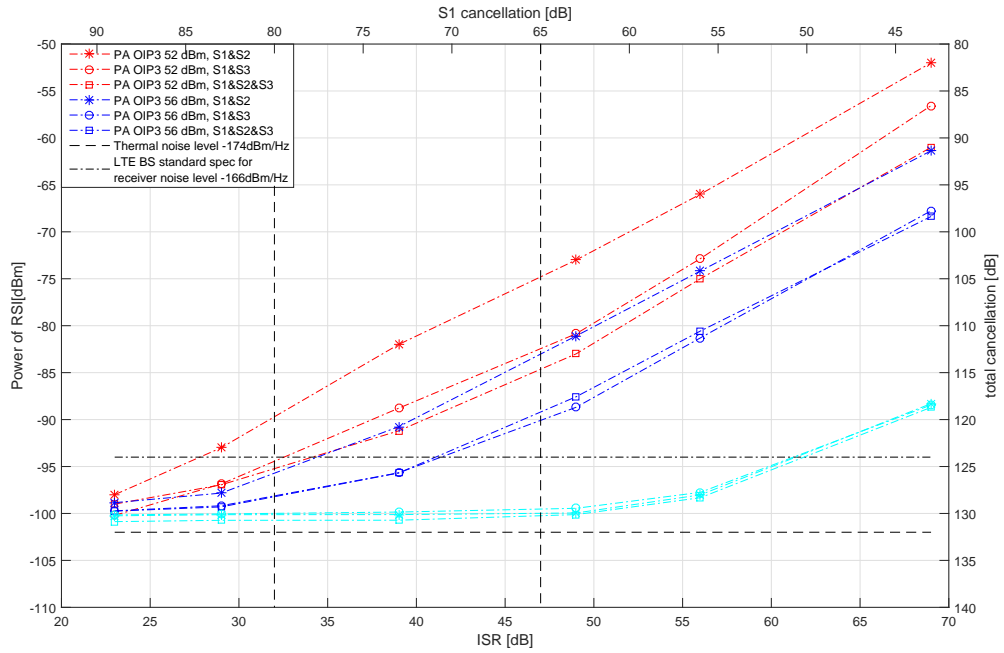


Fig. 4.8 PA nonlinearity effect in architecture 1.

mance between two kinds of power amplifiers, one with linearization while OIP3 is 56 dBm, the other without linearization while the OIP3 is 52 dBm. The plot shows clearly that, applying the linearization techniques gives a better performance. The difference is about 10 dB, when analog SI-cancellation stage contributes less than 80 dB, but it becomes less distinct when the contribution exceeds 85 dB. In our platform, since it is realized by a linear algorithm, PA nonlinearity has a large effect on RF SI-cancellation stage, however the baseband SI-cancellation stage can suppress a part of nonlinearity.

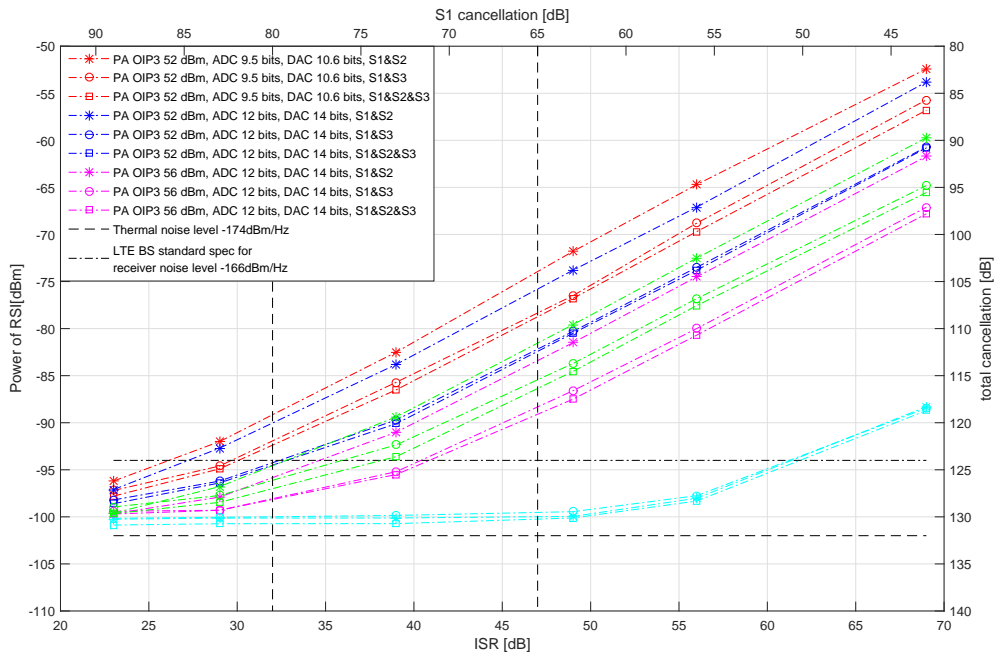


Fig. 4.9 Combined PA nonlinearity and Quantization effect in architecture 1.

The combined performance by PA nonlinearity and quantization effect is shown in Fig. 4.9. The RF SI-cancellation stage is mainly limited by the PA nonlinearity, while the baseband SI-cancellation stage is restricted primarily by the quantization noise of the receiver ADC and S2 DAC. Combined degradation effects of practical 9.5-bit receiver ADC, 10.6-bit S2 DAC, and TX PA OIP3 of 56 dBm, result in total cancellation limit of about 116 dB (for S1 cancellation of 65 dB). Improving quantization with 12-bit ADC and 14-bit DAC increases the total cancellation to about 118 dB (limited by PA OIP3).

Analog SI-Cancellation Nonlinearity Effect

Analog cancellation introduces co-channel nonlinear distortion that cannot be avoided. Taking the nonlinearity of analog cancellation into consideration, the following figures show its effect on cancellation performance.

Table 4.1: Analog SI-Cancellation nonlinearity effect in architecture 1.

S1 IIP3 67 dBm			
	ISR [dB]	26	46
Power of RSI [dBm]	after S2	-93.32	-91.0
	after S3	-96.43	-95.64
	after S2 and S3	-96.44	-95.65

S1 IIP3 70 dBm			
	ISR [dB]	26	46
Power of RSI [dBm]	after S2	-96.31	-95.78
	after S3	-97.48	-97.34
	after S2 and S3	-97.51	-97.48

S1 IIP3 82 dBm			
	ISR [dB]	26	46
Power of RSI [dBm]	after S2	-98.08	-97.93
	after S3	-98.09	-98.09
	after S2 and S3	-99.68	-99.42

Table. 4.1 shows the cancellation performance with various powers of analog SI-cancellation stage nonlinearity. To analyze analog SI-cancellation nonlinearity, we only have two cases to consider: $S1 = 82$ dB for a typical outdoor SI channel, and $S1 = 62$ dB for a typical indoor SI channel. It is clear that analog SI-cancellation stage nonlinearity limits the RF SI-cancellation stage, due to the linear algorithm applied in the RF SI-cancellation stage. Comparing analog SI-cancellation stage nonlinearity and PA nonlinearity, we notice that PA nonlinearity is dominant.

Table 4.2: Combined analog SI-cancellation nonlinearity and quantization effect in architecture 1.

S1 IIP3 67 dBm						
Power of RSI [dBm]	ADC 9.5 bits, DAC 10.6 bits			ADC 12 bits, DAC 14 bits		
	ISR [dB]	26	46	ISR [dB]	26	46
	after S2	-90.36	-81.21	after S2	-91.54	-90.29
	after S3	-90.41	-81.26	after S3	-91.64	-90.39
	after S2 and S3	-94.78	-82.08	after S2 and S3	-95.46	-94.06

S1 IIP3 82 dBm						
Power of RSI [dBm]	ADC 9.5 bits, DAC 10.6 bits			ADC 12 bits, DAC 14 bits		
	ISR [dB]	26	46	ISR [dB]	26	46
	after S2	-96.74	-81.53	after S2	-97.80	-94.90
	after S3	-96.79	-81.58	after S3	-97.90	-95.0
	after S2 and S3	-98.29	-82.28	after S2 and S3	-99.43	-95.22

Table. 4.2 combines the analog SI-cancellation stage nonlinearity and quantization noise. For the case of 9.5-bit ADC and 10.6-bit DAC, the quantization would be the main limiting factor of total cancellation (about 112 dB). With 12-bit ADC and 14-bit DAC, the total cancellation could be improved to 124 dB and 125 dB, for S1 TD-SIC IIP3 of 67 dBm and 82 dBm, respectively.

LNA Nonlinearity Effect

At the receiver, the distortion behavior of LNA also limits the SI-cancellation. Although S1 and S2 suppress SI by a large amount, the residual SI at the output of S2 still introduces some nonlinearity when going through LNA. Fig. 4.10 plots the cancellation performance with the effect of LNA nonlinearity.

Compared with PA nonlinearity, the nonlinearity introduced by LNA is not as strong. From Fig. 4.3 and Fig. 4.10 we can see that the nonlinearity of LNA does not limit the cancellation ability by much, while the noise figure of PA and LNA dominate the limitation of cancellation.

Fig. 4.11 plots the performance after combining both LNA nonlinearity and quantization noise. The existence of LNA nonlinearity limits the cancellation of RF stage. The dominant lim-

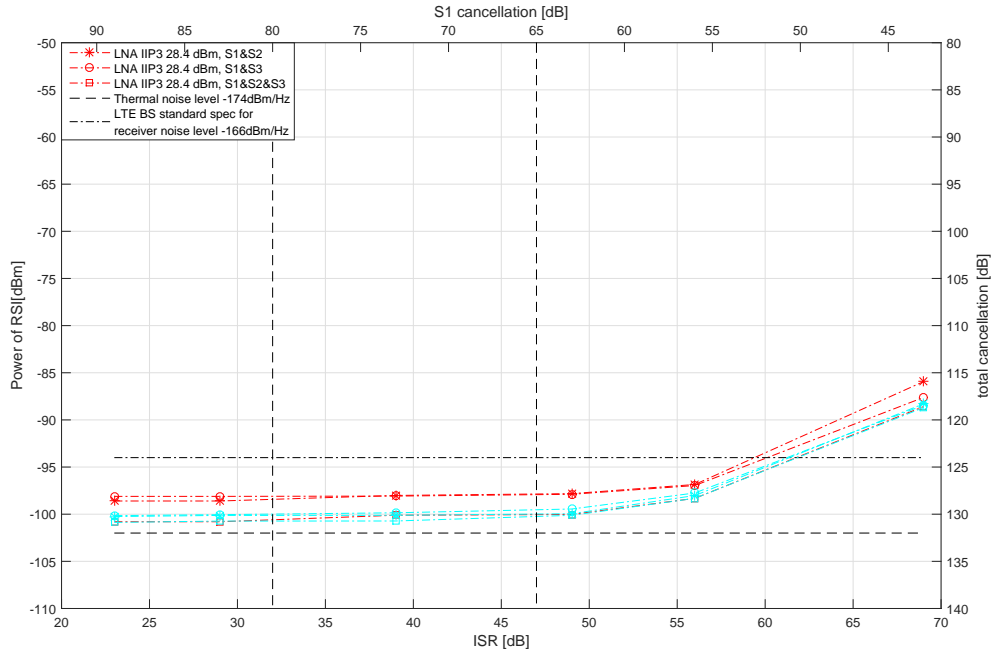


Fig. 4.10 LNA nonlinearity effect in architecture 1.

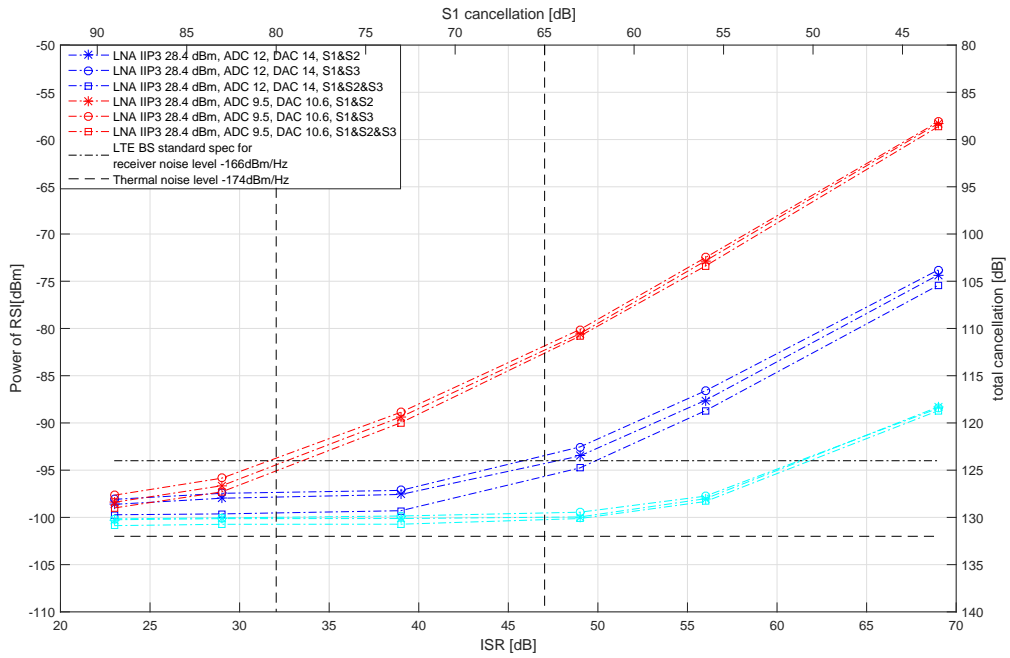


Fig. 4.11 Combined LNA nonlinearity and quantization effect in architecture 1.

itation is the quantization noise. For the case of ADC 9.5-bit and DAC 10.6-bit, the quantization would be the main limiting factor of total cancellation (about 113 dB). With 12-bit ADC and 14-bit DAC, the total cancellation could be improved to 126 dB.

Selected Practical Cases of Combined Nonlinearity and Quantization Effects

Previously, we have showed the effects of each impairment on the SI-cancellation. In this part, we present the performance of some practical cases of combined quantization and nonlinearity:

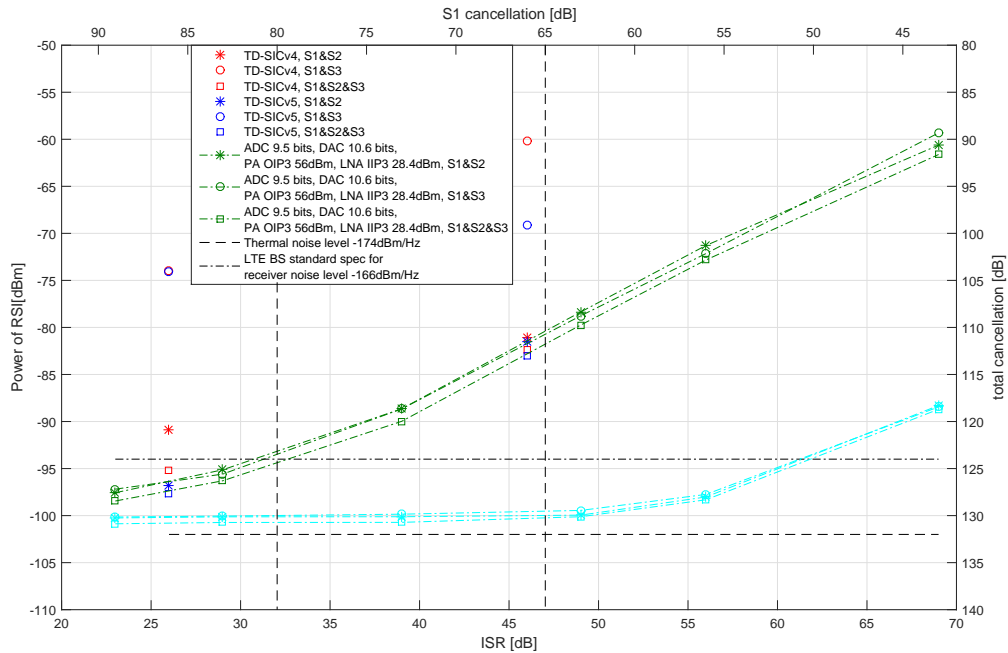


Fig. 4.12 TD-SICv4 case and TD-SICv5 case in architecture 1.

The cancellation performances in practical cases with both nonlinearity and quantization effects are shown in Fig. 4.12. Under TD-SICv4, ADC and DAC have 9.5 and 10.6 bits, while PA OIP3, S1 IIP3 and LNA IIP3 are set to 56 dBm, 67 dBm and 28.4 dBm, respectively. The settings for TD-SICv5 are such that ADC is 9.5-bit, DAC is 10.6-bit, PA OIP3 is 56 dBm, S1 IIP3 is 82 dBm and the LNA IIP3 is 28.4 dBm. It is nonlinearity that mainly limits the RF SI-cancellation stage. For the entire system, the quantization noise introduced by receiver ADC is the dominant factor that limits the cancellation.

Practical 9.5-bit ADCs and 10.6-bit DACs, and assumed nonlinearity of TX PA, S1, and LNA would limit the total cancellation to about 111 dB with S1 cancellation of 65 dB. For negligible contribution to total cancellation limit, the receive ADC and S2 DAC should have at least 12 and 14 effective bits, respectively. However, TX Ref ADC should have at least 14 bits. This total cancellation limit is mainly due to the quantization effects of TX Ref ADC and S2 RF SIC DAC.

4.2.3 Performance of The Second Architecture

The second architecture takes the reference signals for RF and baseband SI-cancellation stages from the output of the PA [10]. Thus, SI signal, transmitter impairments and noise are partially canceled by the RF SI-cancellation stage. The resulting signal is then subtracted from the received signal. This requires an additional receive (Rx) chain containing an RF attenuator and an ADC.

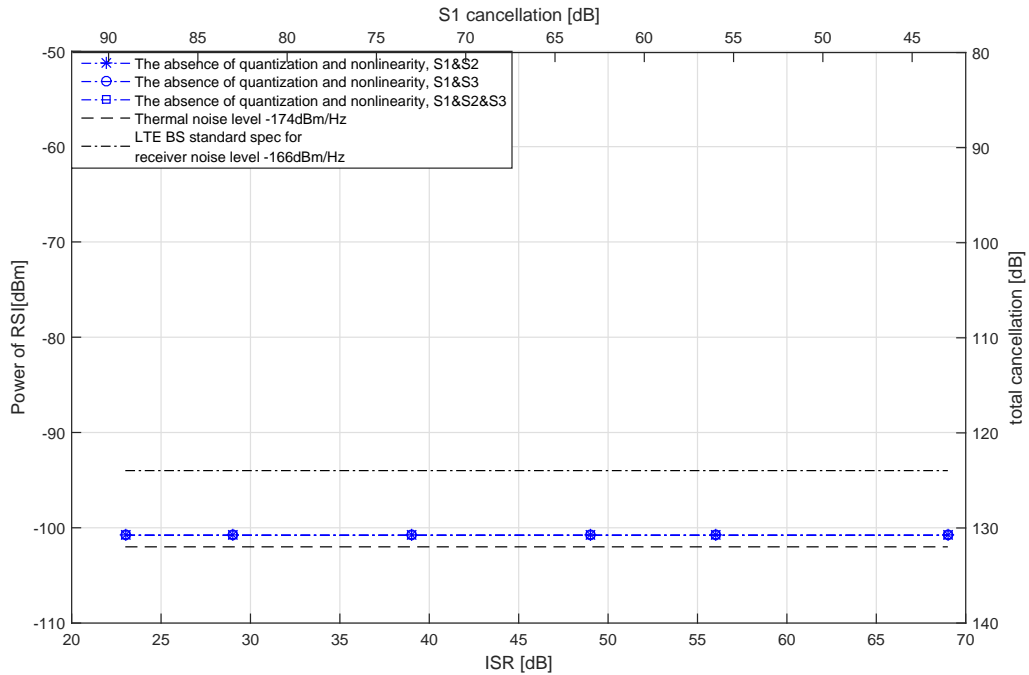


Fig. 4.13 Cancellation performance in the absence of quantization noise and nonlinearities in architecture 2.

Quantization Effect

As shown in Fig. 4.2 (b), quantization noise is introduced by two ADCs and two DACs. In addition to the first architecture, another ADC with down-conversion is required at the input of digital cancellation stages, because the reference signal for RF and baseband are taken from the output of the PA. The following figures show the quantization effect of these components separately.

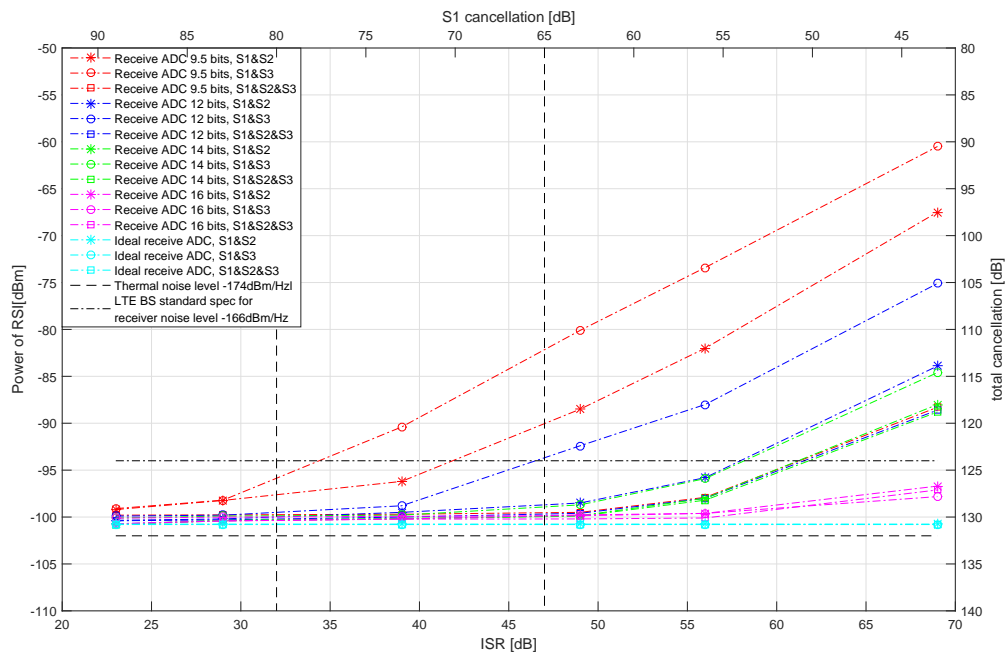


Fig. 4.14 Receive ADC resolution effect in architecture 2.

Fig. 4.14 plots the cancellation performance with various resolutions of ADC in the receiver. It is clear that the quantization noise introduced by ADC in the receiver greatly limits the cancellation ability of our system, especially when the ADC resolution is low (i.e., 9.5 bits). When we increase the resolution of ADC, the power of residual SI decreases quickly. Baseband SI-cancellation stage is more sensitive to receiver ADC when compared with RF SI-cancellation stage, particularly with high ISR. This is due to the fact that without RF SI-cancellation stage the high residual SI passes the ADC and leads to a large amount of quantization, which becomes the dominant noise and makes baseband SI-cancellation stage unable to estimate the SI channel accurately. Thus the ability of cancellation in the system is weakened. Taking the reference after

PA, the signal includes all the PA impairments. Hence, when the resolution of ADC is high and the ISR is great, the cancellation decreases more slowly than that in the first architecture.

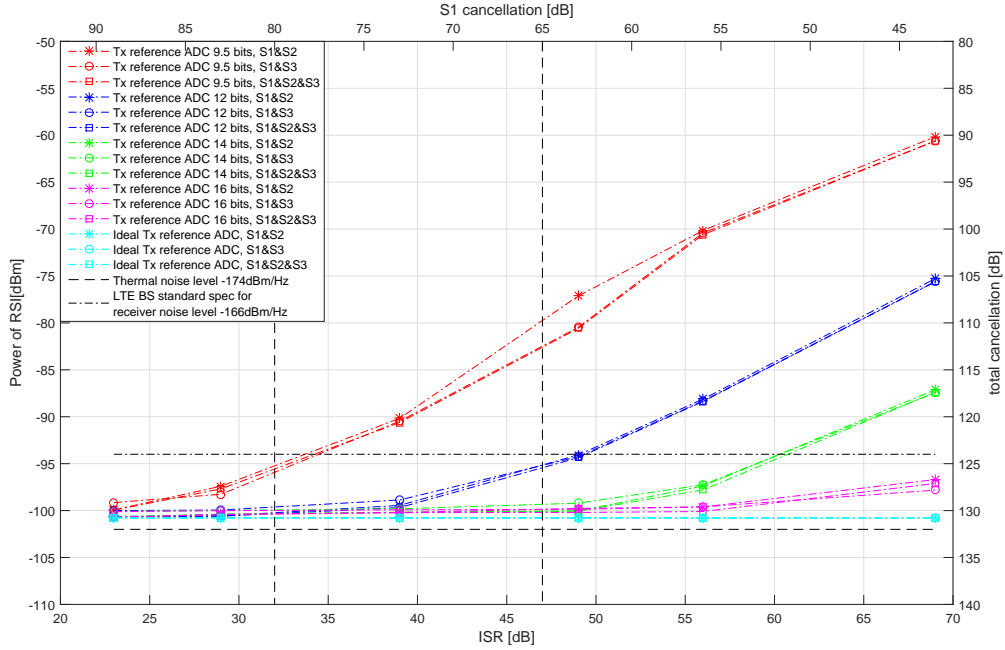


Fig. 4.15 Transmitter reference ADC resolution effect in architecture 2.

Fig. 4.15 plots the cancellation performance with various resolutions of ADC in the reference of cancellation stage. Architecture 1 does not have this ADC block. Similar to the ADC in the receiver, the quantization noise introduced by ADC in the reference of cancellation stage greatly limits the cancellation ability of our system, especially when the ADC resolution is low (i.e., 9.5 bits). However, ADC in the reference of cancellation stage not only limits the RF SI-cancellation stage, but also the baseband SI-cancellation stage. When reference signal passes the ADC, the introduced quantization makes cancellation stage unable to estimate the SI channel accurately. Thus the ability of both RF and baseband SI-cancellation stages in the system are weakened.

Fig. 4.16 presents the cancellation performance under various resolutions of DAC, according to which, when analog SI-cancellation stage contributes more than 55 dB, the power of the residual SI more or less stays unchanged (i.e., -82 dBm with 10.6-bit DAC). Otherwise, when the suppression of SI by the analog SI-cancellation stage is below a threshold, the quantization noise caused by the DAC becomes too large and cannot be suppressed by the RF and baseband SI-cancellation stages. Similar to the case in the first architecture, when we only apply analog

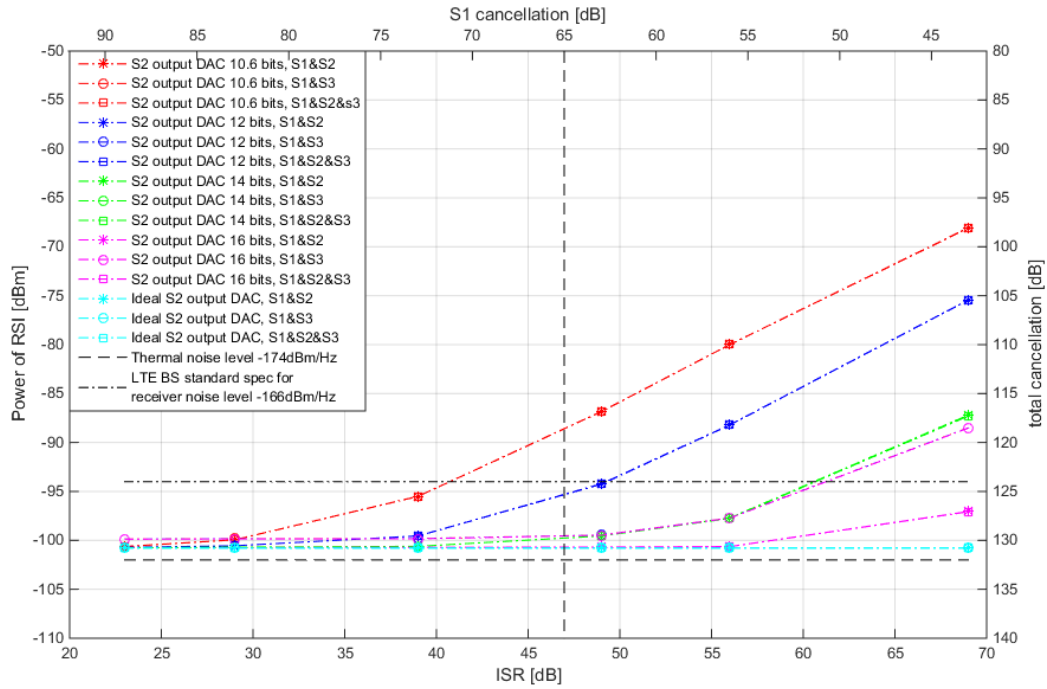


Fig. 4.16 RF cancellation output DAC resolution effect in architecture 2.

and baseband SI-cancellation stages (with the absence of RF-cancellation stage), the quantization noise from the DAC at RF cancellation output is of no concern.

Fig. 4.17 shows the cancellation performance under various resolutions of transmitter DAC. It implies that the main limitations of RF and baseband SI-cancellation stages are the noise figures of PA and LNA, instead of the quantization noise introduced by the transmitter DAC.

The quantization noises introduced by ADCs are the main quantization factors that limit the RF SI-cancellation stage and baseband SI-cancellation stage. The effects of combined cases with ADCs and DACs are shown in Fig. 4.18. For negligible contribution to total cancellation limit (125 dB), the receive ADC and S2 DAC should have at least 12 and 14 effective bits, respectively. Otherwise, with 9.5-bit ADC and 10.6-bit DAC, the total cancellation will be mostly limited by 9.5-bit TX Ref ADC to about 112 dB (for the case of S1 cancellation of 65 dB).

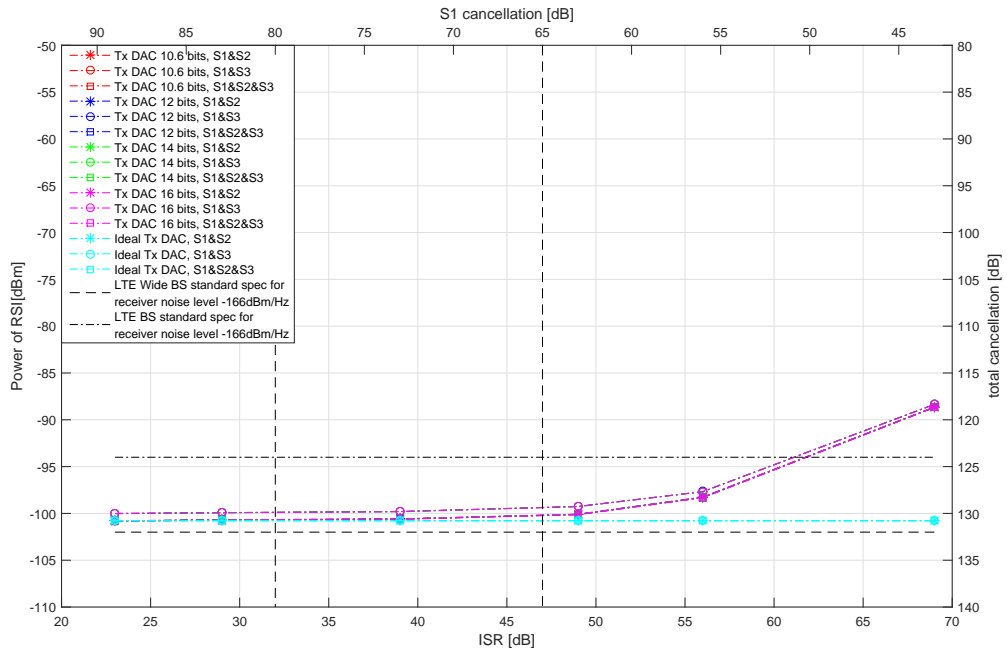


Fig. 4.17 Transmitter DAC resolution effect in architecture 2.

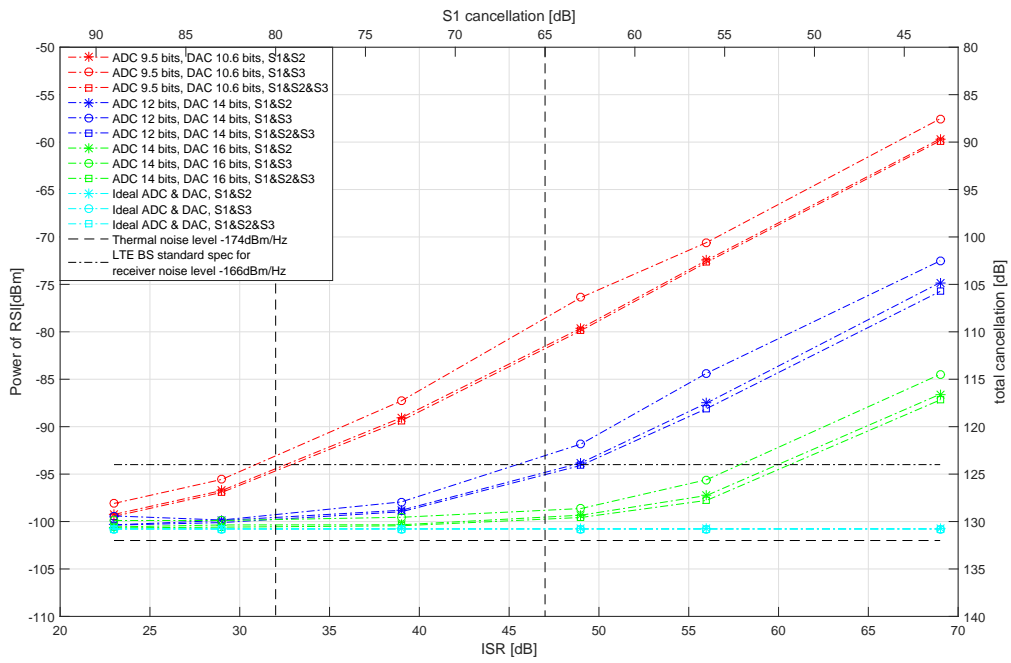


Fig. 4.18 Combined ADC and DAC resolution effect in architecture 2.

PA Nonlinearity Effect

PA nonlinearity is not a limiting factor of SI-cancellation in architecture 2, because the transmitter impairments contained in reference signal are reduced by RF SI-cancellation stage. This is confirmed by the following figures.

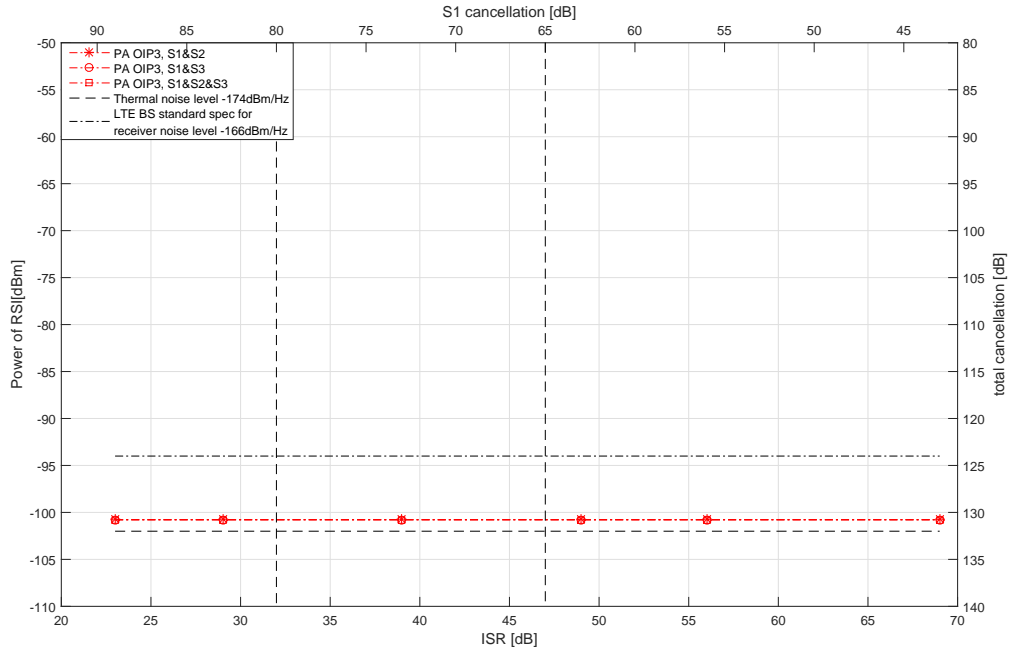


Fig. 4.19 PA nonlinearity effect in architecture 2.

Fig. 4.19 plots the effect of PA nonlinearity on cancellation performance. The reference signal contains the different transmitter impairments, thus the performances of PA with OIP3 of 56 dBm and 52 dBm are the same.

In the second architecture, the performance offer combining PA nonlinearity and quantization effects is shown in Fig. 4.20. Compared with the case that only has quantization shown in Fig. 4.18, we observe the similar cancellation performance. Therefore, it is clear that the baseband SI-cancellation stage is mainly limited by quantization noise. For negligible contribution to total cancellation limit, the ADC and DAC should have at least 12 and 14 effective bits, respectively (total cancellation 126 dB with S1 cancellation of 65 dB. Otherwise, 9.5-bit ADC and 10.6-bit DAC would limit the total cancellation to 112 dB with S1 cancellation of 65 dB.

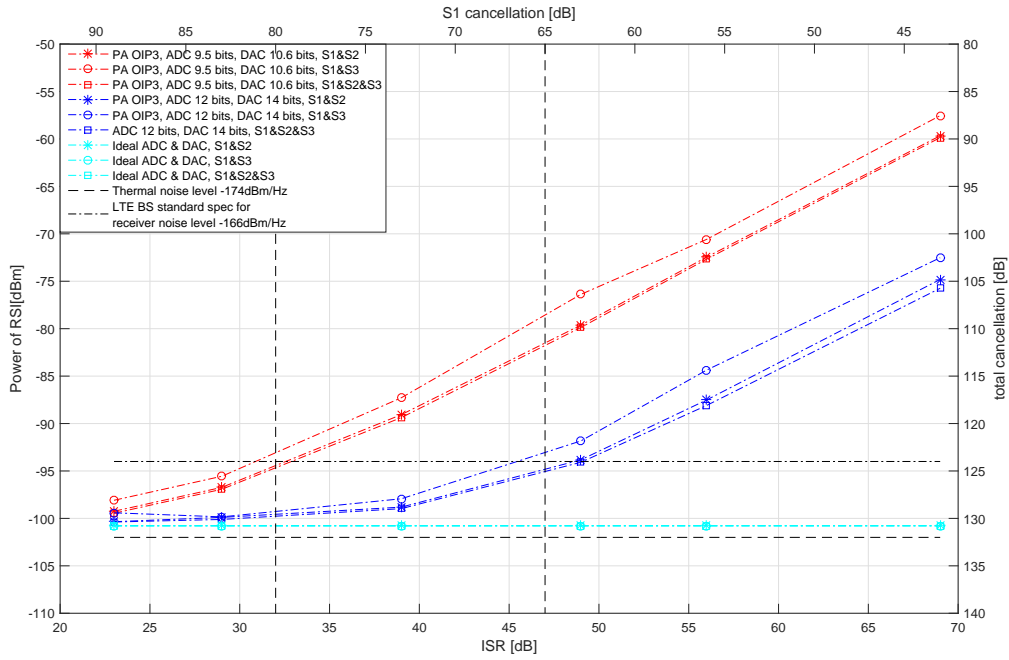


Fig. 4.20 Combined PA nonlinearity and Quantization effect in architecture 2.

Analog SI-Cancellation Nonlinearity Effect

Table 4.3: Analog SI-Cancellation nonlinearity effect in architecture 2.

S1 IIP3 67 dBm			
	ISR [dB]	26	46
Power of RSI [dBm]	after S2	-93.34	-91.52
	after S3	-96.43	-95.67
	after S2 and S3	-96.44	-95.67

S1 IIP3 70 dBm			
	ISR [dB]	26	46
Power of RSI [dBm]	after S2	-96.35	-95.89
	after S3	-97.51	-97.47
	after S2 and S3	-97.52	-97.55

S1 IIP3 82 dBm			
	ISR [dB]	26	46
Power of RSI [dBm]	after S2	-98.64	-98.04
	after S3	-99.03	-98.47
	after S2 and S3	-99.91	-99.42

The co-channel nonlinear distortion introduced by analog cancellation becomes the dominant nonlinearity, since the PA nonlinearity is no longer the limiting factor when taking the reference at the output of PA. Under this situation, the nonlinearity consideration of analog cancellation is shown in subsequent tables.

The effects of nonlinearity in the analog SI-cancellation stage is shown in Table. 4.3. Only two cases are available: $S1 = 82$ dB typically outdoor SI channel, and $S1 = 62$ dB typically indoor SI channel. Due to the linear algorithm, the RF SI-cancellation stage is limited by nonlinearity from the analog SI-cancellation stage.

Table 4.4: Combined analog SI-cancellation nonlinearity and quantization effect in architecture 2.

S1 IIP3 67 dBm						
Power of RSI [dBm]	ADC 9.5 bits, DAC 10.6 bits			ADC 12 bits, DAC 14 bits		
	ISR [dB]	26	46	ISR [dB]	26	46
	after S2	-90.38	-81.21	after S2	-91.66	-90.33
	after S3	-90.40	-81.27	after S3	-91.69	-90.43
	after S2 and S3	-94.78	-82.09	after S2 and S3	-95.49	-94.45

S1 IIP3 82 dBm						
Power of RSI [dBm]	ADC 9.5 bits, DAC 10.6 bits			ADC 12 bits, DAC 14 bits		
	ISR [dB]	26	46	ISR [dB]	26	46
	after S2	-96.73	-81.61	after S2	-97.94	-94.97
	after S3	-96.74	-81.70	after S3	-98.03	-95.56
	after S2 and S3	-98.31	-82.30	after S2 and S3	-99.55	-95.96

For the case of ADC 9.5-bit and DAC 10.6-bit, the quantization would be the main limiting

factor of total cancellation (about 112 dB). With 12-bit ADC and 14-bit DAC, the total cancellation could be improved to 124 dB and 125 dB, for S1 TD-SIC IIP3 of 67 dBm and 82 dBm, respectively.

LNA Nonlinearity Effect

At the receiver, the distortion behavior of LNA also limits the SI-cancellation. Although S1 and S2 suppress SI by a large amount, the residual SI at the output of S2 still introduces some nonlinearity when going through the LNA. Fig. 4.21 plots the cancellation performance with the effect of LNA nonlinearity.

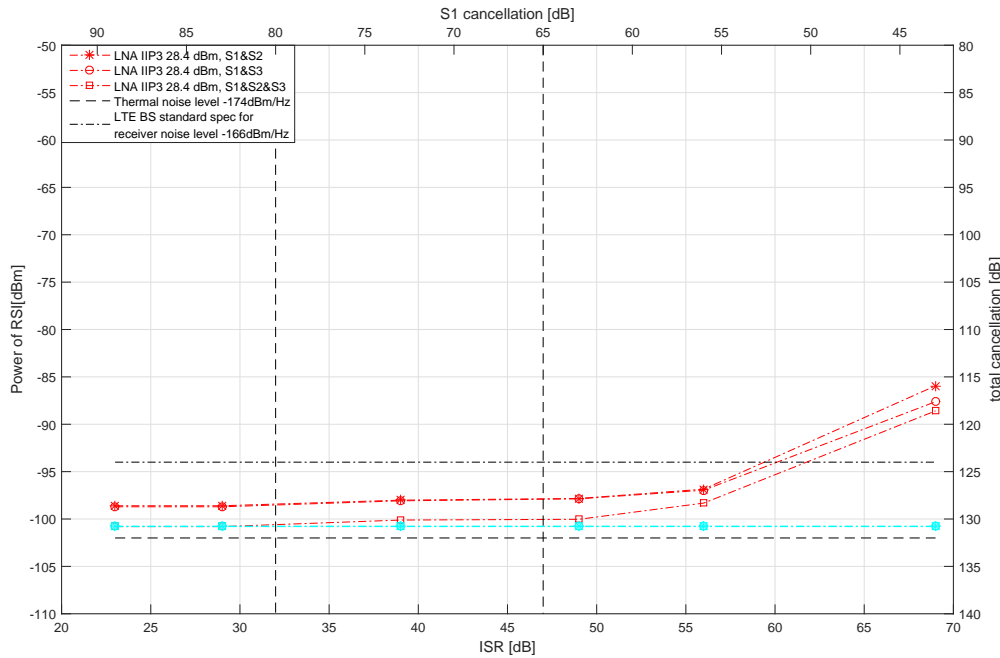


Fig. 4.21 LNA nonlinearity effect in architecture 2.

LNA nonlinearity has less power compared with PA nonlinearity, thus it has less effect on SI-cancellation. When the analog SI-cancellation stage offers more than 60 dB of cancellation, the distortion introduced by LNA can be ignored.

The performance with effects from both LNA nonlinearity and quantization noise is shown in Fig. 4.22. Although the LNA nonlinearity limits the cancellation of the RF stage, for the whole system, the dominant limitation is due to the quantization noise. For negligible contribution to

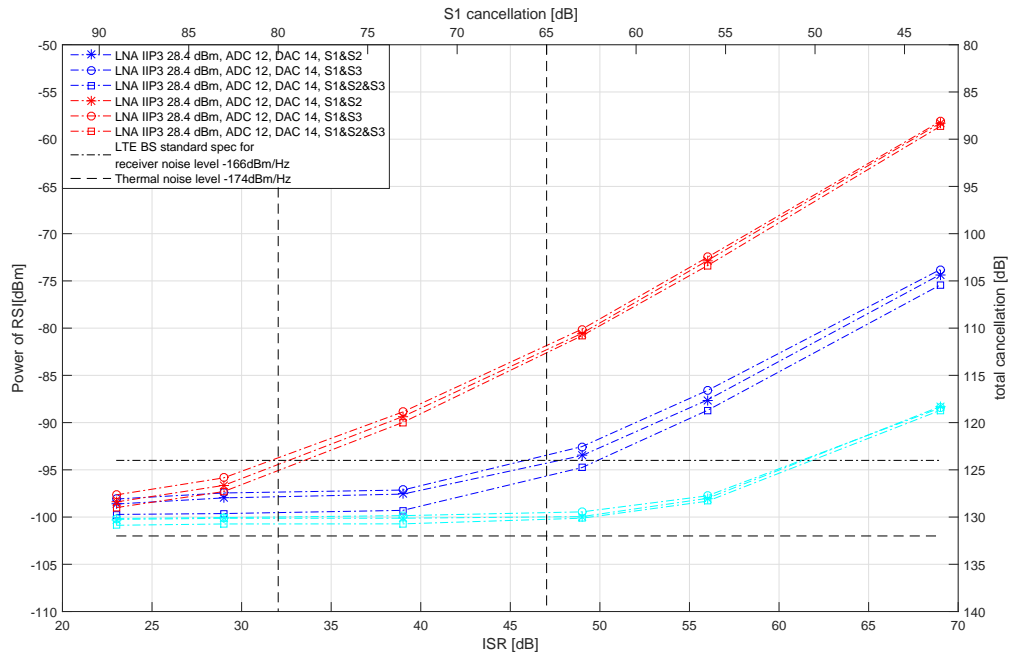


Fig. 4.22 Combined LNA nonlinearity and quantization effect in architecture 2.

total cancellation limit, the receive ADC and S2 DAC should have at least 12 and 14 effective bits, respectively (total cancellation 126 dB with S1 cancellation of 65 dB. TX Ref ADC is the main contributor of limitation, and should be at least 14 bits to improve total cancellation to 129 dB. Otherwise 9.5-bit ADC and 10.6-bit DAC would limit the total cancellation to 113 dB.

Selected Practical Cases of Combined Nonlinearity and Quantization Effects

Previously, we have showed the effects of each impairment on the SI-cancellation. In this part, we present in Fig. 4.23 the performance of some practical cases with combined effects from quantization and nonlinearity.

The settings for the two practical cases are as follows. For TD-SICv4, ADC is 9.5 bits, DAC is 10.6 bits, PA OIP3 is 56 dBm, S1 IIP3 is 67 dBm and the LNA IIP3 is 28.4 dBm. For TD-SICv5, on the other hand, ADC is 9.5-bit, DAC is 10.6-bit, PA OIP3 is 56 dBm, S1 IIP3 is 82 dBm and the LNA IIP3 is 28.4 dBm.

In the second architecture, the reference signal contains all the transmitter impairments, thus the limiting factor is no longer the PA nonlinearity. The ADC in the reference of cancellation

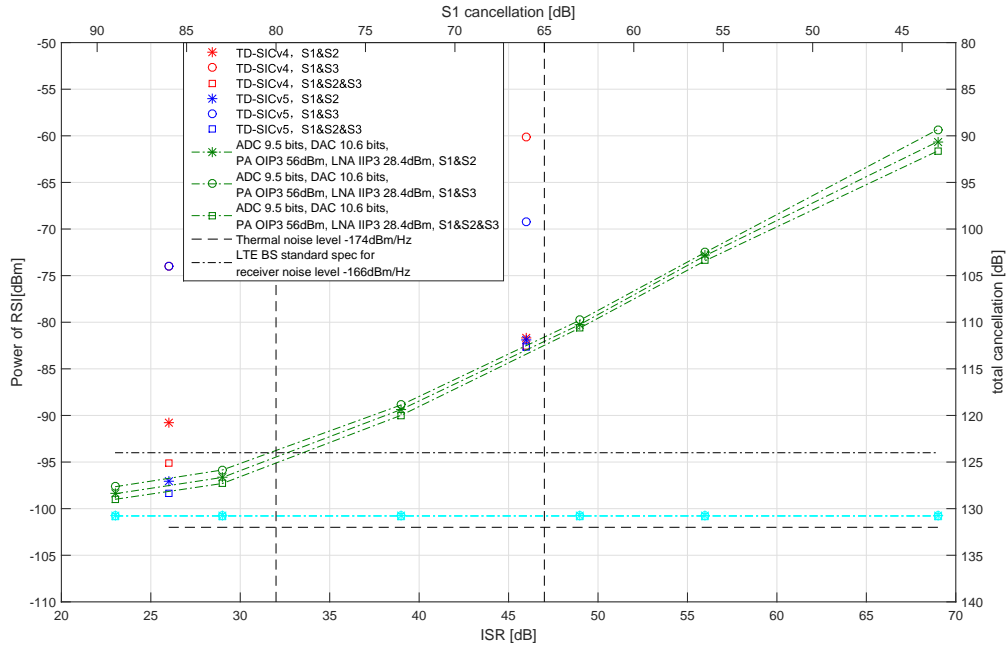


Fig. 4.23 TD-SICv4 case and TD-SICv5 case in architecture 2.

stage introduces the quantization that limits both the RF and baseband SI-cancellation stages, while the quantization noise introduced by the receiver ADC is the another dominant factor that limits the baseband SI-cancellation stage.

Practical 9.5-bit ADCs and 10.6-bit DACs, and the nonlinearities of TX PA, S1 and LNA would limit the total cancellation to about 113 dB with 65 dB S1 cancellation. For negligible contribution to total cancellation limit, the receiver ADC and S2 DAC should have at least 12 and 14 effective bits, respectively. However, TX Ref ADC should have at least 14 bits. This total cancellation limit is mainly due to the quantization effects of TX Ref ADC and S2 RF SIC DAC.

4.3 Limitation of Cancellation

In this section, we gather results from previous sections to evaluate the impact of all the components on overall system performance, in order to identify the factors that limits FD systems for the two architectures.

4.3.1 Limitation of RF SI-Cancellation Stage

The RF SI-cancellation stage subtracts a replica of the received SI, based on an estimate of the SI-channel from the received RF signal. The performance of the RF SI-cancellation stage depends on the accuracy of the SI-channel estimation. We assume an initial HD transmission period (i.e., without the intended signal) in which the SI-channel is estimated, by using the LS estimator.

In the first architecture, all paths of the SI-channel are canceled, leaving the transmitter impairments to be reduced in the baseband. The most significant residual SI is caused by the transmitter impairments, which cannot be reduced by the RF SI-cancellation stage.

The second architecture reduces the paths of the SI-channel along with the transmitter impairments in the RF stage. The quantization noise introduced by ADCs and DACs become the dominant source of residual SI.

4.3.2 Limitation of baseband SI-cancellation stage

The residual SI is reduced in the baseband by subtracting a baseband replica of the SI from the received signal.

In the first architecture, the subtracted samples are generated by processing the known transmitted baseband symbols with an estimate of the nonlinearity coefficients and the residual SI-channel after the RF SI-cancellation stage. The estimated residual SI-channel includes the effects of the transceiver and the multi-path components due to external reflections.

In the second architecture, transmitter nonlinearities are already included in the reference signal for baseband SI-cancellation, which is taken after the PA, and that only linear processing is needed to obtain the canceling signal.

For both architectures, baseband SI-cancellation stage cannot reduce the quantization noise introduced by ADCs and DACs.

4.4 Potential Scenarios with fewer cancellation stages

Suppressing the SI by combining successive cancellation stages is a practical and widely used method. In general, the amount of SI-cancellation increases with the number of stages. However, beyond a certain level, adding more cancellation stages does not help suppress the SI; it only makes the canceler more complex. In fact, having more cancellation stages not only adds

complexity to the communication system, but also increases the cost of building one. In previous work, we applied two digital cancellation stages to achieve a good SI suppression: one RF SI-cancellation stage applied before receiver LNA, and one baseband SI-cancellation stage applied after the receiver ADC. We aim for an improved design, in the sense of having minimal number of stages for the SI canceler, while keeping the cancellation requirement satisfied. In the following subsections, we discuss the trade-off between the amount of SI-cancellation and the number of cancellation stages, based on the simulation results we presented in previous sections. We also propose potential scenarios for operation with one digital cancellation.

4.4.1 Potential Scenarios for operation without RF SI-cancellation stage

RF SI-cancellation stage is more expensive than baseband SI-cancellation stage, because the former requires an auxiliary transmitter chain to convert the baseband signal to RF. We would like to remove the RF SI-cancellation stage without sacrificing the cancellation performance. Presently, the RF SI-cancellation stage results in the suppression of SI to a level sufficiently low prior to the ADC, in order to avoid the saturation of these components. From the cancellation results with quantization effect shown previously, we can see that the distortion made by ADC overloading cannot be reduced by the baseband SI-cancellation stage. Thus, once we suppress the SI sufficiently by the analog SI-cancellation stage, the RF SI-cancellation stage is no longer necessary.

For 12 bits RF ADC, the parameters we used are listed in Table. 4.5:

Table 4.5 The parameters of ADC

parameter	value
SNR (full BW ADC spec)	48 dB
SFDR (full BW ADC spec)	60 dBc
IMD3 (at ADC output)	-64 dBc

Assume the signal at the input of ADC has: $\text{SNR} + \text{ISR} < 64\text{dB} - 10\text{dB} = 54\text{dB}$ (with a back-off of 10 dB). Therefore, when SNR is 20 dB, the ISR is less than $54\text{dB} - 20\text{dB} = 34\text{dB}$. The noise figure of the receiver is about 4 dB, thus the SNR at the input of receiver (output of analog SI-cancellation stage) is 24 dB, and the power of noise P_{noise} is -103 dBm . Under these conditions, the power of intended signal at the input of receiver P_{IS} is -79 dBm , thus P_{SI} , the power of SI at input of receiver, should be less than $-79\text{dBm} + 34\text{dB} = -45\text{dBm}$.

For LNA, we apply the HW Balanced Amplifier, whose parameters are listed in Table. 4.6.

Table 4.6 The parameters of LNA

parameter	value
Noise Figure (NF)	1.8 dB
Gain (G)	15 dB
IIP3	28.4 dBm
$P_{1dB_{in}}$	18.4 dBm

The average input signal power to LNA ($P_{avg_{in}}$) should be less than 6.4 dB ($P_{1dB_{in}} - PAR = +18.4dBm - 12dB = +6.4dBm$). For operation in linear region, assuming an additional back-off of 20 dB, $P_{avg_{in}}$ is no more than -13.6 dBm. Thus for the gain of transmitter PA (P_{tx}) of +30 dBm, we need at least 43.6 dB cancellation after the analog SI-cancellation stage.

According to the above, preliminary calculations considering receiver ADC and LNA indicate that in order to remove the RF SI-cancellation stage, the analog SI-cancellation stage should provide at least 75 dB of SI-cancellation, which agrees with the simulation results shown previously.

4.4.2 Potential Scenarios for operation without baseband SI-cancellation stage

Baseband SI-cancellation stage is very important because it suppresses the residual SI and RF impairments. Nonlinearities introduced by PA, analog SI-cancellation stage and LNA cannot be suppressed by the other two stages. In particular, PA nonlinearity is the dominant limitation.

As previously shown, for the second architecture, the reference signal contains all the transmitter impairments, including PA nonlinearity. The power of LNA nonlinearity is not very strong, so it only has a small effect on SI-cancellation. When the analog SI-cancellation stage offers more than 60 dB cancellation, distortion introduced by the LNA can be ignored. Thus, the factors that make operations without baseband SI-cancellation stage challenging are the quantization noise introduced by ADCs and DACs.

By choosing the second architecture, we can remove the baseband SI-cancellation stage, as long as the analog SI-cancellation stage provides at least 60 dB of SI-cancellation.

4.5 Chapter Summary

We implemented a SIMULINK FD communications system platform to evaluate the SI-cancellation performance and its characteristics in different realistic scenarios. We also investigated the main limitations of each SI-cancellation stage in two widely used architectures for SI-cancellation. When the transmit baseband signal is used as a reference, RF SI-cancellation stage is affected mainly by the transmitter impairments. While if PA output is taken as a reference signal, the RF SI-cancellation stage can sufficiently reduce the transmitter impairments. In this case, the quantization noise of the receiver ADC is the main factor that limits the upper bound of overall cancellation by both RF and baseband SI-cancellation stages. Moreover, the transmitter nonlinearities have to be reduced in the baseband. Intensive simulation results illustrate the effects of the quantization noise and nonlinearity. For reducing the SI-cancellation complexity, we discussed potential scenarios for operations with only analog and RF SI-cancellation stages, or analog and baseband SI-cancellation stages.

Chapter 5

Conclusions and Future Work

5.1 Summary

Along this thesis, we studied the problem of SI-cancellation in FD systems. Conventional approaches subtract the SI from the received signal and thus reveal the need to estimate and reconstruct the received SI. We develop a new estimation algorithm for SI-cancellation to achieve superior accuracy and spectral efficiency than the available approaches. The main contributions and corresponding results are summarized as follows.

A parameters estimation of baseband SI-cancellation is proposed in Chapter 3. In the previous works, the proposed estimators ignore the intended signal by either using a training period to estimate the SI parameters, resulting in a reduced spectral efficiency, or simply considering the intended signal as additive noise. In our work, we incorporate the intended signal in the estimation process by exploiting its second-order statistics and the transmit pilots. The global phase-noise process changes from one sample to another. Thus the equivalent channel coefficients become time-varying. Other works that consider the phase-noise are proposed by alternatively estimating the phase-noise and the SI channel. However, this algorithm suffers from two kinds of errors: the phase-noise increases the estimation error of the SI channel, and then the channel estimation error reduces the phase-noise estimation performance. In our work, BEM is adopted to model the combined phase-noise and channel coefficients. The time-varying phase-noise is captured in

a deterministic way by means of a basis expansion, which reduces the number of parameters. An ML scheme is developed to find the BEM coefficients. Incorporating the intended signal into the estimation process represents the main advantage of the proposed method.

The strong SI, which travels much shorter distance than the remote intended signal, requires multiple cancellation stages at the receiver. In Chapter 4, we studied the power of SI after each cancellation stage for the two widely used architectures, taking into account the transceiver impairments. One SI-cancellation scheme by combining antenna cancellation, RF cancellation and digital cancellation provides results from practical experiments showing the feasibility of an FD design. In general, it is difficult to give an exact number of the SI reduction that can be obtained because of the interaction between many factors such as transceiver impairments, wireless propagation channel and estimation error. What can be done is to identify the main factors that limit the cancellation performance. This makes a better analysis of the entire system performance and leads to the development of more efficient methods to improve the cancellation capability. We addressed the impact of each transceiver impairment in FD systems and specified the limiting factors of the RF and baseband SI-cancellation stages in two architectures. We justified the need to reduce the SI before the LNA/ADC, using the RF SI-cancellation stage, to avoid high quantization noise from the ADC. The analysis reveals also that the transmitter nonlinearities have to be modeled and canceled in the baseband SI-cancellation stage. Finally we discussed the balance between the amount of SI-cancellation and the number of cancellation stages according to the simulation results we presented, and proposed the potential scenarios for operation with one digital cancellation.

5.2 Potential Future Research

Although several issues regarding SI-cancellation in system have been addressed in this thesis, many interesting related problems remain to be answered and hence, deserve further attention. The proposed future work is given as follows:

In Chapter 3, we applied an iterative procedure to calculate the covariance matrix and intended channel coefficients. This is a common approach to deal with these dependent parameters, while it is time consuming and increase the complexity of calculation. A closed-form solution should be applied in this situation.

When developing the ML estimator in Chapter 3, equivalent channels corresponding to, for

example, the direct signal, or the image signal from the IQ mixer, are assumed to be independent. They are, however, related by a multiplicative factor that represents the response of the IQ mixer to the image signal. Thus exploiting this relation can potentially improve the estimation accuracy. Furthermore, the estimator we developed by imposing independent conditions for the covariance matrix and intended channel coefficients is only an approximation of the true ML estimator. Removing the independence assumption and using numerical methods such as Newton-type algorithms would lead to the true form.

Only FD SISO system is analyzed in Chapter 4. While MIMO is an advanced technique that has been proposed as a promising solution for beneficially increasing the networks spectral efficiency, which is currently operational in wireless communications systems. Thus the cancellation performance should be further simulated with MIMO system.

References

- [1] A. C. Cirik, "Fairness considerations for full duplex multi-user MIMO systems," *IEEE Wireless Communications Letters*, vol. 4, no. 4, pp. 361–364, Aug. 2015.
- [2] R. V. Nee and R. Prasad, *OFDM for wireless multimedia communications*. Artech House, Inc., 2000.
- [3] A. J. Paulraj, D. A. Gore, R. U. Nabar, and H. Bolcskei, "An overview of MIMO communications - a key to gigabit wireless," *IEEE Trans. Proceedings.*, vol. 92, no. 2, pp. 198–218, Feb. 2004.
- [4] Z. Zhang, K. Long, A. V. Vasilakos, and L. Hanzo, "Full-duplex wireless communications: Challenges, solutions, and future research directions," *IEEE Trans. Proceedings.*, vol. 104, no. 7, July 2016.
- [5] Z. Zhang, X. Chai, K. Long, A. V. Vasilakos, and L. Hanzo, "Full duplex techniques for 5G networks: self-interference cancellation, protocol design, and relay selection," *IEEE Commun. Mag.*, vol. 53, no. 5, pp. 128–137, May 2015.
- [6] T. Riihonen, S. Werner, and R. Wichman, "Mitigation of loopback self-interference in full-duplex MIMO relays," *IEEE Trans. Signal Process.*, vol. 59, no. 12, pp. 5983–5993, Dec. 2011.
- [7] Y. Sung, J. Ahn, B. V. Nguyen, and K. Kim, "Loop-interference suppression strategies using antenna selection in full-duplex MIMO relays," in *International Symposium on Intelligent Signal Processing and Communications Systems (ISPACS)*, Dec. 2011, pp. 1–4.

-
- [8] T. Gansler and G. Salomonsson, "Nonintrusive measurements of the telephone channel," *IEEE Trans. Commun.*, vol. 47, no. 1, pp. 158–167, Jan. 1999.
- [9] M. Ho, J. M. Cioffi, and J. A. C. Bingham, "Discrete multitone echo cancelation," *IEEE Trans. Commun.*, vol. 44, no. 7, pp. 817–825, July 1996.
- [10] A. Masmoudi and T. Le-Ngoc, "Self-interference cancellation limits in full-duplex communication systems," in *Proc. IEEE Global Commun. Conf. (GLOBECOM)*, Dec. 2016, pp. 1–6.
- [11] M. Heino, D. Korpi, T. Huusari, E. Antonio-Rodriguez, S. Venkatasubramanian, T. Riihonen, L. Anttila, C. Icheln, K. Haneda, R. Wichman, and M. Valkama, "Recent advances in antenna design and interference cancellation algorithms for in-band full duplex relays," *IEEE Commun. Mag.*, vol. 53, no. 5, pp. 91–101, May 2015.
- [12] Z. Zhang, K. Long, A. V. Vasilakos, and L. Hanzo, "Full-duplex wireless communications: Challenges, solutions, and future research directions," *IEEE Trans. Proceedings.*, vol. 104, no. 7, pp. 1369–1409, July 2016.
- [13] "LTE; evolved universal terrestrial radio access (E-UTRA); user equipment (UE) radio transmission and reception (3GPP TS 36.101 version 11.2.0 release 11)," ETSI, Sophia Antipolis Cedex, France.
- [14] Y. Hua, P. Liang, Y. Ma, A. Cirik, and Q. Gao, "A method for broadband full-duplex MIMO radio," *IEEE Signal Process. Lett.*, vol. 19, no. 12, pp. 793–796, Dec. 2012.
- [15] D. Korpi, L. Anttila, V. Syrjala, and M. Valkama, "Widely linear digital self-interference cancellation in direct-conversion full-duplex transceiver," *IEEE J. Sel. Areas Commun.*, vol. 32, no. 9, pp. 1674–1687, Sep. 2014.
- [16] D. Korpi, T. Riihonen, V. Syrjala, L. Anttila, M. Valkama, and R. Wichman, "Full-duplex transceiver system calculations: Analysis of ADC and linearity challenges," *IEEE Trans. Wireless Commun.*, vol. 13, no. 7, pp. 3821–3836, July 2014.
- [17] A. Masmoudi and T. Le-Ngoc, "Channel estimation and self-interference cancellation in full-duplex communication systems," *IEEE Trans. Veh. Technol.*, vol. 66, no. 1, pp. 321–334, Jan. 2017.

-
- [18] —, “A digital subspace-based self-interference cancellation in full-duplex MIMO transceivers,” in *Proc. IEEE Intl. Conf. Commun. (ICC)*, June 2015, pp. 4954–4959.
- [19] E. Ahmed, A. Eltawil, and A. Sabharwal, “Self-interference cancellation with nonlinear distortion suppression for full-duplex systems,” in *Proc. IEEE Asilomar Conf. on Signal, Systems and Computers (ASILOMAR)*, Nov. 2013, pp. 1199–1203.
- [20] V. Syrjala, M. Valkama, L. Anttila, T. Riihonen, and D. Korpi, “Analysis of oscillator phase-noise effects on self-interference cancellation in full-duplex OFDM radio transceivers,” *IEEE Trans. Wireless Commun.*, vol. 13, no. 6, pp. 2977–2990, June 2014.
- [21] T. Riihonen, P. Mathecken, and R. Wichman, “Effect of oscillator phase noise and processing delay in full-duplex OFDM repeaters,” in *Proc. IEEE Asilomar Conf. on Signal, Systems and Computers (ASILOMAR)*, Nov. 2012, pp. 1947–1951.
- [22] A. Sahai, G. Patel, C. Dick, and A. Sabharwal, “On the impact of phase noise on active cancelation in wireless full-duplex,” *IEEE Trans. Veh. Technol.*, vol. 62, no. 9, pp. 4494–4510, Nov. 2013.
- [23] E. Ahmed and A. Eltawil, “On phase noise suppression in full-duplex systems,” *IEEE Trans. Wireless Commun.*, vol. 14, no. 3, pp. 1237–1251, Mar. 2015.
- [24] A. Masmoudi and T. Le-Ngoc, “A maximum-likelihood channel estimator in MIMO full-duplex systems,” in *Proc. IEEE Veh. Tech. Conf. (VTC)*, Sep. 2014, pp. 1–5.
- [25] —, “Self-interference cancellation for full-duplex MIMO transceivers,” in *Proc. IEEE Wireless Commun. Netw. Conf. (WCNC)*, March 2015, pp. 141–146.
- [26] Z. Tang, R. Cannizzaro, G. Leus, and P. Banelli, “Pilot-assisted time-varying channel estimation for OFDM systems,” *IEEE Trans. Signal Process.*, vol. 55, no. 5, pp. 2226–2238, May 2007.

-
- [27] G. Giannakis and C. Tepedelenlioglu, "Basis expansion models and diversity techniques for blind identification and equalization of time-varying channels," *IEEE Trans. Proceedings.*, vol. 86, no. 10, pp. 1969–1986, Oct. 1998.
- [28] R. Li, A. Masmoudi, and T. Le-Ngoc, "Self-interference cancellation with phase-noise suppression in full-duplex systems," in *Proc. IEEE Intl. Symp. on Personal, Indoor and Mobile Radio Commun. (PIMRC)*, Aug. 2015, pp. 261–265.
- [29] A. Masmoudi and T. Le-Ngoc, "A maximum-likelihood channel estimator for self-interference cancelation in full-duplex systems," *IEEE Trans. Veh. Technol.*, vol. 65, no. 7, pp. 5122–5132, July 2016.
- [30] X. Wu, Y. Shen, and Y. Tang, "The power delay profile of the single-antenna full-duplex self-interference channel in indoor environments at 2.6 GHz," *IEEE Antennas Wireless Propag. Lett.*, vol. 13, pp. 1561–1564, 2014.
- [31] A. Sethi, V. Tapio, and M. Juntti, "Self-interference channel for full duplex transceivers," in *Proc. IEEE Wireless Commun. Netw. Conf. (WCNC)*, April 2014, pp. 781–785.
- [32] C. R. Anderson, S. Krishnamoorthy, C. G. Ranson, T. J. Lemon, W. G. Newhall, T. Kummetz, and J. H. Reed, "Antenna isolation, wideband multipath propagation measurements, and interference mitigation for on-frequency repeaters," in *IEEE Trans. Proceedings.*, March 2004, pp. 110–114.
- [33] K. Haneda, E. Kahra, S. Wyne, C. Icheln, and P. Vainikainen, "Measurement of loop-back interference channels for outdoor-to-indoor full-duplex radio relays," in *IEEE Trans. Antennas Propag.* IEEE, 2010, pp. 1–5.
- [34] E. Everett, M. Duarte, C. Dick, and A. Sabharwal, "Empowering full-duplex wireless communication by exploiting directional diversity," in *Proc. IEEE Asilomar Conf. on Signal, Systems and Computers (ASILOMAR)*, Nov. 2011, pp. 2002–2006.
- [35] E. Everett, A. Sahai, and A. Sabharwal, "Passive self-interference suppression for full-duplex infrastructure nodes," *IEEE Trans. Wireless Commun.*, vol. 13, no. 2, pp. 680–694, Feb. 2014.

-
- [36] J. I. Choi, M. Jain, K. Srinivasan, P. Levis, and S. Katti, "Achieving single channel, full duplex wireless communication," in *MobiCom*. ACM, 2010, pp. 1–12.
- [37] J. I. Choi, S. Hong, M. Jain, S. Katti, P. Levis, and J. Mehlman, "Beyond full duplex wireless," in *Proc. IEEE Asilomar Conf. on Signal, Systems and Computers (ASILOMAR)*, Nov. 2012, pp. 40–44.
- [38] Z. Zhang, X. Chai, K. Long, A. V. Vasilakos, and L. Hanzo, "Full duplex techniques for 5G networks: self-interference cancellation, protocol design, and relay selection," *IEEE Commun. Mag.*, vol. 53, no. 5, May 2015.
- [39] D. Korpi, M. Heino, C. Icheln, K. Haneda, and M. Valkama, "Compact inband full-duplex relays with beyond 100 dB self-interference suppression: Enabling techniques and field measurements," *IEEE Trans. Antennas Propag.*, vol. 65, no. 2, pp. 960–965, Feb. 2017.
- [40] M. Duarte and A. Sabharwal, "Full-duplex wireless communications using off-the-shelf radios: Feasibility and first results," in *Proc. IEEE Asilomar Conf. on Signal, Systems and Computers (ASILOMAR)*, Nov. 2010, pp. 1558–1562.
- [41] M. Duarte, C. Dick, and A. Sabharwal, "Experiment-driven characterization of full-duplex wireless systems," *IEEE Trans. Wireless Commun.*, vol. 11, no. 12, pp. 4296–4307, Dec. 2012.
- [42] D. Bharadia, E. McMillin, and S. Katti, "Full duplex radios," *ACM SIGCOMM Computer Communication Review*, vol. 43, no. 4, pp. 375–386, 2013.
- [43] K. E. Kolodziej, J. G. McMichael, and B. T. Perry, "Adaptive RF canceller for transmit-receive isolation improvement," in *IEEE Radio and Wireless Symposium (RWS)*, Jan. 2014, pp. 172–174.
- [44] —, "Multitap RF canceller for in-band full-duplex wireless communications," *IEEE Trans. Wireless Commun.*, vol. 15, no. 6, pp. 4321–4334, June 2016.

-
- [45] K. E. Kolodziej, P. T. Hurst, A. J. Fenn, and L. I. Parad, "Ring array antenna with optimized beamformer for simultaneous transmit and receive," in *Proc. IEEE Intl. Symp. on Personal, Indoor and Mobile Radio Commun. (PIMRC)*, July 2012, pp. 1–2.
- [46] M. Jain, J. I. Choi, T. Kim, D. Bharadia, S. Seth, K. Srinivasan, P. Levis, S. Katti, and P. Sinha, "Practical, real-time, full duplex wireless," in *IEEE Proceedings of international conference on Mobile computing and networking*, 2011, pp. 301–312.
- [47] A. Sahai, G. Patel, and A. Sabharwal, "Pushing the limits of full-duplex: Design and real-time implementation," *arXiv preprint arXiv:1107.0607*, 2011.
- [48] J. H. Lee, "Self-interference cancelation using phase rotation in full-duplex wireless," *IEEE Trans. Veh. Technol.*, vol. 62, no. 9, pp. 4421–4429, Nov. 2013.
- [49] Z. Zhang, Y. Shen, S. Shao, W. Pan, and Y. Tang, "Full duplex 2×2 MIMO radios," in *IEEE Wireless Communications and Signal Processing*, Oct. 2014, pp. 1–6.
- [50] E. Ahmed and A. M. Eltawil, "All-digital self-interference cancellation technique for full-duplex systems," *IEEE Transactions on Wireless Communications*, vol. 14, no. 7, pp. 3519–3532, July 2015.
- [51] Y. Pan, C. Zhou, G. Cui, W. Wang, and X. Li, "Self-interference cancellation with RF impairments suppression for full-duplex systems," in *Proc. IEEE Veh. Tech. Conf. (VTC)*, Sep. 2015, pp. 1–5.
- [52] F. Gregorio, J. Cousseau, S. Werner, T. Riihonen, and R. Wichman, "EVM analysis for broadband OFDM direct-conversion transmitters," *IEEE Trans. Veh. Technol.*, vol. 62, no. 7, pp. 3443–3451, Sep. 2013.
- [53] L. Ding, G. Zhou, D. Morgan, Z. Ma, J. Kenney, J. Kim, and C. Giardina, "A robust digital baseband pre-distorter constructed using memory polynomials," *IEEE Trans. Commun.*, vol. 52, no. 1, pp. 159–165, Jan. 2004.
- [54] D. Morgan, Z. Ma, J. Kim, M. Zierdt, and J. Pastalan, "A generalized memory polynomial model for digital predistortion of RF power amplifiers," *IEEE Trans. Signal Process.*, vol. 54, no. 10, pp. 3852–3860, Oct. 2006.

- [55] L. Anttila, D. Korpi, E. Antonio-Rodríguez, R. Wichman, and M. Valkama, “Modeling and efficient cancellation of nonlinear self-interference in MIMO full-duplex transceivers,” in *Proc. IEEE Global Commun. Conf. (GLOBECOM)*, Dec. 2014, pp. 777–783.
- [56] K. wan Nam, “Direct down-conversion system with I/Q correction,” Texas Instruments, <http://www.ti.com/lit/ug/slwu085/slwu085.pdf>.
- [57] X. Ma and G. Giannakis, “Maximum-diversity transmissions over doubly selective wireless channels,” *IEEE Trans. Inf. Theory*, vol. 49, no. 7, pp. 1832–1840, July 2003.
- [58] H. Ochiai and H. Imai, “Performance analysis of deliberately clipped OFDM signals,” *IEEE Trans. Commun.*, vol. 50, no. 1, pp. 89–101, Jan. 2002.
- [59] D. Petrovic, W. Rave, and G. Fettweis, “Effects of phase noise on OFDM systems with and without PLL: Characterization and compensation,” *IEEE Trans. Commun.*, vol. 55, no. 8, pp. 1607–1616, Aug. 2007.
- [60] A. Mehrotra, “Noise analysis of phase-locked loops,” *IEEE Trans. Circuits Syst. I*, vol. 49, no. 9, pp. 1309–1316, Sep. 2002.
- [61] Q. Gu, *RF system design of transceivers for wireless communications*. Springer Science & Business Media, 2005.
- [62] A. Parssinen, J. Jussila, J. Ryyanen, L. Sumanen, and K. A. I. Halonen, “A 2-GHz wide-band direct conversion receiver for WCDMA applications,” *IEEE J. Solid-State Circuits*, vol. 34, no. 12, pp. 1893–1903, Dec. 1999.
- [63] H. Yoshida, T. Kato, T. Toyoda, I. Seto, R. Fujimoto, T. Kimura, O. Watanabe, T. Arai, T. Itakura, and H. Tsurumi, “Fully differential direct conversion receiver for W-CDMA using an active harmonic mixer,” in *IEEE Radio Frequency Integrated Circuits (RFIC) Symposium*, June 2003, pp. 395–398.
- [64] A. Masmoudi and T. Le-Ngoc, “Residual self-interference after cancellation in full-duplex systems,” in *Proc. IEEE Intl. Conf. Commun. (ICC)*, June 2014, pp. 4680–4685.

-
- [65] T. Riihonen and R. Wichman, "Analog and digital self-interference cancellation in full-duplex MIMO-OFDM transceivers with limited resolution in A/D conversion," in *Proc. IEEE Asilomar Conf. on Signal, Systems and Computers (ASILOMAR)*, Nov. 2012, pp. 45–49.
- [66] S. Wei, D. L. Goeckel, and P. A. Kelly, "Convergence of the complex envelope of bandlimited OFDM signals," *IEEE Transactions on Information Theory*, vol. 56, no. 10, pp. 4893–4904, Oct. 2010.
- [67] H. Rowe, "Memoryless nonlinearities with gaussian inputs: Elementary results," *Bell System Technical Journal*, vol. 61, no. 7, pp. 1519–1526, 1982.
- [68] F. Chen, H. H. Lee, R. Morawski, and T. Le-Ngoc, "RF/Analog self-interference canceller for 2x2 MIMO full-duplex transceiver," May 2017.
- [69] J. C. Pedro and N. B. de Carvalho, "Evaluating co-channel distortion ratio in microwave power amplifiers," *IEEE Trans. Microw. Theory Tech.*, vol. 49, no. 10, pp. 1777–1784, Oct. 2001.
- [70] W. Cheng, A. J. Annema, J. A. Croon, D. B. M. Klaassen, and B. Nauta, "A general weak nonlinearity model for LNAs," in *IEEE Conference on Custom Integrated Circuits*, Sep. 2008, pp. 221–224.